AM-FM signal Analysis by Teager Huang Transform: application to underwater acoustics

Abdelkhalek Bouchikhi

N° d'ordre : 4301 **ANNÉE 2010**

THÈSE / UNIVERSITÉ DE RENNES 1
sous le sceau de l'Université Européenne de Bretagne

pour le grade de

DOCTEUR DE L'UNIVERSITÉ DE RENNES 1

Mention : TRAITEMENT DU SIGNAL et TELECOMMUNICATIONS

Ecole doctorale MATISSE

Présentée par

Abdelkhalek BOUCHIKHI

Préparée à l'IRENav, EA 3634, Ecole Navale
(SPM)

Analyse des Signaux AM-FM par Transformation de Huang-Teager : Application à l'acoustique sous-marine

Thèse soutenue à l'Ecole Navale le 7 décembre 2010

devant le jury composé de :

Nadine MARTIN
DR CNRS, Univ. Grenoble / Rapporteur

Messaoud BENIDIR
Professeur, Paris-Sud / Rapporteur

Jean Marc BOUCHER
Professeur, Télécom Bretagne / Examinateur

Xavier NEYT
Professor, Ecole Royale Militaire / Examinateur

Ali KHENCHAF
Professeur, ENSIETA / Directeur de thèse

Abdel-Ouahab BOUDRAA
MCF, HdR, Ecole Navale / Encadrant

Jean Christophe CEXUS
Enseignant-Chercheur, ENSIETA / Invité

Remerciements

Je tiens à remercier en premier lieu Abdel-Ouahab Boudraa, mon encadrant de thèse. Sans son enthousiasme et son amical soutien, je ne sais si cette thèse sur la thématique de l'analyse des signaux AM-FM par l'EMD aurait été menée à son terme, "Rabi yarham waldik, abdel-ouahab". Je remercie aussi mon directeur de thèse Ali Khenchaf, Professeur des Universités à ENSTA Bretagne, pour sa disponibilité malgré son emploi de temps assez chargé. Ses conseils m'étaient toujours indispensables. Je remercie également ici avec la plus grande sincérité les personnes qui ont participé de près ou de loin à ce travail de thèse.

Je tiens tout d'abord à remercier les membres du jury qui m'ont fait l'honneur d'évaluer ce travail. Je remercie Jean-Marc Boucher, Professeur à Télécom Bretagne, d'avoir apporté son regard personnel et de m'avoir fait le plaisir de présider le jury. Je remercie Madame Nadine Martin, Directrice de Recherche au CNRS (GIBSA-lab), et Messaoud Benidir, Professeur des Universités à Paris 11, d'avoir pris le temps de soigneusement étudier ce manuscrit et de le rapporter en me faisant part de leurs nombreuses questions et recommandations. Je remercie également Xavier Neyt, Professeur à l'Ecole Royale Militaire (Bruxelles), d'avoir apporter un regard critique sur le contenu scientifique de cette thèse. Je remercie beaucoup Jean Christophe Cexus, Enseignant-Chercheur à ENSTA Bretagne, d'avoir accepté de participer à ce jury et surtout d'avoir apporté son soutien à mes travaux de recherche, ça m'a fait beaucoup de plaisir de travailler avec toi " J. Christophe Sénior ! ". Je remercie également Laurent Guillon, Maître de Conférences à l'Ecole Navale, Docteur Elhadji Diop, Gérard Maze, Professeur des Universités à l'Université du Havre, et le Docteur John Fawcett, Chercheur au DRDC Atlantic (Canada), pour les discussions enrichissantes et les nombreuses remarques qui ont participé à l'avancement de ce travail de recherche. Mes remerciements vont aussi au personnel de l'Institut de Recherche de l'Ecole Navale (IRENav) en particulier, Jacques André Astolfi, Maître de Conférences à l'Ecole Navale, Christophe Claramunt, directeur de l'IRENav, ainsi que Radjesvarane Alexandre, Professeur des Universités à l'Ecole Navale, pour leurs soutiens. Je remercie également l'équipe du laboratoire d'Extraction et Exploitation de l'Information en Environnements Incertains (E3I2) de l'ENSIETA et en particulier Mme Annick Billon-Coat pour son aide.

Je tiens à remercier ici mes collèges à l'équipe RESO de l'ENIB, en particulier Maîtres de Conférences Abdesslam Benzinou, Yan Boucher et Docteur Kamal

Nasseredine pour leurs soutiens.
Mon amitié et mes remerciements à mes voisins de bureau : Patrice, Jean-luc, Jean-Michel et Pierre-Loic pour leur encouragement et à l'équipe ASM, Valérie, Delphine, Rozenn, Kais, Samuel et Louay. Je tiens également à remercier ici mon ami Sobhi, "Rabi ybarek Fik" et tout les Doctorants et Docteurs de l'IRENav sans que j'oublie personne, pour les inoubliables repas des doctorants et les sorties de cohésions, c'étaient des moments vraiment agréables. Je tiens aussi à remercier mes collègues de travail de l'Ecole Navale: département des langues, formation militaire, et en particulier tout le personnel du département des CENOE.
Finalement, il me reste à remercier mes parents, ma femme, Assia, mes trois soeurs, mes frères et mes amis en Algérie, ici en France et partout dans le monde à qui je dois la curiosité qui m'a amené jusqu'ici, et dont le soutien m'a été toujours précieux, "Rabi yhfadkom".

Contents

Contents **1**

List of Figures **5**

List of Tables **10**

Abbreviations **12**

List of publications **13**

Résumé étendu **16**

Introduction **22**

I Time-frequency representations **28**

I.1 Introduction 29

I.2 Fourier transform 29

I.3 Short-Time Fourier Transform 30

I.4 Wavelet Transform 31

I.5 Wigner-Ville Distribution 32

I.5.1 The cross-term issue 32

I.6 Reassigned TF Distributions 32

I.7 Summary 33

II Empirical Mode Decomposition **36**

II.1 Introduction 38

II.1.1 Linear systems 39

II.2 Empirical Mode Decomposition 39
II.2.1 Sifting process 40
II.2.2 Illustrative example 41
II.3 Some aspects of the EMD 45
II.3.1 IMF criteria 45
II.3.2 Number of sifts 45
II.3.3 Number of IMFs 46
II.3.4 Sampling and mode mixing issues 46
II.3.5 Orthogonality 47
II.3.6 Bivariate EMD 47
II.3.7 Ensemble EMD 47
II.3.8 A PDE for sifting process 48
II.4 Smooth B-spline interpolation of IMF 48
II.4.1 Polynomial spline signal 49
II.4.2 Noise reduction 52
II.4.3 Forced oscillatory motion 56
II.5 Summary 56

III Instantaneous frequencies and amplitudes tracking 62

III.1 Introduction 63
III.2 Multicomponent AM-FM Signal Model 63
III.3 ESA or HT ? 65
III.4 HT demodulation 66
III.5 TKEO 67
III.5.1 Discrete energy demodulation 68
III.5.1.1 DESA-1a 69
III.5.1.2 DESA-1 69
III.5.1.3 DESA-2 70
III.5.2 Continue energy demodulation 70
III.5.2.1 Demodulation by exact splines 71
III.6 Results and Discussion 75

III.7 Summary 83

IV Teager Huang Transform **86**

IV.1 Introduction 87

IV.2 Teager-Huang Transform 87

IV.3 Teager-Kaiser spectrum 88

IV.3.1 TKS generation 91

IV.4 Results and discussions 92

IV.4.1 Example 1: Hyperbolic frequencies law 92

IV.4.2 Example 2: Monocomponent FM signal 96

IV.5 Conclusions 98

V Teager Huang Hough Transform **102**

V.1 Introduction 103

V.2 Hough-Transform 103

V.3 THT and Hough-Transform: THHT 104

V.4 Detection in noise free environment 106

V.4.1 Results 106

V.5 Detection in noisy environment 109

V.5.1 EMD denoising 109

V.5.2 Results 113

V.6 Conclusions 122

VI Application to underwater acoustics **124**

VI.1 Introduction 125

VI.2 IMFs versus physical modes 125

VI.2.1 Physical Modes for a spherical shell 126

VI.2.2 IMFs 128

VI.3 Comparison and discussion 131

VI.4 Backscattering signal analysis 133

Conclusion and perspectives **144**

A Analysis of white gaussian Noise by EMD **148**

B The first derivatives of IMF in B-Spline space **154**

C Determinant for an empty shell **158**

Bibliography **160**

List of Figures

I.1 Jean Baptiste Joseph Fourier. 21 March 1768 Auxerre, Yonne, France [36] 29

II.1 Initialization of the sifting process for $s(t)$, envelope mean detection (red line) and the first sift of IMF1. Over- and undershoots are indicated by arrows. 42

II.2 Extraction of the 5 Hz component from $s(t)$ at first iteration. The local mean envelope is null (red line) and the component contain an acceptable number of extremas. 43

II.3 Extraction of the second candidate IMF from $s(t)$. Envelope mean detection (red line). 43

II.4 Extraction of the third candidate IMF from $s(t)$. Envelope mean detection (red line). 44

II.5 Extraction of the third candidate IMF from $s(t)$. Envelope mean detection (red line). 44

II.6 IMFs extracted from signal given in (cf, Eq. II.2.2). The two components of frequencies 5 Hz and 1 Hz correspond to IMF1 et IMF2, respectively. 45

II.7 EMD-RBS diagram. The modified EMD is distinguished from the coventional EMD on integrating the smooth B-splines, or Regularized B-splines (RBS) interpolation instead of the cubic splines interpolation. Also as in [15] we use the acronym EMD-RBS to refer to the modified EMD. 50

II.8 Cubic B-splines functions in the segment $[t_k, t_{k+1}]$. 51

II.9 Extracted IMFs by EMD from noisy signal $s(t)$ (SNR=0dB). The conventional EMD failed to extract directly the 5Hz sinusoid. For getting a smooth version of the sinusoidal signal one must add the IMF 5, the IMF 6 and part of the IMFs 4 and 7. 53

II.10 Extracted IMFs by EEMD from noisy signal $s(t)$ (SNR=0dB). The sum of IMF 4, 5 and 6 give a noisy version of the sinusoidal signal but not the original one. 54

II.11 Extracted IMFs by EMD-RBS of the noisy signal $s(t)$ (SNR=0 dB). The 5Hz tone is extracted successfully, it corresponds to IMF number 2. 55

II.12 variation of the parameter λ 56

II.13 Signal generated by an hydrodynamical system. 57

II.14 Extracted IMFs by conventional EMD from hydrodynamical measured signal. In top square IMF1 to IMF5. The square of middle, IMF6 to IMF10 and last one contain remainder IMFs and the residue. 58

II.15 Extracted IMFs by EMD-RBS from hydrodynamical measured signal. In top square, IMF1 to IMF4. The square of middle, IMF5 to IMF8 and last one contain remainder IMFs and the residue. The number of IMFs in the present figure is less than the previous figure. 59

III.1 Two AM-FM components ($M = 2$) 64

III.2 AS of the two AM-FM components, this representation shows in 3D the complex form of the signal, with their imaginary part and real part. The horizontal axis contain the samples points position. We note that a projection of this signal in the plane (Real part-sample) give the real signal, figure (III.1) 67

III.3 Decomposition of the noisy AM-FM signal, $s(t)$, (SNR=20 dB) with EMD 74

III.4 Decomposition of the noisy AM-FM signal, $s(t)$, (SNR=20 dB) with modified EMD 74

III.5 IAs estimation of noise free signal, $s(t)$, by EMD-ESA-BS 75

III.6 IFs estimation of noise free signal, $s(t)$, by EMD-ESA-BS 76

III.7 IA estimation of signal $s(t)$ (SNR= 20dB) by EMD-ESA-BS 77

III.8 IA estimation of signal $s(t)$ (SNR= 20dB) by EMD-ESA-RBS 77

III.9 IF estimation of signal $s(t)$ (SNR= 20dB) by EMD-ESA-BS 78

III.10IF estimation of signal $s(t)$ (SNR= 20dB) by EMD-ESA-RBS 78
III.11IA estimation of signal $s(t)$ (SNR= 20dB) by EMD-HT 78
III.12IA estimation of signal $s(t)$ (SNR= 20dB) by EMD-DESA1 79
III.13IA estimation of signal $s(t)$ (SNR= 20dB) by EMD-DESA1a 79
III.14IA estimation of signal $s(t)$ (SNR= 20dB) by EMD-DESA2 80
III.15IF estimation of signal $s(t)$ (SNR= 20dB) by EMD-HT 80
III.16IF estimation of signal $s(t)$ (SNR= 20dB) by EMD-DESA1 80
III.17IF estimation of signal $s(t)$ (SNR= 20dB) by EMD-DESA1a 81
III.18IF estimation of signal $s(t)$ (SNR= 20dB) by EMD-DESA2 81
III.19MSE as function of input SNR for different IF estimations of signal $s_2(t)$ 82
III.20MSE as function of input SNR for different IA estimations of signal $s_2(t)$ 82

IV.1 IFs and IAs estimating by EMD-ESA 88
IV.2 (a) On top a sinusoidal signal, on bottom the corresponding Fourier spectrum and mean marginal TKS in black and red colors, respectively. (b) THT (EMD-ESA) of the signal 90
IV.3 TFRs of the signal $s_1(t)$. (a) Spectrogram with Length of window ($Lw = 64$), number of overlaps samples in each segment of signal ($Nov = 32$) and number of frequency points ($Nfft = 1024$) (c) Spectrogram ($Lw = 256$, $Nov = 64$, $Nfft = 1024$) (d) Scalogram performed by Daubechies wavelet (db2) and in scales $S = [1 : 64]$ (d) Scalogram (Morlet, $S = [1 : 64]$). The red dashed line corresponds to the real frequency law. 93
IV.4 TFRs of the signal $s_1(t)$. (a) WVD. (b) SPWVD. (c) RSPWVD. The red dashed line corresponds to the real frequency law 94
IV.5 Decomposition of the signal $s_1(t)$ by EMD, the signal is plotted in the first row, the IMF1 to IMF8 correspond to the rows 1 to 8, respectively. The last one is the residue. 95
IV.6 TFRs of the signal $s_1(t)$., (a) EMD-HT. (b) EMD-ESA. The red dashed line correspond to the real frequency law 96
IV.7 Spectrum analysis of $s_2(t)$, (a) Spectrogram. (c) Scalogram. (d) SPWVD (e). RSPWVD (a) EMD-HT. (c) EMD-ESA. The red dashed line corresponds to the real frequency law 97

V.1 Illustration of Hough transform 104
V.2 Block diagram of the THHT. 106
V.3 Ideal TFR of the free noise signal $x_1(t)$. 107
V.4 Components tracking in THT plane of $x_1(t)$ 108
V.5 THHT applied to $x_1(t)$. 109
V.6 Components tracking in WVD plane of $x_1(t)$ 110
V.7 WVD-H$_g$T applied to $x_1(t)$. 111
V.8 Components tracking in SPWVD plane of $x_1(t)$ 112
V.9 Ideal TFR of the free noise signal $x_2(t)$. 113
V.10 Components tracking in THT plane of $x_2(t)$ 114
V.11 Components tracking in SPWVD plane of $x_2(t)$ 115
V.12 Block diagram of the EMD$_{\text{SG}}$ 116
V.13 Ideal TFR of noisy signal $x_2(t)$ (30dB). 116
V.14 WVD and THT of $x_2(t)$. 117
V.15 WVD-H$_g$T applied to $x_2(t)$. 117
V.16 WVD-H$_g$T applied to $x_2(t)$. 118
V.17 IF estimation (red) with WVD-H$_g$T (on the left) and THHT (on the right) of $x_2(t)$. 118
V.18 Estimation of β_0 119
V.19 Estimation of ν_0 119
V.20 Components tracking in THT plane of $x_3(t)$ (SNR=7dB) 120
V.21 Components tracking in SPWVD plane of $x_3(t)$ (SNR=7dB) 121

VI.1 Scattering geometry. This cartoon depicts a plane wave, traveling in the z direction, incident upon a fluid sphere (radius a, density ρ_1 and sound velocities c_l c_t), entrained in a second fluid (density ρ, sound speed c). For simplicity, the scattered waves are shown as spherical, which they are in time, although not generally in phase and amplitude. In the forward region, the scattered field and incident field interfere, and may produce a shadow [47]. 125
VI.2 225 kHz echo signal from a spherical shell of radii ratio equal to 0.96. 126
VI.3 Geometry of the scattering calculation. The sphere is centered on the z axis of the plan wave. 127

VI.4 On top, filtered time signal (the specular echo is replaced by zeros). The signal is reconstructed from the associated time series of the IMRs of the spherical shell($b/a = 0.94$). On bottom, resonance spectrum . . 128

VI.5 Associated time series of the IMRs of a spherical shell, modes 1-10 . . 129

VI.6 IMFs 1-10 extracted from the backscattering signal from a spherical shell. 130

VI.7 PSDs of IMRs 131

VI.8 PSDs of the IMFs 131

VI.9 superposition of PSDs of the IMRs, IMF1 and IMF2 dark and green dashed lines respectively 132

VI.10(a) Signal and FFT of signal 1. (b) Spectrogram. (c) Scalogram. (d) SPWVD. (e) HHT. (f) THT. 135

VI.11(a) Signal and FFT of signal 2. (b) Spectrogram. (c) Scalogram. (d) SPWVD. (e) HHT. (d) THT. 136

VI.12(a) Signal and FFT of signal 3. (b) Spectrogram. (c) Scalogram. (d) SPWVD. (e) HHT. (d) THT. (g) Zooming on HHT, (h) Zooming on THT ($[1.5, 1.55]$ ms). 138

VI.13(a) Signal and FFT of signal 4. (b) Spectrogram. (c) Scalogram. (d) SPWVD. (e) HHT. (d) THT. (g) Zooming on HHT, (h) Zooming on THT ($[1.5, 1.55]$ ms). 140

VI.14(a) Signal and FFT of signal 5. (b) Spectrogram. (c) Scalogram. (d) SPWVD. (e) HHT. (d) THT. (g) Zooming on HHT, (h) Zooming on THT ($[1.5, 1.55]$ ms). 142

A.1 IMF power spectra in the case of White Gaussian Noise. The spectrum densities (PSD) is plotted as a function of the logarithm of the period for IMFs 1 to 7. The spectral estimates have been computed on the basis of 5000 independent sample paths of 4096 data points . . 149

A.2 IMF power spectra in the case of White Gaussian Noise. The spectrum densities (PSD) is plotted as a function of the logarithm of the periode for IMFs 1 to 7. The spectral estimtes have been computed on the basis of 5000 independent sample paths of 4096 data points . . 152

A.3 Histograms of IMFs from 2 to 7 for a WGN sample with 4096 data points.The superimposed black lines are the Gaussian fits for each IMF, except IMF3 153

List of Tables

II.1 Sifting process 41

III.1 Mean Square Error between estimated IFs and real ones for the noise free signal. 76

IV.1 Proprieties comparison of Fourier analysis, TFRs of Cohen class and THT. 100

VI.1 Statistical parameters of the IMRs. 131

VI.2 Statistical parameters of the IMFs. Because the amplitudes of IMF8-10 are very small the values of the statistical parameters are considered null with the fixed precision 132

Abbreviations

AF	Ambiguity Function
AM	Amplitude Modulation
AS	Analytical Signal
DESA	Discrete Energy Separation Algorithm
EEMD	Ensemble Empirical Mode Decomposition
EMD	Empirical Mode Decomposition
ESA	Energy Separation Algorithm
FM	Frequency Modulation
FT	Fourier Transform
FFT	Fast Fourier Transform
HHT	Hilbert Huang Transform
HT	Hilbert Transform
IMF	Intrinsic Mode Function
IMR	Isolated Modal Resonance
IA	Instantaneous Amplitude
IF	Instantaneous Frequency
LFM	Linear Frequency Modulated
LS	Least Squares
ML	Maximum Likelihood
MSE	Mean Square Error
PDE	Partial Differential Equation
PSD	Power Spectral Densities
QTFR	Quadratic Time Frequency Representation
RADAR	RAdio Detection And Ranging
RBS	Regularized B-Spline
RSPWVD	Reassigned Smooth Pseudo Wigner-Ville Distribution
SD	Standard Deviation
SNR	Signal to Noise Ratio
SONAR	SOund Navigation And Ranging
SPWVD	Smooth Pseudo Wigner-Ville Distribution
STFT	Short Time Fourier Transform
SG	Savitzky-Golay
TF	Time Frequency
TFR	Time Frequency Representation
THT	Teager-Huang Transform
THHT	Teager-Huang-Hough Transform
TKEO	Teager-Kaiser Energy Operator
TKS	Teager-Kaiser Spectrum
WT	Wavelet Transform
WVD	Wigner-Ville Distribution

List of publications

International Journal Papers :

[1] **A. Bouchikhi** and A.O. Boudraa, "Multicomponent AM-FM signals analysis based on EMD-B-Splines ESA", *Signal Processing* (submitted).
[2] **A. Bouchikhi**, J.C. Cexus and A.O. Boudraa, "A combined Teager-Huang and Hough transforms for LFM signals detection", *Signal Processing.* (submitted).
[3] A.O. Boudraa. J.C. Cexus and **A. Bouchikhi**, "Time-frequency representation of multicomponent AM-FM signals by Teager-Huang transform", *IEEE Trans. Instrum. Meas.* (submitted).
[4] J.C. Cexus, A.O. Boudraa , **A. Bouchikhi**, et A. Khenchaf, "Analyse des échos de cibles Sonar par transformation de Huang-Teager (THT)", *Traitement du Signal*, vol. 24, no. 1-2, pp. 119-129, 2008.
[5] K. Khaldi, A.O. Boudraa, **A. Bouchikhi** and M. Turki-Hadj Alouane, "Speech enhancement via EMD", *EURASIP Journal on Advances in Signal Processing*, vol. 2008, Article ID 873204, 8 pages, 2008.

International Conference Papers :

[1] **A. Bouchikhi**, A.O. Boudraa, G.Maze, "Analysis of acoustics signals echos from cylindrical elastic shells by HHT and THT", *Proc. International Conference in Underwater Measurements*, pp 1455-1460, Nafplion, Greece, 2009.
[2] **A. Bouchikhi**, A.O. Boudraa, S. Benramdane and E.H.S. Diop, "Empirical mode decomposition and some operators to estimate instantaneous frequency: A comparative study", *Proc. IEEE ISCCSP*, pp. 608-613, Malta,2008.
[3] K. Khaldi, A.O. Boudraa, **A. Bouchkhi**, M. Turki-Hadj Alouane and E.H.S. Diop, "Speech signal noise reduction by EMD", *Proc. IEEE ISCCSP*, pp. 1155-1158, Malta, 2008.
[4] A.O. Boudraa, E.H.S. Diop and **A. Bouchikhi**, "Teager-Kaiser energy bilevel

thresholding", *Proc. IEEE ISC-CSP*, pp. 1086-1090, Malta, 2008.
[5] A.O. Boudraa, T. Chonavel, J.C. Cexus, S. Benramdane and **A. Bouchikhi**, "On the detection of transient signals using cross-Psi-B-energy operator", *Proc. IEEE IS-CCSP*, pp. 1445-1449, Malta, 2008.
[6] E.H.S. Diop, A.O. Boudraa and **A. Bouchikhi**, "An improved image demodulation algorithm based on Teager-Kaiser operator", *Proc. IEEE ISCCSP*, pp. 876-881, Malta, 2008.
[7] J.C. Cexus, A.O. Boudraa and **A. Bouchikhi**, "A combined Teager-Kaiser and Hough transforms for LFM signals detection", *Proc. IEEE ISCCSP*, 5 pages, Limassol, Cyprus, 2010.
[8] J.C. Cexus, A.O. Boudraa et **A. Bouchikhi**, "THT et transformation de Hough pour la détection de modulations linéaires de fréquence", *GRETSI*, 4 pages, 2009, Dijon, France.
[9] **A. Bouchikhi** et A.O. Boudraa, "Estimation des FIs d'un signal multi-composantes par décomposition modale empirique et une version B-splines de l'opérateur d'énergie de Teager-Kaiser", *GRETSI*, pp. 817-820, Troyes, France, 2007.
[10] A.O. Boudraa, E.H.S. Diop, F. Salzenstein, **A. Bouchikhi**, "Seuillage d'images basé sur l'opérateur de Teager-Kaiser", *GRETSI*, pp. 885-888, Troyes, France, 2007.

Résumé étendu

Les signaux issus des phénomènes physiques sont en général de nature non-stationnaire et dans certains cas ils sont également formés de plusieurs composants fréquentielles (multi-composante). On peut citer comme exemples de signaux non-stationnaires, les signaux, Radar, Sonar, de Parole, sismique ou biomédicaux [12]. Les Représentations Temps-Fréquence (RTF) sont des transformations conjointes forment le cadre idéal pour l'analyse et le traitement de tels signaux. Les RTF de la classe de Cohen constituent un outil puissant pour l'analyse des signaux non-stationnaires. La nature bilinéaire des RTF introduit des interférences (termes croisés) qui nuit à la lisibilité de ces dernières. Le lissage temps-fréquence permet de réduire ces interférences des RTF, mais certaines de leurs propriétés telles que les marginales ne seront plus vérifiées. Par ailleurs la plupart des RTF sont liées au noyau de Fourier et par conséquent auront intrinsèquement plus ou moins les mêmes limites que la transformée de Fourier. De plus aussi bien les RTF de la classe de Cohen que la transformée en ondelettes nécessitent la connaissance d'un noyau ou d'une fonction de base. Or, il n'existe pas de noyau universel pour représenter tous les signaux. L'idéal est de trouver une décomposition qui s'adapte à chaque signal, sans informations a priori et qui permette une description temps-fréquence. Une solution à ce problème a été proposée par Huang et *al.* [64] en introduisant la décomposition modale empirique (EMD pour Empirical Mode Decomposition). Cette décomposition est entièrement pilotée par les données et la RTF associée obtenue par Transformation d'Hilbert (TH) [12] ou l'algorithme de séparation d'énergie (ESA pour Energy Separation Algorithm) [83] ne présente pas d'interférences. L'EMD est dédiée à l'analyse de signaux non-stationnaires issus ou non de systèmes linéaires. La décomposition d'un signal par EMD produit des composantes qui sont des formes d'ondes oscillantes potentiellement non harmoniques dont les caractéristiques (fréquence, amplitude) varient au cours du temps. Ces composantes oscillantes modulées en amplitude (AM) et en fréquence (FM) sont

appelées modes empiriques ou IMFs (pour Intrinsic Mode Functions) :

$$s(t) = \sum_{j=1}^{N} \mathrm{IMF}_j(t) + \mathrm{r}_N(t), \tag{1}$$

où N est le nombre d'IMFs et $\mathrm{r}_N(t)$ est le résidu de la décomposition.

L'EMD est définie par la sortie d'un algorithme appelé processus de tamisage.
Dans cette thèse on explore les potentialités de cette méthode en analyse temps-fréquence pour l'estimation d'attributs important tels que l'Amplitude Instantanée (AI) et la Fréquence Instantanée (FI) ou la détection de Modulations Linéaires de Fréquence (MLF) dans le plan temps-fréquence. L'apport de l'EMD est illustré par une application à l'Acoustique Sous-Marine (ASM) ou les signaux sont de nature non-stationnaire.

Nous rappelons dans un premier temps l'intérêt de la représentation fréquentielle d'un signal et de la nécessité de l'analyse temps-fréquence dans le cas non-stationnaire. Nous mettons l'accent sur les limites des Représentations Temps-Fréquence (RTF) et le besoin d'un nouveau cadre de description des signaux s'affranchissant de la contrainte du noyau de décomposition et supprimant les termes d'interférences.

Dans un deuxième temps, nous nous penchons sur l'outil EMD et ses variantes. Nous mettons en avant les problématiques inhérentes au tamisage telles que les conditions d'une IMF, l'échantillonnage, l'interpolation des enveloppes du signal à décomposer, la condition d'orthogonalité des modes ou le critère d'arrêt. La version conventionnelle de l'EMD utilise la famille des B-splines [109] pour l'interpolation des enveloppes de maxima et de minima du signal [64]. Les modes ainsi extraits sont des sommes d'interpolations [14],[109]:

$$\mathrm{IMF}_j^n(t) = \sum_{l \in \mathbb{Z}} c_j\,[l]\,\beta_j^n(t-l) \tag{2}$$

où $\beta_k^n(t)$ est la B-spline centrale de degré n [99] et $c_j\,[k]$ les coefficients du modèle. Une propriété intéressante des fonctions B-splines est liée à leur support compact, ce qui limite la propagation des erreurs d'approximation d'un intervalle ("*box*") à l'autre. Cela étant, les enveloppes basées sur les fonctions B-splines ne sont pas assez robustes en présence de bruit car la contrainte d'interpolation est trop forte [15]. Une des conséquence de l'interpolation rigide est la génération d'IMFs artificielles. Dans ce cas, la solution est donc de s'orienter vers une courbe d'approximation des données

et non plus d'interpolation:

$$E = \sum_{l=-\infty}^{\infty} (\mathrm{IMF}_j^n(l) - h_j^n(l))^2 + \lambda \int \left(\frac{\partial^r h_j^n(t)}{\partial t^r} \right)^2 dt \tag{3}$$

où λ est une constante de régularisation, $h_j^n(l)$ est le modèle et $\mathrm{IMF}_j^n(l)$ sont les données mesurées. La valeur de λ est ajustée de manière heuristique ou sur la base de simulations intensives. Sur la base de cette interpolation régularisée un nouveau processus de tamisage est développé. Les résultats obtenus sur des signaux bruités en terme de décomposition et de nombre de modes extraits montrent l'intérêt de la régularisation des enveloppes du signal.

Nous nous sommes ensuite intéressés à l'apport du nouveau tamisage pour l'analyse temps-fréquence des signaux multi-composante associé à l'ESA. Le signal multi-composant analysé est de la forme suivante:

$$s(t) \triangleq \sum_{j=1}^{N} \underbrace{a_j(t) \cos(\int_0^{\tau} 2\pi f_j(t) dt)}_{s_j(t)} \tag{4}$$

où $a_j(t)$ et $f_j(t)$ sont la FI et la AI de la i^{eme} IMF $s_j(t)$ respectivement, et N est le nombre de composante ou IMF. La démodulation ESA est définie par les relations suivantes:

$$f_j(t) \approx \frac{1}{2\pi} \sqrt{\frac{\overline{\Psi[\dot{s}_j(t)]}}{\Psi[s_j(t)]}}, \quad \mid a_j(t) \mid \approx \frac{\Psi[s_j(t)]}{\sqrt{\Psi[\dot{s}_j(t)]}}, \tag{5}$$

où Ψ est l'opérateur de Teager-kaiser définit par,

$$\Psi[s_j(t)] \triangleq (\dot{s}(t))^2 - s(t)\ddot{s}(t) \tag{6}$$

$$\Psi[s_j(t)] \simeq 4\pi^2 a_j^2(t) f_j^2(t) \tag{7}$$

En approximant une IMF par un modèle B-spline d'ordre trois

$$g_j^3(t) = c_j[1]t^3 + c_j[2]t^2 + c_j[3]t + c_j[4]$$

nous montrons que l'ESA peut s'écrire

$$a_j(t) = \frac{A(t) + B(t)}{\sqrt{C(t)}} \tag{8}$$

$$f_j(t) = \frac{1}{2\pi} \sqrt{\frac{C(t)}{A(t) + B(t)}} \tag{9}$$

$$\begin{aligned} A(t) &= 3c_j^2[1]t^4 + 4c_j[1]c_j[2]t^3 + 2c_j^2[2]t^2, \\ B(t) &= (2c_j[2]c_j[3] - 6c_j[1]c_j[4])t + c_j^2[3] - 2c_j[2]c_j[4], \\ C(t) &= 18c_j^2[1]t^2 + 12c_j[1]c_j[2]t + 4c_j^2[2]t - 6c_j[1]c_j[3]. \end{aligned} \tag{10}$$

Les FI $f_j(t)$ et les AI $a_j(t)$ du signal $s(t)$ sont estimées en utilisant l'EMD et l'ESA. L'avantage d'une telle stratégie est la combinaison de deux approches locales et non-linéaires pour estimer des attributs instantanés. De plus, l'approche proposée n'est pas contrainte par l'estimation du nombre de composantes et ne fait pas d'hypothèse sur le modèle de la phase du signal à analyser. La méthode ESA régularisée obtenue est illustrée sur des signaux multi-composante bruités et les résultats comparés à ceux de la méthode basée sur la TH. Les résultats obtenus en terme de démodulation montrent l'apport des approches ESA-régularisée et EMD.

La combinaison de l'EMD et l'estimation des FI et AI est connue sous le nom de Transformée de Huang-Teager (THT). Cette RTF a été introduite par Cexus [22]. La THT n'est pas limitée par le principe d'incertitude et n'est pas contrainte par le théorème de Bedrosian. De plus elle évite le problème d'interférences des RTF de la classe de Cohen. Cela étant, jusqu'à présent la THT a été uniquement utilisée comme une simple représentation du signal. Nous proposons dans cette thèse une formulation mathématique de cette représentation qui va permettre de définir certaines notions telles que les marginales ou d'estimer des attributs tels que l'index de stationnarité. En utilisant l'équation (5), nous formulons la THT comme suit :

$$K(t,f) = \sum_{j=1}^{N} a_j(t, f_j(t)) = \sum_{j=1}^{N} a_j(t,f)\delta(f - f_j(t)) \tag{11}$$

où $K(t,f)$ est le spectre de Teager-Kaiser. Le but de cette nouvelle formulation (Eq. (11)) est d'étendre les applications de la THT autant qu'un outil d'analyse temps-fréquence.

Comme application de la nouvelle formulation de la THT (Eq. (11)), nous montrons comment la THT associée à la transformée de Hough (outil de traitement d'images) peut être utilisée pour la détection des signaux MLF dans le plan temps-fréquence. La méthode de détection des MLF est appelée Teager-Huang-Hough Transform (THHT). La THHT d'un signal $s(t)$ est définie comme la ligne intégrale du spectre de Teager-Kaiser $K(t,f)$ le long du modèle de FI $f(t;\Theta_j)$ où $\Theta_j := (\nu_j, \beta_j)$ est le vecteur de paramètres.

$$h(\Theta_j) = \int_{-\infty}^{-\infty} K(t, f(t;\Theta_j))dt \quad j \in \{0, 1, \ldots N-1\} \tag{12}$$

Ainsi la détection dans le plan temps-fréquence d'un chirp (ν_j, β_j) consiste à chercher

un pic dans le plan de Hough définit par les paramètres (ρ_j, θ_j):

$$(\rho_j, \theta_j) = \underset{\Theta_j}{Arg\,max}\,[h(\Theta_j)] \tag{13}$$

où $\nu_j = \dfrac{\rho_j}{\sin\theta_j}$ et $\beta_j = -\text{cotang}\,\theta_j$. La THHT est illustrée par des signaux MLF bruités et les résulats comparés à ceux de la distribution de Wigner-Ville (WVD) et de la Pseudo-WVD. Les résultats montrent que la suppression des termes d'interfé rences améliorent la détection des chirps dans le plan temps-fréquence.

Enfin, nous illustrons la THT par une application à l'ASM. Plus exactement, nous nous intéressons à l'analyse des échos de cibles Sonar qui sont des signaux non-stationnaires. Nous commençons d'abord par étudier les relations entre les IMFs et les modes de résonances des cibles (IMR pour Isolated Modal Resonance). Si ces les relations entre IMFs et IMRs sont établies alors le processus de classification de cibles ne peut être que facilitée. Les résultats préliminaires montrent qu'il n'y a pas de correspondance directe entre un mode empirique et un mode physique du même niveau; par contre l'analyse des densités spectrales de puissance des IMF et des IMR montre qu'une IMF peut être approximée par une somme réduite d'IMR. L'analyse des paramètres statistiques (moyenne, énergie, Skewness, Kurtosis) des IMF et des IMR va dans le même sens que celle des densités spectrales de puissance. Pour terminer, la THT a été appliquée à une série de signaux d'échos de cibles réels (coques cylindriques) avec différentes caractéristiques physiques (matériau, épaisseur,...). Les résultats de la THT ont été comparés à ceux du spectrogramme, le scalogramme et la Pseudo-WVD. L'analyse des cartes temps-fréquences des échos de cibles montre que seule la THT est sensible aux changements des paramètres physiques des cibles, ce qui montre que la décomposition par EMD s'adapte bien aux caractéristiques du signal à analyser.

Introduction

1. The need for time-frequency

Time-Frequency (TF) analysis is an area of active interest in the signal processing domain. The fundamental goal is to understand and describe situations where the frequency content of a signal varies in time (nonstationary signal). Important features of nonstationary signal are provided by its Instantaneous Frequency (IF) and Instantaneous Amplitude (IA) [12]. Estimating these time features is a first step for signals analysis. In different areas such as in seismic, Radar or Sonar, signals under consideration are known to be nonstationary and could be generated by a nonlinear process. It has been proven that estimations of IFs and IAs of measured data, remain the best way for detecting and analyzing hidden physical phenomena (e.g., signal scattering from obstacle, temperature changing in some areas and a period of time, acoustics signal generated by crustacean,...). Furthermore, IF determines what frequencies are present, how strong they are, and how they change over time. However, only meaningful IFs or IAs may really help us to explain the production, variation and evolution of physical phenomena. The problem of the interpretation of the IFs of signal has been largely addressed in the literature [11, 32, 64, 12, 64]. It has been argued that the interpretation of IF functions may be physically appropriate only for monocomponent signals where there is only "one spectral component" or "narrow band component" [32]-[12],[65]. Additionally, to reveal the true physical meaning of IF or IA, their estimation must be robust against noise.

Though the Hilbert Transform (HT) [12] and the Energy Separation Algorithm (ESA) [83] are accepted demodulation methods, when applied to multicomponent signal or AM/FM oscillatory functions, the tracked IF and IA features can lose their physical signification [65]. To overcome this problem, the Empirical Mode Decomposition (EMD) a time signal decomposition was developed so that a multicomponent signal can be analyzed in physically meaningful time-frequency-amplitude space by reducing it to a collection of monocomponent functions. This

signal processing technique breaks down any signal derived from linear or nonlinear system into a sum of oscillatory modes called Intrinsics Modes Functions (IMFs) so that meaningful IFs and IAs are derived [64]. Many works have been shown that decomposing a signal by EMD can really break out physical features [64]-[65],[49].

Once IMFs are extracted, it is possible to perform a spectral analysis, or three dimension plot (time-frequency-amplitude) that represents the variation of frequency and amplitude (or energy) of IMFs over time. Based on the EMD two Time-Frequency Representations (TFRs) are recently introduced [64],[22]. Applying the HT or the ESA to each IMF the derived TFR is designated as Hilbert-Huang Transform (HHT) [64] or Teager-Huang Transform (THT) [24]. While the HT uses the whole signal, the ESA is based on signal differentiation and thus it is an instantaneous approach and has a good time localization. Note that different from classical TFRs such as Wigner-Ville Distribution (WVD), neither do the HHT and the THT define an explicit equation that maps one dimension signal into a three dimension representation that provides information about time, frequency and amplitude (energy). It has been shown that the THT gives interesting results compared to the HHT and particularly for signals with sharp transitions [22]. The THT works well in free and in moderately noisy environments, but like the HHT it performs poorly for very noisy signals. This THT limitation is due to the sensitivity to noise of the ESA, which is based on the differentiation of the signal. Thus, to reduce noise sensitivity a more systematic approach is to use continuous-time expansions of discrete-time signals to numerically implement the required differentiations without approximation. In EMD, the core idea is the fitting splines to extrema in the process of extracting the IMFs and a residual in the decomposition of the input signal. Since extracted IMFs are represented in B-spline expansions [14], a close formulae of the ESA which ensure robustness again noise is derived. Also, by means of a smooth version of B-splines for interpolating, the tracked IFs and IAs are more robust against noise.

Based on the EMD, the THT is well dedicated to analyze any signal without any requirement of stationarity or linearity. As the HHT, the THT is not based on the convolution pairs from priori basis function sets, the result is not limited by the Heisenberg-Gabor uncertainty principle. Both THT and HHT are cross-terms free compared to TFRs of Cohen's class. Nevertheless, there is a limit on the precision, because of the infinite many adaptive IMF basis sets the EMD can generate. Furthermore, unlike the HHT which is based of the HT, the THT is not limited by the Bedrosian theorem. However, until now the THT is still used just

as a representation of the signal. No TF attributes or other relevant informations (marginals,...) are derived from such representation. We propose in this thesis a mathematical formulation of the TF map of the THT such as some useful definitions or information such as the marginals or stationarity index can be estimated. Furthermore, this new formulation allows the extension of the application field of the THT. Thus, based on this formulation a new tracking scheme (detection and estimation) of multicomponent Linear Frequency Modulation (LFM) signals using the Hough transform is introduced and compared to WVD-Hough transform. The introduced detection method is called Teager Huang Hough Transform (THHT) for short.

2. Application

One of the most challenging applications of TFRs deal with the analysis of the underwater acoustic signals. In this work, the THT is illustrated on real world underwater acoustics signals derived from spherical targets which can be viewed as nonlinear systems. The problem of discrimination of immersed targets was initiated with the works of Hoffman [56] who investigated time-domain approaches and Chesnut and Floyd who tested multiple frequency based techniques [26]. Time-domain techniques based on neural network inversions have been developed to discriminate Sonar objects [59],[3]. TF approaches have also been used for target classification [81]-[42] and have given high potentiality for discrimination between solid and hollow targets as well as for determining the target material [28]. For example in [28] WVD is used as TF description. Indeed, WVD has been shown to be a relevant for understanding of echo formation mechanisms and for surface waves that circumnavigate the targets [81]-[42]. In [27] a Sonar target classification approach based on the TF projection filtering, proposed by Hlawatsch and Kozek [55], is presented. The WVD associated to the Impulse response (IR) (acoustic response) of a Sonar target generates a TF plane (image) showing different patterns. These patterns can be classified into two categories 1) Interferences due to the bilinear nature of the WVD [11]. 2) High energy pattern: the first one, non dispersive, is associated with the specular echo on the target and the two following patterns correspond to the arrival of surfaces waves (antisymmetric Lamb waves) that circumnavigate the target [27]. The two pertinent patterns for classification are the specular reflection and the Lamb waves. The function of a TF filter is to extract from the signal to be analyzed the pertinent patterns. The filter is designed from the WVD of a reference signal and more particularly from its TF support R containing the relevant information. This region R is derived manually (isolation of the echoes by an expert operator).

The limit of the WVD is the severe cross terms due to the existence of negative power for some frequency ranges. Although most of these difficulties are overcome by using proper kernel functions, the method is still Fourier based; therefore all the possible complications associated with Fourier Transform (FT) still exist. To circumvent this drawback we use the THT which is cross-terms free and we investigate this tool for signal analysis task. Here we deal with the analysis of the acoustic signature without classification. Before analyzing the resulted TF maps of backscattering signals by simple shells, we first investigate possibles relationships between Isolated Modal Resonances (IMRs) of a spherical shell and IMFs extracted from the backscattering signal by this shell. Such links between empirical and physical modes, may be useful for Sonar target detection and classification purposes.

3. Main contributions of the thesis

- Introduction of a new sifting process where smoothing interpolation is used instead of exact interpolation, to construct the upper and lower envelopes of the signal to be decomposed. Main advantages of this new sifting are to give the EMD more robustness against noise and to reduce the number of unwanted or insignificant IMFs of the conventional EMD (over-decomposition).
- Application of the new sifting processus to signals denoising.
- Coupling two local and nonlinear approaches namely EMD and ESA as the basis of a multicomponent signal analysis framework. Moreover, different discrete versions of the EMD-ESA depending on the used derivation schemes are studied.
- Based on B-splines model, continuous version of the EMD-ESA is proposed. This new approach is used for tracking IFs and IAs of multicomponent AM-FM signal embedded in additive white Gaussian Noise.
- TF analysis by means of THT is introduced. Mathematical formulation of the THT is presented and some useful attributes calculated.
- Introduction of new detection approach of multicomponent LFM signals combining the THT and the Hough Transform (THHT).
- Investigation of possibles links between physical modes of spherical shell and the IMFs extracted from the backscattering signal by this shell.
- TF analysis by THT and HHT of real world under water reflected acoustics signal.

4. Contents and organization of the manuscript

In the first chapter, the definition of FT is recalled and a brief insight on some popular and largely used TFRs of the Cohen's class is given. A classification of these representations is given at the end of the chapter. In order to understand how they work, in next chapters these representations are applied to synthetic and real world signals. Furthermore, in the fourth chapter we compare the resulting representations to each other and to the THT.

In the second chapter basics of the EMD are presented. Contrary to the former decomposition methods, the EMD is intuitive and direct, with the basis functions derived from the data. Conventional EMD is detailed and some of its issues discussed. To improve the results of the conventional EMD in term of decomposition a new sifting process is introduced. This new sifting is firstly tested for separating sinusoidal signal from other components embedded in white Gaussian Noise. Finally application of the new EMD to real data is presented (isolation of an oscillatory component in forced motion [94]).

In the third chapter, a demodulation approach of multicomponent AM-FM is proposed. This method combines the EMD and the ESA, designated as EMD-ESA for short. A multicomponent AM-FM is first decomposed by EMD into a set of IMFs, then the IF and IA of each IMF tracked using the ESA. We introduce different variants of the discrete version of the EMD-DESA. To improve the tracking results, a continuous version of the approach is proposed. The investigation is completed by a comparative study between the proposed methods and the EMD-HT approach.

In the fourth chapter the THT is introduced. Unlike classical approaches this TFR dose not need any predefined decomposition basis. The THT is compared to classical TFRs on synthetic signals. We analyze the results of each approach and discuss its limits.

In the fifth chapter a formulation of the detection problem of LFM signals (mono- or multicomponent) in the TF plane of the THT is presented. This new detection scheme combines the THT and the Hough transform. LFM components are detected and their parameters are estimated in terms of peaks and their locations in the parameter space. In order to evaluate the performance of the proposed approach we have tested it in noisy environment and the results are

compared to classical approaches such as the WVD-Hough transform.

In the last chapter, preliminary results of the possibles relationships between the IMRs of a thin empty spherical shell and the associated extracted IMFs from the acoustic signal backscattered by this spherical shell, are presented. The study is carried out quantitatively and qualitatively. Finally, different TFRs of backscattering signal from simple shells (cylinder) for several physical parameters are analyzed.

CHAPTER I

Time-frequency representations

Contents

I.1 Introduction 29

I.2 Fourier transform 29

I.3 Short-Time Fourier Transform 30

I.4 Wavelet Transform 31

I.5 Wigner-Ville Distribution 32

I.5.1 The cross-term issue 32

I.6 Reassigned TF Distributions 32

I.7 Summary 33

In this chapter, the definition of FT is recalled and a brief insight on some popular and largely used TFRs of the Cohen's class is given. A classification of these representations is given at the end of the chapter. In order to understand how they work, in next chapters these representations are applied to synthetic and real world signals. Furthermore, in the fourth chapter we compare the resulting representations to each other and to the THT.

I.1 Introduction

A large number of applications need adequate signal processing and analysis tools to extract relevant information. Time-Frequency (TF) analysis is becoming a topic of much interest in the signal processing domain. The main goal of this analysis is to understand and describe situations where the frequency content of a signal varies in time (nonstationary signal). Actually, for resolving the problems in hand [13, 81, 86, 87, 108], one can easily find sophisticated mathematical models and approaches [12, 31, 48, 92]. We remark that all these approaches have a common beginning point, the Fourier Transform (FT).

Figure I.1: Jean Baptiste Joseph Fourier. 21 March 1768 Auxerre, Yonne, France [36]

I.2 Fourier transform

Joseph Fourier, (Fig. (I.1)) developed trigonometric series in order to resolve a physical problem [111]. He was originally interested in heat propagation in metals. Fourier main motivation was to find an equation governing the behavior of heat. His formulation of the heat equation and the proposed solution are considered one of the most fascinating mathematical models for physical phenomena [93]. The Fourier series would then be very useful for solving problems in many fields of applications, such as electrotechnics, electric circuits, mechanics, radio propagation and telecommunications systems. Since the second half of the last century, the emergence of powerful calculators, which still continue offering a computational processing time, the Fourier series, that are limited to periodic signal of finite energy [113] have been generalized to the FT, then to a sophisticate and rapid algorithm, the Fast Fourier Transform (FFT) [113][20][45]. Today,

engineers and scientists use systematically the FT for processing a signal. In this Chapter we would like to highlight some sophisticated approaches, derived from the FT. In order to understand the philosophy of the TFRs, we firstly define the FT.

FT decomposes a signal into a set of weighted harmonics components with fixed frequencies. To be Fourier-transformed, a signal $s(t)$ must be stationary and have a finite energy (Eq. I.1).
Finite energy signals satisfy the condition of summability:

$$\int_{-\infty}^{+\infty} |s(t)|^2 dt < \infty \tag{I.1}$$

By definition, the FT $S_1(f)$ of a signal $s(t)$ is given by [92]:

$$S_1(f) = \int_{-\infty}^{+\infty} s(t) e^{-j2\pi ft} dt = |S_1(f)|\, e^{j\phi(\omega)} \tag{I.2}$$

$$s(t) = \int_{-\infty}^{+\infty} S_1(f) e^{j2\pi ft} df \tag{I.3}$$

where $|S_1(f)|$ and $\phi(\omega)$ are the module and the phase of the spectrum $S_1(f)$, respectively. $e^{j\phi(\omega)}$ is the Fourier kernel.

It has been proven that analysis of nonstationary signals by FT does not bring interesting information about spectral contnent [20][45]. As we have illustrated with this simple example, the FT dose not allow good analysis of signals if their spectral content is varying in time. In order to overcome the limitation of the FT and to provide new tools for analyzing nonstationary signals, TF analysis tools are introduced.

I.3 Short-Time Fourier Transform

In order to add time-dependency in the FT, a simple and intuitive solution consists in dividing a time-domain signal into a series of small overlapping pieces; each of these pieces is windowed and then the FT is applied to each one. The obtained transformation is called Short-Time Fourier Transform (STFT). For a signal $s(t)$, the STFT is given by [32]:

$$S_2(f,t) = \int_{-\infty}^{\infty} s(\tau) h(\tau - t) e^{-i2\pi f\tau} d\tau \tag{I.4}$$

where $h(t)$ is a window function. The energy density spectrum of the STFT is defined as

$$E_2(f,t) = |S_2(f,t)|^2 \tag{I.5}$$

Equation (I.5) is named spectrogram; it is real-valued and has non-negative distribution. The width of the window function h remains a problematic issue. It is not possible to achieve good localization simultaneously in the time and the frequency domains. For instance, contracting a function in the time domain in order to improve its time localization cannot be done without dilating it in the frequency domain, i.e., weakening its frequency localization. This limitation is named the Heisenberg uncertainty principle [21],[53].

I.4 Wavelet Transform

Instead of a fixed window function, the Wavelet Transform (WT) uses TF atoms or wavelets. The WT of signal $s(t)$ is defined as [33],[92]:

$$S_3(a,b) = \int_{-\infty}^{\infty} s(t)\psi^*_{a,b}(t)dt \tag{I.6}$$

where * denotes the complex conjugate, and the wavelet basis $\psi_{a,b}(t)$ is generated from a basis (mother) wavelet (Eq. I.7) $\psi(t)$ by dilatations and translations. An example of wavelet is the Morlet wavelet (Eq. I.8) which has a wider effective support to provide more accurate results.

$$\psi_{a,b}(t) = \frac{1}{a}\psi(\frac{t-b}{a}) \tag{I.7}$$

$$\psi(t) = \exp(-t^2/2).\cos(5t) \tag{I.8}$$

where a is the scale factor, b is the translation factor, and $1/\sqrt{a}$ is a factor for the normalization in terms of energy. It becomes $1/a$ for the normalization in terms of amplitude. The energy density function of a WT is defined as $E_3 = |S_3(a,b)|^2$ and is called scalogram.

I.5 Wigner-Ville Distribution

A TF energy distribution which is particularly used in SONAR and RADAR [115] is the Wigner-Ville distribution (WVD) defined as [92]:

$$S_4(f,t) = \int_{-\infty}^{\infty} e^{-i2\pi f\tau} s(t+\frac{\tau}{2}) s^*(t-\frac{\tau}{2}) d\tau \tag{I.9}$$

An advantage of the WVD is that it can exactly localize sines or Dirac impulses which is not the case for the spectrogram and the scalogram. However, it suffers from signal interferences or cross terms.

I.5.1 The cross-term issue

Bilinear distributions produce so-called "cross-terms", which arise because the distribution is a nonlinear, specifically bilinear, function of the signal. A major advance in mitigating the cross terms was made by Williams, who developed the concepts needed to generate bilinear distributions that reduce the cross items while simultaneously preserving desirable properties of the distributions, particularly the marginal function [29],[70]. To avoid this interference, a smoothed version of WVD is introduced [11]

$$S_5(f,t) = \int \int_{-\infty}^{\infty} G(f-f', t-t') S_4(f',t') d\tau' df' \tag{I.10}$$

which filters the original WVD of Eq. (I.9) with a two dimensional filter, G [32]. In practice the filter G is composed of two one-dimension window filters (h, g). The WVD in this case is named Smooth Pseudo WVD (SPWVD)

I.6 Reassigned TF Distributions

Pioneering work on the method of reassignment was first published by Kodera [76] under the name of Modified Moving Window Method. The technique enhances the resolution in time and frequency of the classical Moving Window Method, the TFR constructed from the squared magnitude of the moving window transform defined in equation (I.9) or (I.10), by assigning to each data point a new TF coordinate that better-reflects the distribution of energy in the analyzed signal. Auger and Flandrin have generalized the technique to large TF distributions [4].

A much more relevant choice is to assign the total mass to the center of gravity of the distribution within the domain, and this is precisely what reassignment does:

at each TF point (t, f) where a spectrogram value is computed, one also computes the two quantities:

$$\hat{t}_s(f,t) = \frac{1}{S_5(f,t)} \int \int_{-\infty}^{\infty} \tau' G(f-f', t-t') S_4(f',t') d\tau' df' \tag{I.11}$$

$$\hat{f}_s(f,t) = \frac{1}{S_5(f,t)} \int \int_{-\infty}^{\infty} f' G(t-t', f-f') S_4(f',t') d\tau' df' \tag{I.12}$$

The spectrum value is then moved from the point (f, t) where it has been computed to the new centroid $(\hat{t}_s(f,t), \hat{f}_s(f,t))$. The new Reassigned SPWVD (RSPWVD) is now defined by [88]:

$$S_6(f,t) = \int \int_{-\infty}^{\infty} S_5(f',\tau') \delta(f - \hat{f}_s(f',\tau'), t - \hat{t}_s(f',\tau')) d\tau' df' \tag{I.13}$$

I.7 Summary

In this chapter we loosely give brief insight of TFR approaches. Our work focuses on the most popular one. We can summarize it, as it has been done in [12] and [88] to:

- A linear TFR $S(f,t)$ satisfies the linearity superposition principle that states that if $s(t) = as1(t) + bs2(t)$ is a linear combination of $s1(t)$ and $s2(t)$, then the TFR of the sum must satisfy $S(f,t) = aS1(f,t) + bS2(f,t)$ where a and b are complex coefficients. Two linear TFRs that have been used in many applications are the STFT and the WT. The STFT is the only linear TFR that preserves both time and frequency shifts on the analysis signal, an important property for speech, image processing and filterbank decoding applications. The WT preserves scale changes (compressions or expansions) on the signal, an important property for multiresolution analysis applications such as detection of singularities or edges in images. Note that as these TFRs are based on windowing techniques, their TF resolution depends on the choice of window characteristics.

- Quadratic TFRs. Any quadratic TFR (QTFR) can be expressed as

$$S(f,t) = \int_{-\infty}^{\infty} \int_{-\infty}^{\infty} s(t_1) s^*(t_2) K(t_1, t_2; f, t) dt_1 dt_2 \tag{I.14}$$

  where K is a signal-independent function that characterizes the QTFR. These representations satisfy the quadratic superposition principle as a QTFR

of $s(t) = \alpha s1(t) + \beta s2(t)$ satisfies $S(f,t) = |\alpha|^2 S1(f,t) + |\beta|^2 S2(f,t) + 2\Re[\alpha\beta^*.S_{1,2}(f,t)]$. The term $S_{1,2}(f,t)$ is the cross term of the QTFR and $\Re[]$ denotes real part. For QTFRs, windowing techniques are not required because the objective is to form energy distributions so that the signal energy, also a quadratic representation, can be distributed in the TF plane. However, windowing techniques are often used to suppress the cross term that may impede processing because they are oscillatory. Two important QTFRs include the WVD, its smoothed version, and the spectrogram.

- Some TFRs were proposed to adapt to the signal TF changes. Like reassigned TFRs adapt to the signal by employing other QTFRs of the signal such as the spectrogram and the WVD or others TFRs.

We conclude from this chapter that the classical TFRs such the STFT, the WVD or the WT, suffer from several limitations. There is need for a new TF framework to overcome those limitations and for analyzing properly signals. In particular, we look for a TFR that is well dedicated for nonlinear and nonstationary data. For this reason, this TFR must be adaptive (data driven approach), cross-terms free, not limited by the uncertainty principle and produces physically meaningful representation of the data from complex processes. We see in next chapters that this TFR can be obtained by combining the EMD of Huang and a demodulation technique such as the Hilbert Transform (HT) or the Energy Separation Algorithm (ESA). The proposed approche as we should illustrated is an alternative for the classical TFRs, but of corse like others it has limites and advantages. In next chapters this points will be discussed.

CHAPTER II

Empirical Mode Decomposition

Contents

II.1 Introduction 38

II.1.1 Linear systems 39

II.2 Empirical Mode Decomposition 39

II.2.1 Sifting process 40

II.2.2 Illustrative example 41

II.3 Some aspects of the EMD 45

II.3.1 IMF criteria 45

II.3.2 Number of sifts 45

II.3.3 Number of IMFs 46

II.3.4 Sampling and mode mixing issues 46

II.3.5 Orthogonality 47

II.3.6 Bivariate EMD 47

II.3.7 Ensemble EMD 47

II.3.8 A PDE for sifting process 48

II.4 Smooth B-spline interpolation of IMF 48

II.4.1 Polynomial spline signal 49

II.4.2 Noise reduction 52

II.4.3 Forced oscillatory motion 56

II.5 Summary 56

We present in this chapter basics of the EMD. Contrary to the former decomposition methods, the EMD is intuitive and direct, with the basis functions derived from the data. Conventional EMD is detailed

and some of its issues discussed. To improve the results of the conventional EMD in term of decomposition a new sifting process is introduced. This new sifting is firstly tested for separating sinusoidal signal from other components embedded in white Gaussian Noise. Finally application of the new EMD to real data is presented (isolation of an oscillatory component in forced motion [94])

II.1 Introduction

The strength of using TFRs compared to time or frequency representations, is their capacity to quantitatively resolve changes in the frequency content of nonstationary signals. Their major weaknesses in some cases: are to generates representations that are meaningless or difficult to interpret. In some cases, one can analyze the resulted TF maps and explain some misunderstood patterns: For example, the WVD by definition generates added cross terms, and could be identified some time in the TFR [77, 81, 102, 22, 24, 16]. For kernel-based approaches, the major weakness is the priori imposed by the basis choice. Finding a decomposition basis that can optimally represent the original signal is a serious issue; when one is faced to inexplicable results given by the STFT for analyzing signal [32, 118, 16] Usually, the length and the type of the temporal truncation window is suspected (i.e, the Heisenberg identity [1][32]). Even the WT, for some applications perform better than others kernel-based TFRs [33], the choice of the wavelet function that optimally represents the analyzed signal, remains a great challenge.

The type of signals of natural phenomena or man made signals vary greatly. A signal is said to be stationary if, in the deterministic case, it can be written as a sum of discrete sinusoids which have constant IF and IA. In the random case, statistical properties of the signal are invariant by shift of the beginning of time; Otherwise when it changes in some sense then one says it is nonstationary [32]. Recall that nonstationarity is a "non-property".

Instantaneous Frequency (IF) is an important notion and very useful physical quantity for characterizing nonstationary signals. It can be defined for monocomponent as the frequency present at short time laps [11][32]. The opinions are devised on this subject, because usually people are influenced by the Fourier spectral analysis. For a full wave (harmonic in the Fourier sense), the frequency and amplitude do not change. However, for nonstationary case where the frequency content changes in time, this simplistic definition does not make sense.

There is not one way to define mathematically the IF. The most popular definition involve the analytic signal, where the frequency is derived from the phase information (see chapter.III). For a lack of precise definition of the monocomponent and the IF, the notion of "narrow band" was introduced as a limitation on the data to make sense for the IF [100]. The bandwidth B_W is defined in terms of the spectral

[1] the Heisenberg principal led to trade off to resolve between having good resolution in time and frequency. $\Delta t.\Delta f \leq \frac{1}{2}$

moment of the signal as follows

$$N_0 = \frac{1}{\pi}\left(\frac{m_2}{m_0}\right)^{1/2}$$
$$N_1 = \frac{1}{\pi}\left(\frac{m_4}{m_2}\right)^{1/2}$$

$$B_W = N_1^2 - N_0^2 = \frac{1}{\pi^2}\frac{m_4 m_0 - m_2^2}{m_2 m_0} \tag{II.1}$$

$$B_W = \frac{1}{\pi^2}\nu^2 \tag{II.2}$$

where N_0, N_1 are the expected numbers of zero crossing and of extrema per unit of time, respectively. m_i is the ith moment of the spectrum. The parameter ν, offers a standard bandwidth measure.

For a narrow band signal we have

$$B_W = 0 \Rightarrow N_0 = N_1$$

as consequence of $\nu = 0$, the number of the expected numbers of extrema and zero crossings must to be the same.

- The main motivation of Huang et *al* [64],[61] was to develop an approach allowing the analysis of nonstationary and nonlinear process. The EMD is introduced for that purpose, moreover, the EMD has given a meaningful sense to the IF (in the Hilbert Transform sens) for real world signal. In the following paragraphs we introduce the EMD, we explain how it works and we discuss some aspects of the EMD.

II.1.1 Linear systems

For the nonlinear systems the superposition principle could not apply. For linear physical system having many sources, one can analyze separately the effect of each source. Then, for studying the effect of the whole system, it is possible to add the results from each source.

II.2 Empirical Mode Decomposition

It has been noted in large number of areas, especially where analysis and interpretation are needed like sub-marine observation, analysis of natural phenomena such

as climate change and heat variation, that traditional TF techniques such as the STFT are unable to calculate the spectral content of highly transient signals with sufficient accuracy. New signal processing methods such as wavelets, WVD, others TFRs and multiscale methods for some areas of application have been developed. These solutions can provide useful TF decompositions by adaptively decomposing data. However, most of TFRs, including those presented in chapter one are kernel dependent approaches. In fact, adding priori on the resulted TFRs could change the nature of the analyzed data and, of course, the interpretation of the results. EMD has been recently introduced by Huang et *al.* for adaptively decomposing signals into sum of "well-behaved" AM-FM components, that hold of natural "intrinsic" building blocks that describe the physical phenomena [64]. The main motivation of Huang et *al.* was to develop an approach allowing the estimation of meaningful IF for real world signal. The EMD decomposes any signal $s(t)$ into a series of Intrinsic Mode Functions (IMFs) through an iterative process called *sifting*.

II.2.1 Sifting process

The decomposition is based on the local time scale of signal $s(t)$, and yields adaptive basis functions. The EMD can be seen as a type of wavelet decomposition, whose sub bands are built up as needed, to separate the different components of $s(t)$. Each IMF replaces the signal detail at certain frequency band [49]. Each IMF has distinct time scales [64]. By definition[64], an IMF satisfies two conditions:

1. the number of extrema, and the number of zeros crossings must differ by no more than one;

2. the mean value of the envelope defined by the local maxima, and the envelope defined by the local minima, is zero

To be successfully decomposed into IMFs, the signal $s(t)$ (Step 3) must have at least two extrema: one minimum and one maximum. The decomposition is defined by an intuitive algorithm called the sifting process. It involves the following steps :

The sifting is repeated several times (i) until the component $h()$ satisfies the conditions (1) and (2). At the end of the sifting $s(t)$ is reconstructed as follows :

$$s(t) = \sum_{j=1}^{N} \mathrm{IMF}_j(t) + \mathrm{r}_N(t). \tag{II.3}$$

where N is the number of IMFs and $\mathrm{r}_N(t)$ is the residual. To guarantee IMF components retain enough physical sense of both amplitude and frequency modulation,

Step 1: Fix the threshold ϵ and set $j \leftarrow 1$ (j^{th} IMF)
Step 2: $\mathrm{r}_{j-1}(\mathrm{t}) \leftarrow x(t)$ (residual)
Step 3: Extract the j^{th} IMF :
(a) : $\mathrm{h}_{j,i-1}(\mathrm{t}) \leftarrow \mathrm{r}_{j-1}(\mathrm{t})$, $i \leftarrow 1$ (i number of sifts)
(b) : Extract local maxima/minima of $\mathrm{h}_{j,i-1}(\mathrm{t})$
(c) : Compute upper and lower envelopes
$\mathrm{U}_{j,i-1}(\mathrm{t})$ and $\mathrm{L}_{j,i-1}(\mathrm{t})$ by interpolating, using cubic spline, respectively local maxima and minima of $\mathrm{h}_{j,i-1}(\mathrm{t})$
(d) : Compute the mean of the envelopes:
$\mu_{j,i-1}(t) = (\mathrm{U}_{j,i-1}(\mathrm{t}) + \mathrm{L}_{j,i-1}(\mathrm{t}))/2$
(e) : Update : $\mathrm{h}_{j,i}(t) := h_{j,i-1}(t) - \mu_{j,i-1}(t)$, $i := i + 1$
(f) : Calculate the stopping criterion :

$$\mathrm{SD} = \sum_{t=1}^{T} \frac{|h_{j,i-1}(t) - h_{j,i}(t)|^2}{(h_{j,i-1}(t))^2}$$

(g) : Repeat steps (b)-(f) until SD$< \epsilon$ and then put
$\mathrm{IMF}_j(\mathrm{t}) \leftarrow \mathrm{h}_{j,i}(\mathrm{t})$ (j^{th} IMF)
Step 4: Update residual : $r_j(t) := r_{j-1}(t) - \mathrm{IMF}_j(t)$.
Step 5: Repeat Step 3 with $j := j + 1$ until the number of extrema in $r_j(t)$ is ≤ 2.

Table II.1: Sifting process

we have to determine Standard Deviation (SD) value for the sifting. This is accomplished by limiting the size of the SD, computed from the two consecutive sifting results. Usually, ϵ is set between 0.2 to 0.3 [64]. The sifting has two effects: (a) it eliminates riding waves and (b) smooths uneven amplitudes [64]. Locally, each IMF contains lower frequency oscillations than the just extracted one. The EMD does not use pre-determined filter, or wavelet function, and is a fully data driven method.

II.2.2 Illustrative example

We illustrate in first example how EMD separates two pure tones and we discuss some issues of the sifting process. The signal in question is two free superimposed tones defined as follows:

$$s(t) = \cos(2\pi.1t) + \cos(2\pi.5t) \tag{II.4}$$

In figure (II.1) components of 1Hz and 5Hz are extracted at the first iteration of the sifting process. For this example, the two components satisfy perfectly the IMF condition (section. II.2.1). At iteration 0(i=1), the 5Hz and 1Hz components could be identified directly in the first IMF and the residue, respectively (Fig.

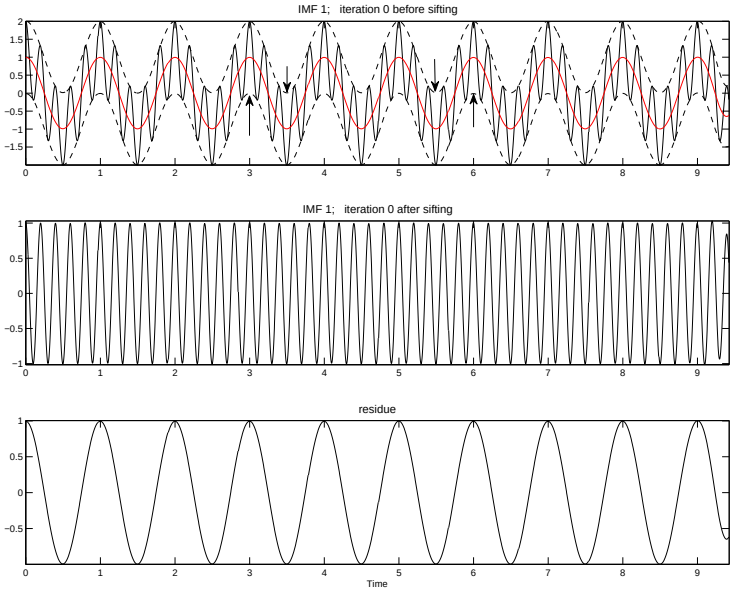

Figure II.1: Initialization of the sifting process for $s(t)$, envelope mean detection (red line) and the first sift of IMF1. Over- and undershoots are indicated by arrows.

(II.1)). But, in practice the algorithm continues the process and generate additive components (see the final results in figure (II.6)). The over decomposition in the sifting is due principally to the approximation errors caused by the interpolation accomplished in step 3 in the sifting process. Cubic splines are known to exhibit over- and undershoot problems [109] (see figure II.1). A solution to overcome this issue and others difficulties are given by the authors [15] and discussed in section (II.4).

After several iterations, the algorithm is not able to extract a third IMF. The sifting can not converge to the final solution directly, because after extraction of the second IMF, the residue remains an oscillatory signal. So, the algorithm continues the decomposition of the signal $s(t)$, probably after subtraction of the residue from $s(t)$ the result is in turn an IMF.

While the stopping criteria is not fulfilled, the process may not converge as quickly as it should. In practice, after a number of iterations, the process is forced to stop. This over- decomposition is due to ghosts extremum generated by the interpolation, in [34],[109] a complete study of this problem can be found.

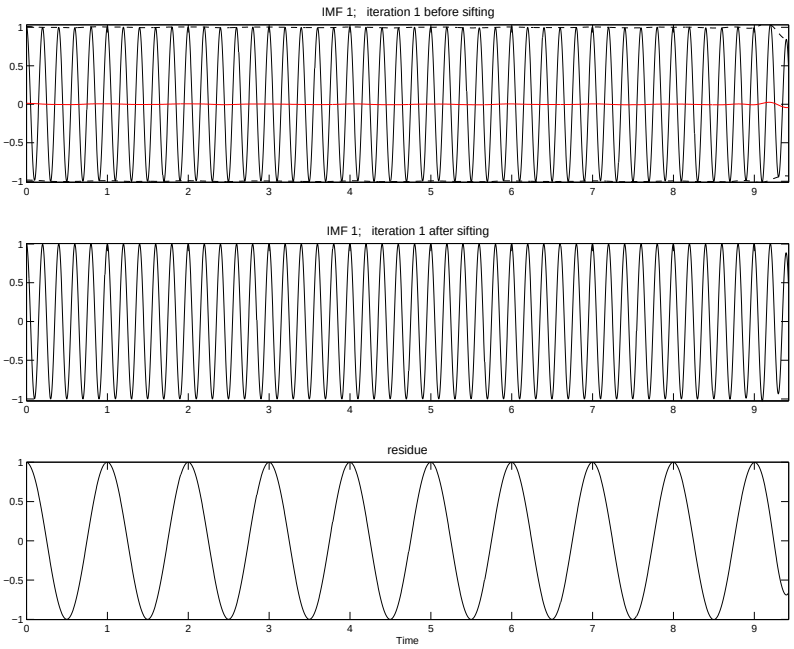

Figure II.2: Extraction of the 5 Hz component from $s(t)$ at first iteration. The local mean envelope is null (red line) and the component contain an acceptable number of extremas.

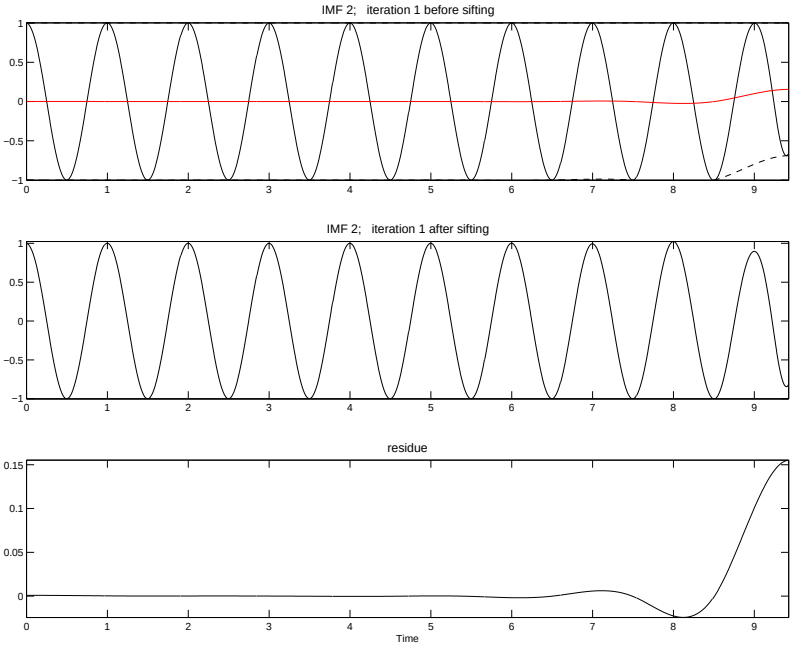

Figure II.3: Extraction of the second candidate IMF from $s(t)$. Envelope mean detection (red line).

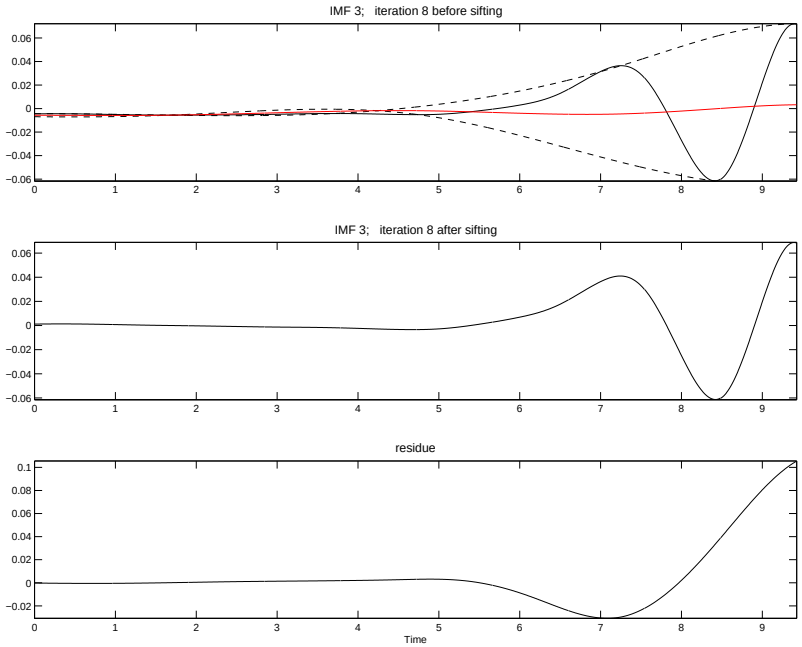

Figure II.4: Extraction of the third candidate IMF from $s(t)$. Envelope mean detection (red line).

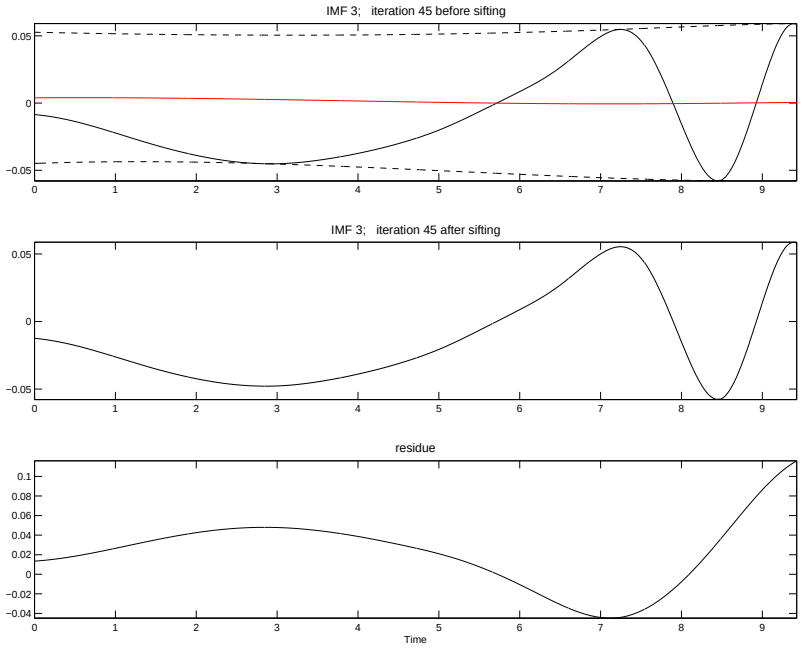

Figure II.5: Extraction of the third candidate IMF from $s(t)$. Envelope mean detection (red line).

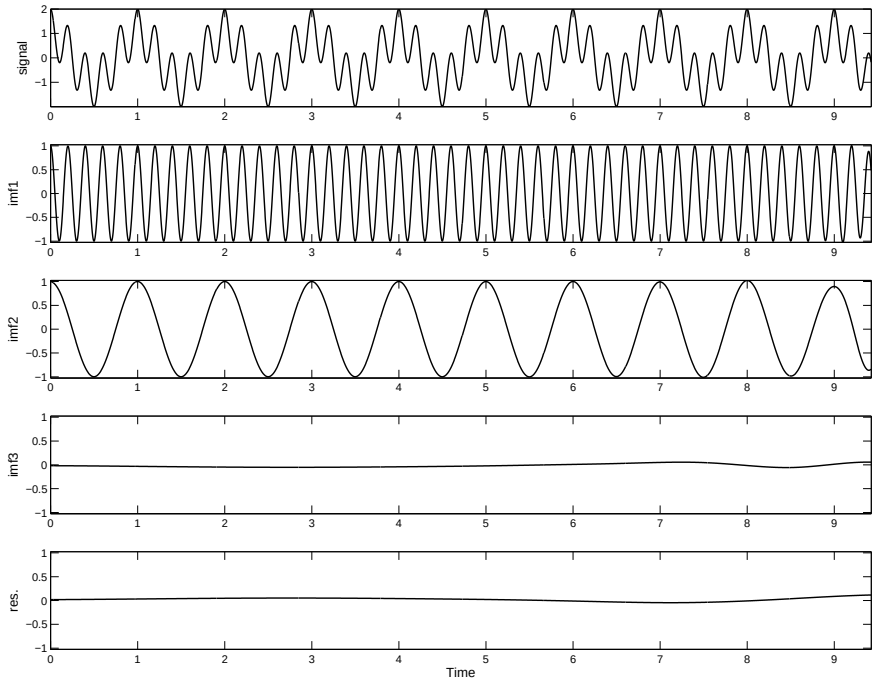

Figure II.6: IMFs extracted from signal given in (cf, Eq. II.2.2). The two components of frequencies 5 Hz and 1 Hz correspond to IMF1 et IMF2, respectively.

II.3 Some aspects of the EMD

II.3.1 IMF criteria

The first point is the IMF criteria. To guarantee the IMF; specifically, their IF must have a meaningful interpretation, the SD value has been limited or fixed by Huang et *al.* [64] (Step (f)). The SD has been changed by Rilling et al [96] to 3-threshold criterion θ_1, θ_2 and α by: $a(t) = (U(t) - L(t)/2)$ and $\sigma(t) = |a(t)/\mu(t)|$. The sifting process is iterated until $\sigma(t) < \theta_1$ for a period of $(1 - \alpha)$ of the total time, and $\sigma(t) < \theta_2$ for the remaining fraction of time. The typical values of the thresholds are $\theta_1 = 0.05$, $\theta_2 = 0.5$, and $\alpha = 0.05$. The problem of these thresholds is that they can not be automatically adapted to each analyzed signal. Except the criteria used in the conventional EMD, to best of our knowledge until now there is no criteria in the literature to efficiently retrieve meaningful IMFs. So, what stopping criteria should one choose? For us the best one should allow to extract a meaningful IMF.

II.3.2 Number of sifts

The second point is the number of sifts. This number is directly conditioned by the above criteria, where physical meaningful amplitude variation may be sifted away.

Indirectly, until the IMF conditions (1) and (2) are not satisfied, this number is seen in grow. There is a tradeoff between the number of sifts and the over-sifting, which tends to produce smooth amplitude IMFs (see third IMF in Fig. II.6). In fact, the stopping criteria defined before ($SD < 0.3$): minimizing the difference between residuals in successive sifts to below a predetermined level, does not explicitly take into account the two IMF conditions. The chosen level (0.3) could be reached without the IMF conditions being satisfied [62]. Since that, Huang and Shen have proposed in [62] a new stopping rule, where the sifting is stopped when the number of extrema and the number of zero crossing differ by one. They found that IMFs produced under this rule (satisfying the first IMF condition) were not oversifted and also consistently orthogonal. Then, can we say : the least the number of sifts the best is the decomposition?

II.3.3 Number of IMFs

The third point is the number of IMFs. The aim of EMD, as explained by Huang, is to decompose any nonstationary/stationary and nonlinear/linear dataset to a finite and often small number of IMFs that admit well-behaved HT [64],[62],[63]. It means, that large number of IMFs in the decomposition could not bring useful information and could add a confusion in the analysis of the data. This problem is not specific to the EMD; it is frequent in modeling time series even when they are stationary; if the data are nonstationary and in case of nonlinearity, this problem is inflamed.

II.3.4 Sampling and mode mixing issues

Another serious problem is when mode mixing occurs. By definition this problem can be viewed as scales confusion, where an IMF move from its natural scales, where it can represent a physical source, to another insignificant scale. Even though the final TF projection could compensate the mixed mode to some degree, the alias at each transition from one scale to another would irrecoverably damage the clean separation of scales. Such a drawback was first illustrated in [62] in which the modeled data was a mixture of intermittent high frequency oscillations riding on a continuous low frequency sinusoidal signal. This point was also investigated by Rilling [95]; the aim of this study was to understand the behavior of the EMD; very interesting points were discussed. Especially, Rilling investigated two situations, the sums of two sine waves and white Gaussian noise. Since, the first situation has helped address the issue of the sampling influence on EMD. And in the second points (Appendix. A), authors verified that EMD act as a dyadic filter [116],[49].

To avoid the mode mixing, Stevenson et *al.* [105] discussed and proposed a sampling limit for the EMD. For an acceptable decomposition the frequency sampling (F_s) must be at least eight times the maximum frequency(F_{max}) or four times the Nyquist-Shannon frequency ; i.e, $F_s > 8F_{max}$.

II.3.5 Orthogonality

The last point concerns the orthogonality of IMFs. The orthogonality has been largely discussed by the EMD community [64, 62], [96, 89]. Undoubtedly Huang et *al.*, discussed this point, because he wanted to use this criterion (The index of orthogonality) to reject the IMFs sets that are grossly non-orthogonal. Then, one can check at any moment the ability of the IMFs set to form an orthogonal basis. Thus, we think that Huang et *al.* introduced the orthogonality index just for comparing the EMD to existing approaches. But, from a physical point of view, must the components of natural processes be orthogonal? And if is not the case, how can they be separated and analyzed via a set of orthogonal basis like exponential or wavelets functions? Thus, the EMD came to overcome a this shortcoming usually escaped in the classical approaches (Fourier series, wavelets,...). The index of orthogonality used in EMD algorithm, for any two components, $C_i(t)$ and $C_j(t)$, can be defined as,

$$IO_{ij}(t) = \sum_t \frac{C_i(t)C_j(t)}{C_i(t)^2 + C_j(t)^2} \tag{II.5}$$

II.3.6 Bivariate EMD

The EMD being initially limited to real-valued time series is extended to bivariate (or complex-valued) time series by Rilling et al [97]. The IMF in EMD is known to be a zero-mean oscillating components; in the bivariate extension, the proposed algorithm is designed to extract zero-mean rotating components [97]. The authors illustrate the approach on a real-world signal for validation, and they discuss properties of the output components.

II.3.7 Ensemble EMD

To alleviate the mode mixing problem occurring in EMD, ensemble EMD (EEMD) was introduced by Hu and Huang [117]. EEMD decomposes by the same process (sifting) an ensemble of signal with additive white Gaussian noise. Then, the noise is averaged out with sufficient number of trials; thus, the only persistent part survives

the averaging process is the signal. As showed in [117], on synthetic example and real world data, EEMD can separate signals of different scales and reduce the mode mixing.

II.3.8 A PDE for sifting process

For a lack of a solid theoretical framework of the EMD, people are suspicious. In order to overcome this issue, a preliminary work had initiated by Sharpley [101] to characterize weak-IMF (IMFs that satisfy only the first condition) as solutions of self-adjoint second-order differential equation. Then, Delechelle [35] proposed to replace the mean envelope detection by a resolution of parabolic partial differential equation (PDE).

Recently, an attempt by Diop et *al.* [39] to provide some theoretical contributions on the comprehension of the sifting process. The authors proposed to perform the sifting process by the resolution of PDEs, and analytical characterizations of modes were then proposed. A suitable way for getting rid of interpolation's issues is also provided. However, as they are cited in the letter the big drawback of the PDEs based approach is δ (cf. Eq. II.6), the parameter of the proposed PDE, which is actually chosen empirically. Furthermore, the PDE approach is very sensitive to noise. More explanations and mathematical developments ca be found in [101],[35],[39]. The study is in the preliminary stage. The studied cases are all noise free signals. The sifting process is fully determined by the sequence defined by [39],

$$\begin{cases} \dfrac{\partial h}{\partial t} + \dfrac{1}{\delta^2} h + \dfrac{1}{2} \dfrac{\partial^2 h}{\partial x^2} = 0 \\ h(x,0) = h_0(x) \end{cases} \tag{II.6}$$

where $h_0(x)$ is the signal to decompose, x is the abscissa. Once the first IMF is extracted by resolving equation (II.6), $h_0(x)$ is set to the residual between the signal and the first IMF and we resolve again equation (II.6) to compute the second IMF; and so on for other IMFs.

II.4 Smooth B-spline interpolation of IMF

In this section, we present some developments and our contribution to improve the decomposition results of the conventional EMD. A smooth version of the EMD is introduced and the new sifting process illustrated on a tone embedded in

additive white Gaussian noise. The obtained results are compared to those of the conventional EMD and the EEMD.

Splines interpolation play an important role in the sifting process, as all extracted IMFs of decomposed signal are linear combinations of splines. As one can see in the EMD diagram (Fig. II.7), the interpolation is integrated at the beginning of the sifting process. As the sifting is iterative, any approximation error will propagate to the present loop (see Tab.II.1,i), and also, to the whole process. This is why we are suggesting to handle interpolation step carefully and we propose a new approach based on B-splines interpolation. We propose also, using smoothing spline interpolation instead of exact approximation.

II.4.1 Polynomial spline signal

In digital signal processing applications, the signals to be manipulated are represented by a set of uniformly spaced sampled values $s(k)$, where k is a vector of integer indexes. Although most processing algorithms are purely discrete, there is a variety of problems that are best formulated by considering a function $s(t)$ of continuous variable t; the most known processing being signal differentiation. So, it is very interesting to use a simple procedure for mapping discrete signal into continuous ones and vice versa; classical polynomial spline interpolation offering this possibility [34]. However, the use of B-splines function [109],[110], which are piece-wise polynomials as well, have a number of advantages. Firstly, higher order polynomials tend to oscillate while spline functions are usually smooth and well behaved. Secondly, the juxtaposition of local polynomial approximations may produce strong discontinuities in the connecting points. B-spline curves, by contrast, are continuous everywhere. The polynomial segments are patched together (Fig. II.8) so that the interpolating function and all derivatives up to order $n-1$ are continuous [109].

The signal $s(t)$ in our case is the extracted IMF. In terms of a B-spline expansion the IMF can be rewritten as follows [14],[109]:

$$\mathrm{IMF}_j^n(t) = \sum_{k\in\mathbb{Z}} c_j\,[k]\,\beta_k^n(t-k) \tag{II.7}$$

where $\beta_k^n(t)$ and $c_j\,[k]$ are the Schoenberg's central B-spline of order n [99] and the B-spline coefficients of the jth mode, respectively. The interpolation coefficients $c_j\,[k]$ can be obtained by inverse filtering [109] or by the classical approaches using matrix algorithms[34].

The basis functions $\beta_k^n(t)$ can be generated iteratively by repeating convolution

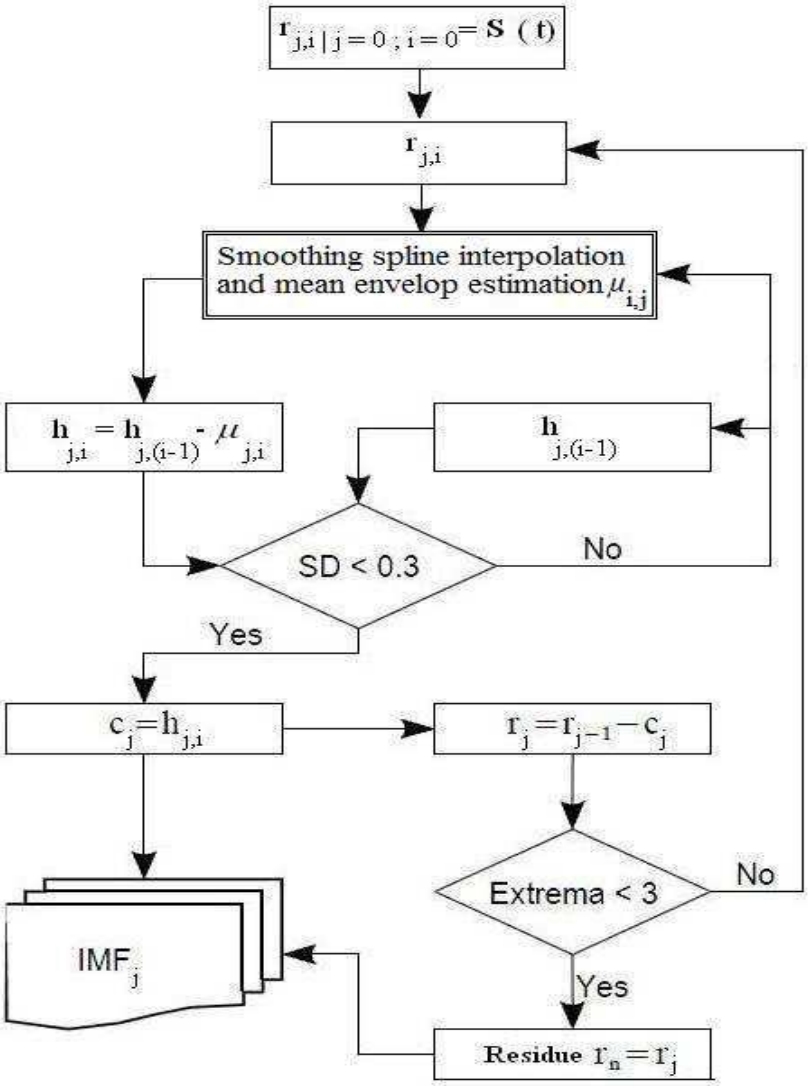

Figure II.7: EMD-RBS diagram. The modified EMD is distinguished from the coventional EMD on integrating the smooth B-splines, or Regularized B-splines (RBS) interpolation instead of the cubic splines interpolation. Also as in [15] we use the acronym EMD-RBS to refer to the modified EMD.

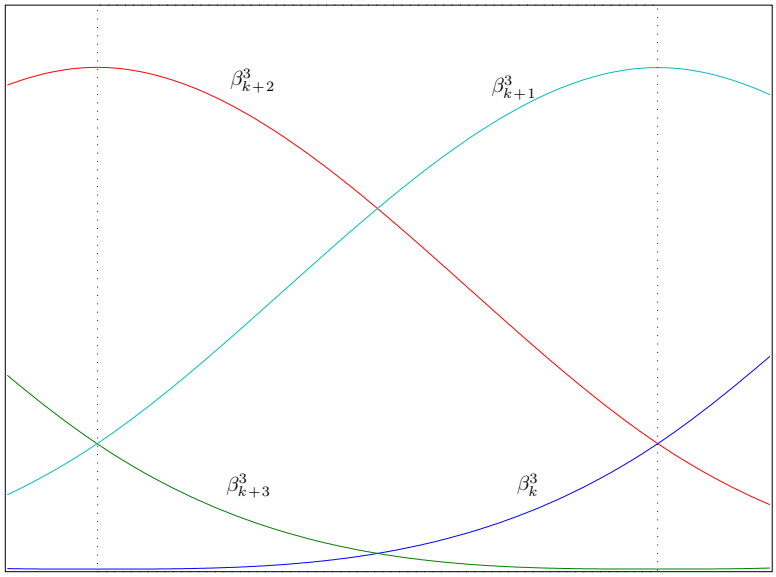

Figure II.8: Cubic B-splines functions in the segment $[t_k, t_{k+1}]$.

of a B-spline of order 0:

$$\beta^n_k(t) = \beta^0_k(t) * \beta^{n-1}_k(t) \tag{II.8}$$

where $\beta^0_k(t)$, $\forall k \in \mathbb{N}$, is the indicator function in the interval $[-\frac{1}{2}, \frac{1}{2})$

$$\beta^0_k(t) = \begin{cases} 1 & t \in [-\frac{1}{2}, \frac{1}{2}) \\ 0 & \text{otherwise} \end{cases}$$

An interesting property of B-splines functions is their compact support (Eq. II.8); this is very important, because it limits the propagation of approximation errors from a box to another. But, in each box, the splines fit all the points without distinguishing between the data and the noise [15]. To improve the performance of the EMD in very noisy environment, smoothed splines are used. This is done by relaxing the interpolation constraint and finding a function (solution) of order $n = 2r - 1$ that minimize E (Eq. (II.9)).

$$E = \sum_{l=-\infty}^{\infty} (\text{IMF}^n_j(n) - h^n_j(l))^2 + \lambda \int \left(\frac{\partial^r h^n_j(t)}{\partial t^r} \right)^2 dt \tag{II.9}$$

Equation (II.9) is a well-posed regularized least-squares problem where the first term measures the error between the model $h^n_j(l)$ and the measured data $\text{IMF}^n_j(n)$. The second term imposes a smoothness constraint on the solution $h^n_j(l)$. The regularization factor λ measures how smooth the interpolating function will be and how close

to the data samples the interpolant will pass [90]. For $\lambda = 0$ there is no smoothing, and the interpolation curve fits exactly the signal samples. if $\lambda \neq 0$, the deviation from the data samples increases with the value of λ.

II.4.2 Noise reduction

In the next chapter, the performance of the proposed sifting method is investigated for demodulating a noisy multicomponent AM-FM signal of varying Signal to Noise Ratio (SNR). Here, we illustrate the effect of regularized B-splines interpolation on the extracted IMFs in noisy environment. Especially, the signal $s(t)$ is corrupted with additive white Gaussian noise $n(t)$ with SNR=0dB:

$$s(t) = \sin(10\pi t) + n(t) \tag{II.10}$$

The signal $s(t)$ is shown in the first row on the top of figures (II.9),(II.10) and (II.11). The conventional EMD extracts ten IMFs (Fig. II.9) while the EEMD generates eleven IMFs (Fig. II.10). The EMD-RBS extracts only six IMFs (Fig.II.11). The last row of each figure corresponds to the final residue.

In the decomposition performed by the conventional EMD and the EEMD, both noise components and sinusoidal component are split into different IMFs. Thus, even the original signal (sinusoid) is a true IMF, from the classical EMD and EEMD, we are not able to recover or to identify this sinusoid. For both decomposition this IMF may be obtained using partial reconstruction by summing some selected IMFs (Figs. II.9 and II.10). To recover the sinusoidal component, which can not be extracted directly from the resulting IMFs of the decomposition, one could add IMF3 to IMF6. In practice, the number of the selected IMFs is noise-dependent.

For the resulted IMFs of EMD-RBS (Fig. II.11), the original signal can be identified to second IMF. The first components and the remainder IMFs are a part of noise. The energy of $s(t)$ is mainly concentrated in the first IMF, the amplitudes of the other IMFs are small. These results show the interest of the regularized interpolation of the envelopes, compared to exact interpolation to recover the original components from $s(t)$ and to reduce the number of unwanted IMFs.

The optimal parameter λ remains in general an unsolved problem because the noise type and magnitude are unknowns. The smoothing parameter determines the relative weight we would like to place on the contradictory demands of having $h(t)$ smooth or having $h(t)$ close to the data, (Eq. II.9). For $\lambda = 0$, is the variational, or natural cubic spline. When λ moves from 0 to 1, the smoothing spline changes. The

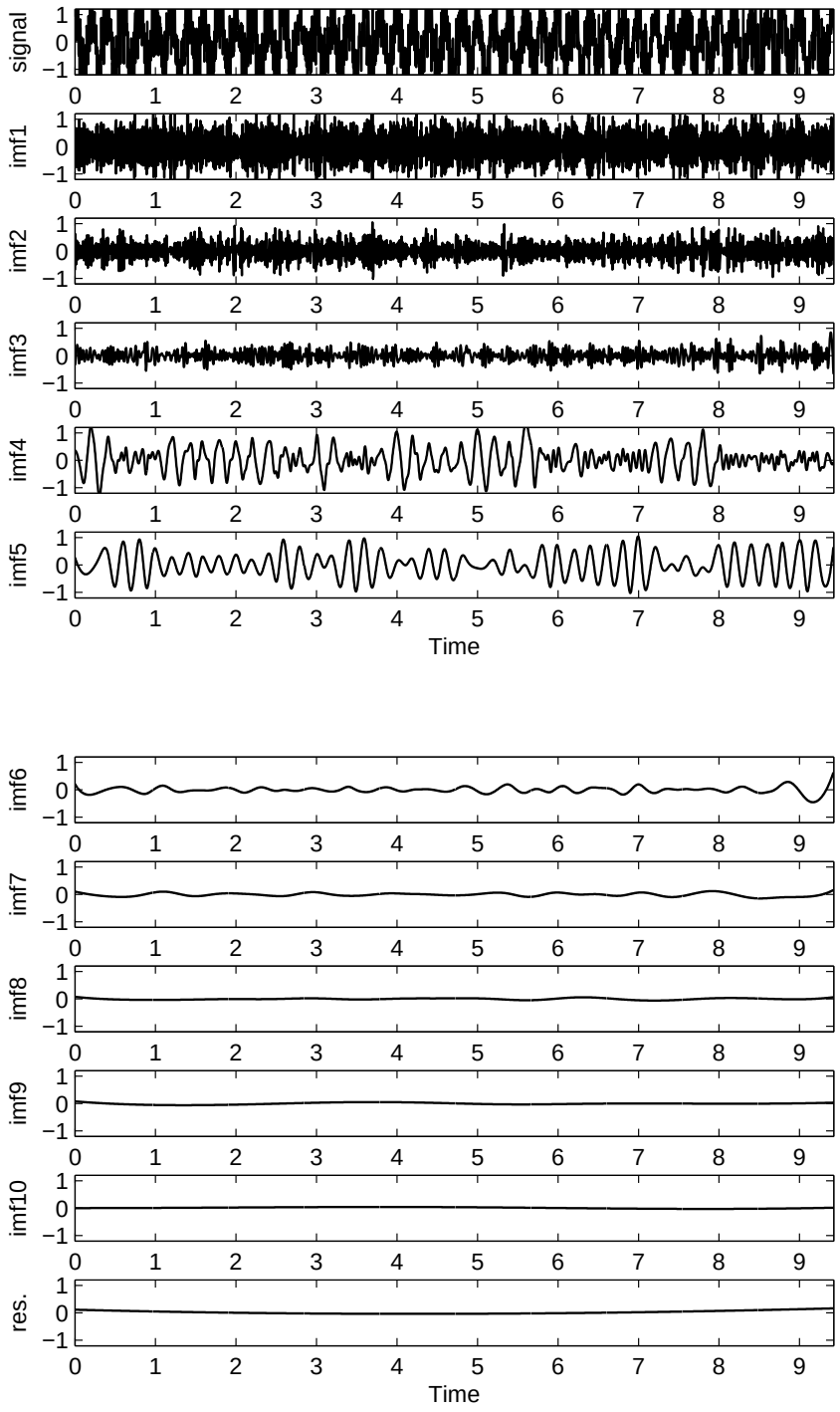

Figure II.9: Extracted IMFs by EMD from noisy signal $s(t)$ (SNR=0dB). The conventional EMD failed to extract directly the 5Hz sinusoid. For getting a smooth version of the sinusoidal signal one must add the IMF 5, the IMF 6 and part of the IMFs 4 and 7.

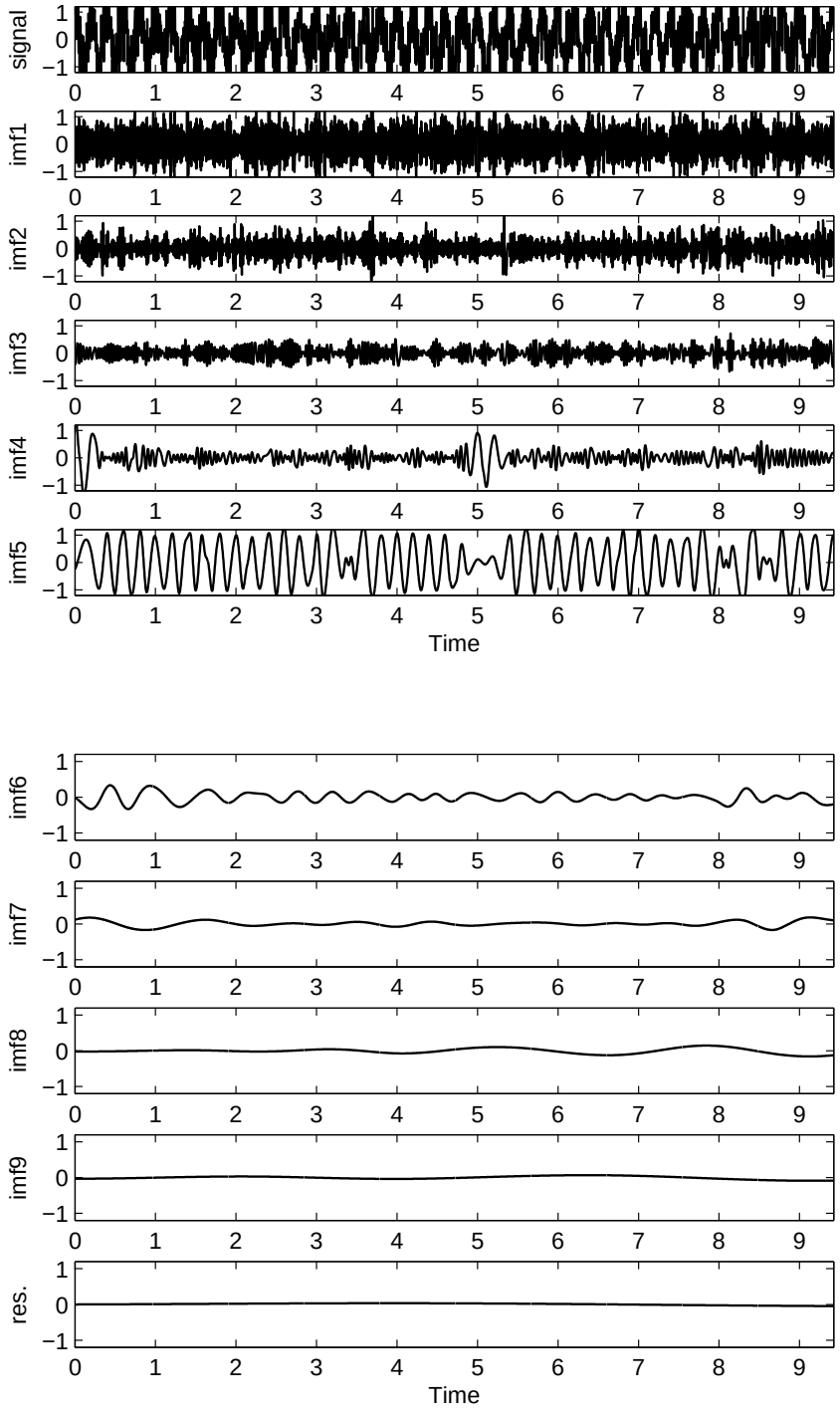

Figure II.10: Extracted IMFs by EEMD from noisy signal $s(t)$ (SNR=0dB). The sum of IMF 4, 5 and 6 give a noisy version of the sinusoidal signal but not the original one.

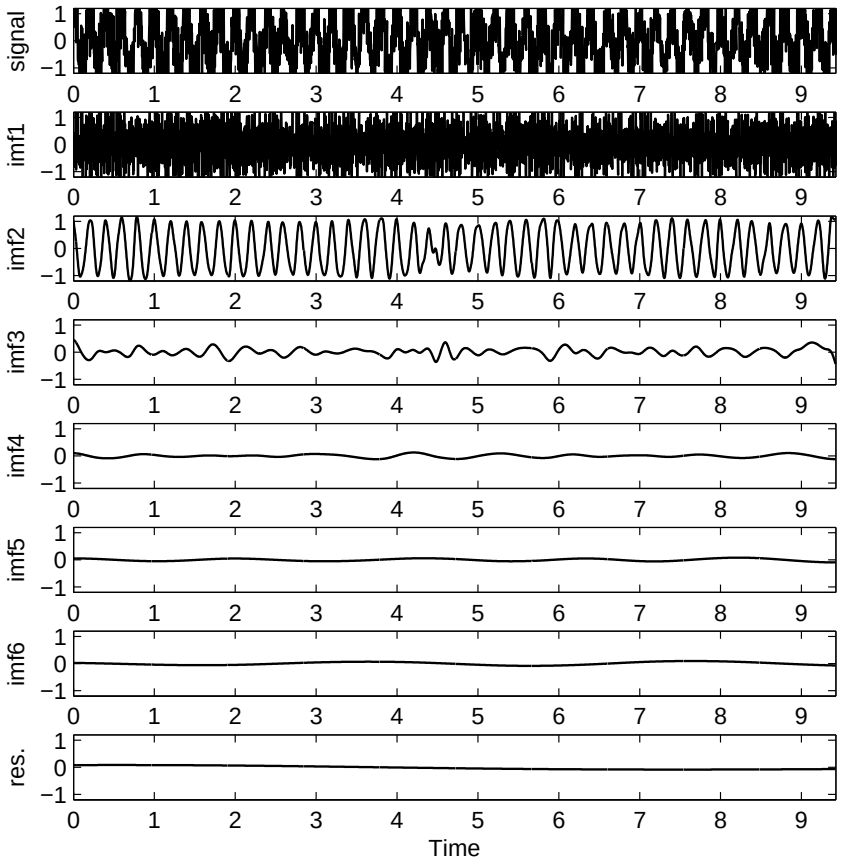

Figure II.11: Extracted IMFs by EMD-RBS of the noisy signal $s(t)$ (SNR=0 dB). The 5Hz tone is extracted successfully, it corresponds to IMF number 2.

choice of λ is not completely arbitrary. We have attempted to find experimentally a good value for λ for different input SNRs. Figure (II.12) plots the Mean Square Error (MSE) against λ and the input SNRs. The MSE is calculated between the extracted IMF (IMF2) and the true signal (sinusoid). In these experiments the corresponding MSE curves had minima for particular values of λ. More particularly, the minima occurred around λ equal to 0.01 independently of the input SNR's values (ranging from -10dB to 30dB). The principal result : the smoothing spline interpolation improves the decomposition, and extracts directly and efficiently pure frequency components, the 5Hz component here. Thus, one avoid partial reconstruction from the resulting IMFs.

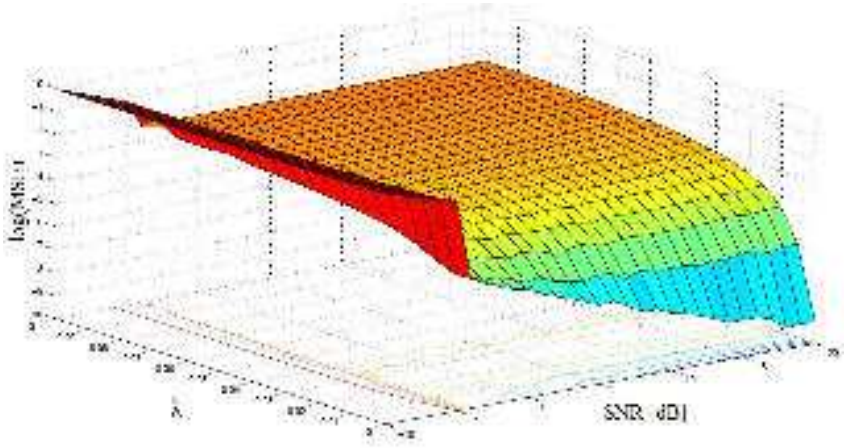

Figure II.12: variation of the parameter λ

II.4.3 Forced oscillatory motion

The new sifting is tested on real world signal from an hydrodynamic system. In forced oscillatory motion, one looks at the first step to separate the component of mechanical forcing (periodical oscillatory component with a known frequency) from the signal. The residual signal would have rich physical content. Figure (II.13) shows a measured signal of forced oscillatory motion [94]. With conventional bandpass filtering methods, one can separate the periodical oscillatory component. However, the bandpass filtering supposes that filters parameters (central frequency of each filter, bandwidth,...) are known. Since the conventional EMD failed to extract (directly identify) the oscillatory component, another solution based on EMD has been introduced by Benramdane [94]. He proposed to extract this component by partial reconstruction of a number of IMFs empirically identified. Using the EMD-RBS the decomposition is obtained with a reduced number of IMFs (II.15). The number of IMFs generated by the conventional EMD (Fig. II.14) is larger than that of the EMD-RBS (II.15). Furthermore, the oscillatory component is identified in the last IMF, (Fig. II.15). To extract the same component from the extracted IMFs by the conventional EMD, we sum IMF12 and IMF13.

II.5 Summary

In this chapter an insight on the EMD and some important works around it are given. Most developed works are an alternative for more comprehension of the EMD, then a real solution to some serious problems of interpretation of some resulting IMFs of real world data. Then we propose a new sifting process,

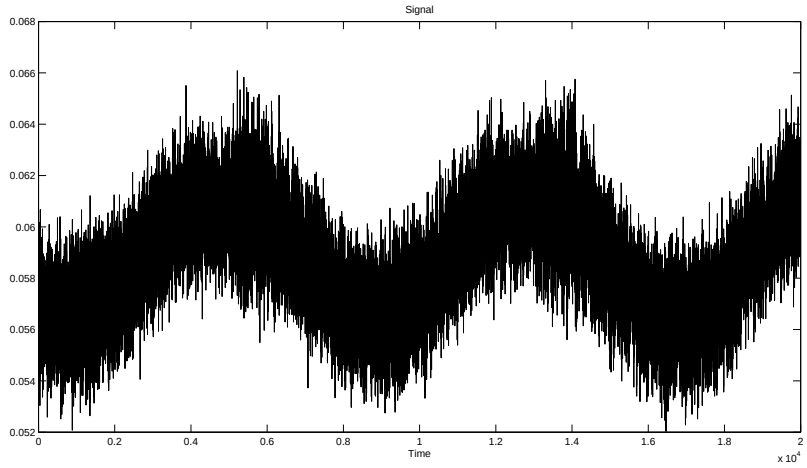

Figure II.13: Signal generated by an hydrodynamical system.

called the EMD-RBS, to improve the results of classical EMD. In case of a single component embedded in noise, EMD-BSR with $\lambda = 0.01$, separates properly the component. In addition, the EMD-RBS performs better than the conventional EMD and the EEMD for separating the forced oscillatory component. In the EMD diagram (Fig. II.7) the interpolation is integrated at the beginning of the sifting process. Since the sifting is an iterative process, any approximation error is propagated in the present loop (i) and also to the whole process. To resolve this problem, instead of exact splines a smoothing spline interpolation is used. A direct consequence on the EMD, is the reduction of the number of insignificant IMFs. The smoothing spline has softly filtered the original signal. In each sifting loop, the spline function pass through the filtering points. However, decomposition of the same signal by conventional EMD, where interpolations are performed by the cubic spline without regularization generates too much insignificant IMFs (Fig. II.10). In the next chapter, the EMD-RBS is tested on a multicomponent AM-FM signal and its performances compared to classical methods.

The contribution on this chapter is the following:

- Introduction of a new sifting process where smoothing interpolation instead of exact interpolation, to construct the upper and lower envelopes of the signal to be decomposed. The main advantages of this new sifting are to give the EMD more robustness against noise and to reduce the number of unwanted or insignificant IMFs of the conventional EMD (over-decomposition).

Based on a very important study done by Unser [109],[110] and Huang et *al.* [64], we chose the cubic B-spline model. This type of interpolation or representation is

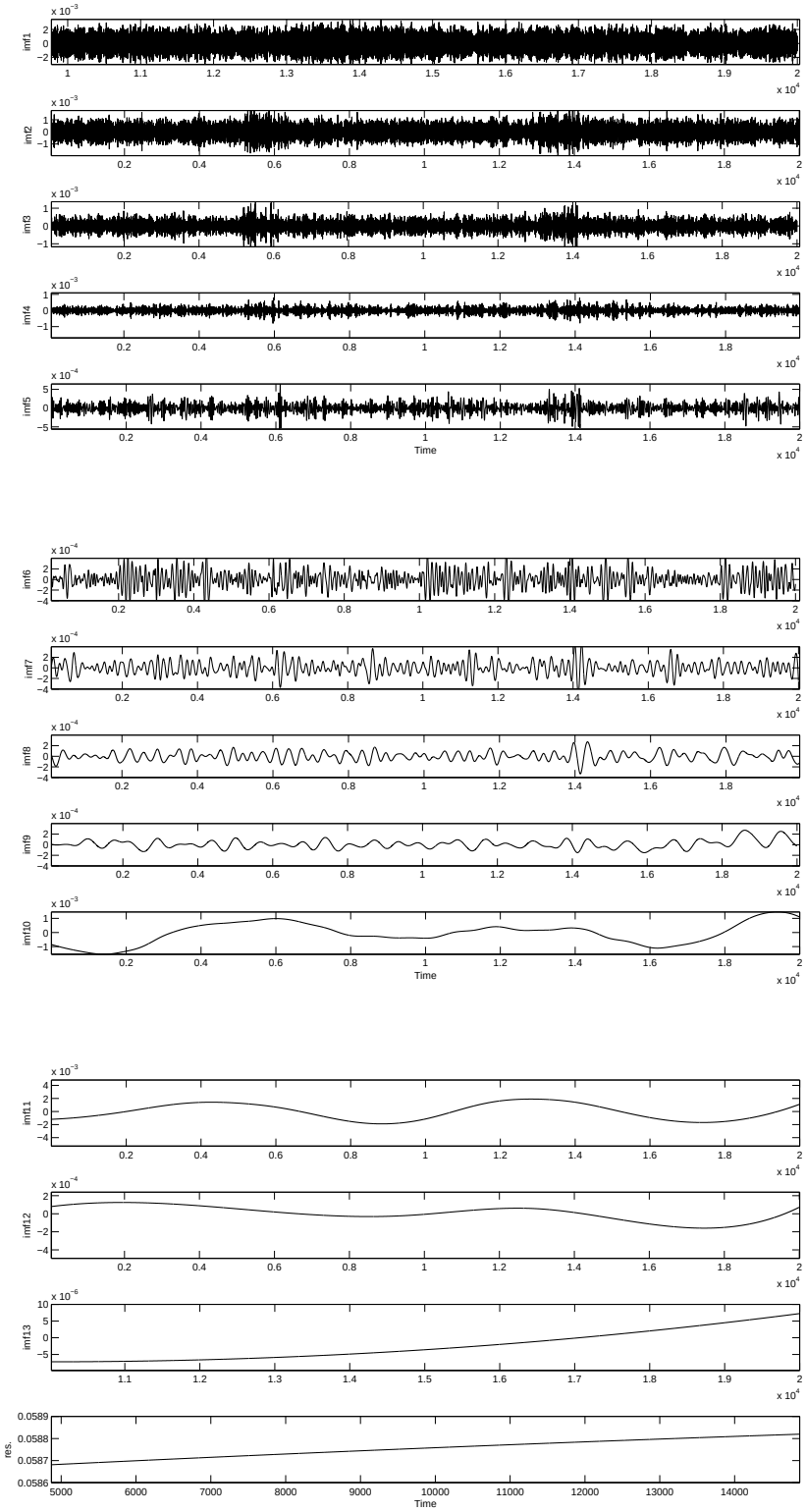

Figure II.14: Extracted IMFs by conventional EMD from hydrodynamical measured signal. In top square IMF1 to IMF5. The square of middle, IMF6 to IMF10 and last one contain remainder IMFs and the residue.

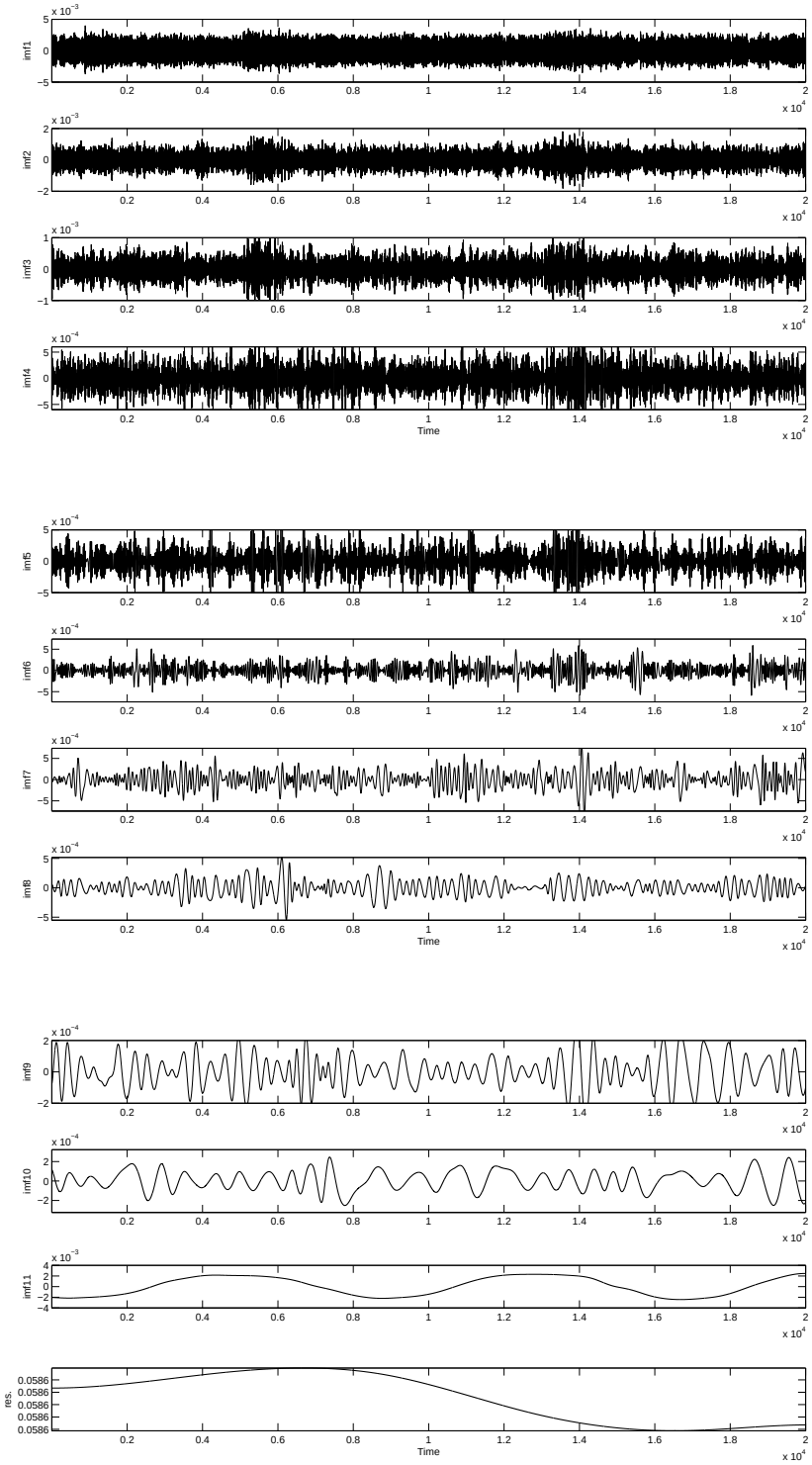

Figure II.15: Extracted IMFs by EMD-RBS from hydrodynamical measured signal. In top square, IMF1 to IMF4. The square of middle, IMF5 to IMF8 and last one contain remainder IMFs and the residue. The number of IMFs in the present figure is less than the previous figure.

useful in a variety of problems that are best formulated in continuous rather than a discrete framework. Particularly, the search for extrema, differentiation, or the integration are simple to perform in the transformed B-spline domain.

CHAPTER III

Instantaneous frequencies and amplitudes tracking

Contents

III.1 Introduction 63

III.2 Multicomponent AM-FM Signal Model 63

III.3 ESA or HT ? 65

III.4 HT demodulation 66

III.5 TKEO 67

III.5.1 Discrete energy demodulation 68

III.5.2 Continue energy demodulation 70

III.6 Results and Discussion 75

III.7 Summary 83

Demodulation approach of multicomponent AM-FM is proposed in this chapter. This method combines the EMD and the ESA, designated as EMD-ESA for short. A multicomponent AM-FM is first decomposed by EMD into a set of IMFs, then the IF and IA of each IMF is tracked using the ESA. We introduce different variants of the discrete version of the EMD-DESA. To improve the tracking results, a continuous version of the approach is proposed. The investigation is completed by a comparative study between the proposed methods and the EMD-HT approach.

III.1 Introduction

Estimating time-varying amplitude and frequency functions of a multicomponent AM-FM signal is an area of active interest in signal processing domain. The aim is to understand and describe situations where the frequency content of a signal varies in time (non-stationary signal). Important features of non-stationary signal are provided by IF and IA [12]. In areas such as in seismic, Radar or Sonar, signals under consideration are known to be non-stationary. Thus, estimations of IF and IA remains the best way for understanding hidden physical phenomena which generating measured data. More particularly, IF determines what frequencies are present and how they change over time and the IA inform us how strong is the IF. But, only meaningful IFs could really help one to explain the production, variation and evolution of physical phenomena [12]-[65]. The interpretation of IF function may be physically appropriate only for monocomponent signals where there is only one spectral component and in narrow band of frequencies [12]-[32],[65]. Additionally, to reveal true physical meaning of the IF, its estimation must be robust against noise.

Both the HT and the ESA, based on Teager-Kaiser Energy Operator (TKEO) [83], are accepted demodulation methods provided that the analyzed signals are monocomponents or narrow-bands. For multicomponents signals these demodulations can not be applied. To extend these demodulation methods to wide-band signals, a sub-band filtering is required. A solution to this problem is the EMD which is a data driven sub-band filtering method [64]. We show in this chapter how the EMD combined with the ESA can track both IA and IF features of signal in both noise free and noisy environments.

III.2 Multicomponent AM-FM Signal Model

Monocomponent AM-FM signals are defined by

$$s(t) \triangleq a(t)cos(\int_0^t 2\pi f(\tau)d\tau) \tag{III.1}$$

$$s(t) \triangleq a(t)cos(\phi(t))$$

this definition contain both AM function, $a(t)$ and FM function, $f(t)$. These signals are largely used because that can efficiently modeled system as: (1) transmission of information over communication channels; (2) target information in SONAR and RADAR systems; (3) speech resonances. They are also often present in signals

created and processed by some biological sources. The signal processing task that is of interest is the extraction of the information bearing IF signal $f(t)$ and IA signal $a(t)$ from the modulated signal $s(t)$. Discrete time monocomponent AM-FM signals are defined have the following form

$$s[n] = a[n]cos(\phi[n]) = a[n]cos(\int_0^n 2\pi f[k]dk), \quad f[n] = \frac{d\phi}{dn}[n] \tag{III.2}$$

where, $\phi[n]$ is the instantaneous phase signal.
The superpositions of these discrete time monocomponent AM-FM signals give time multicomponent AM-FM signals [46].

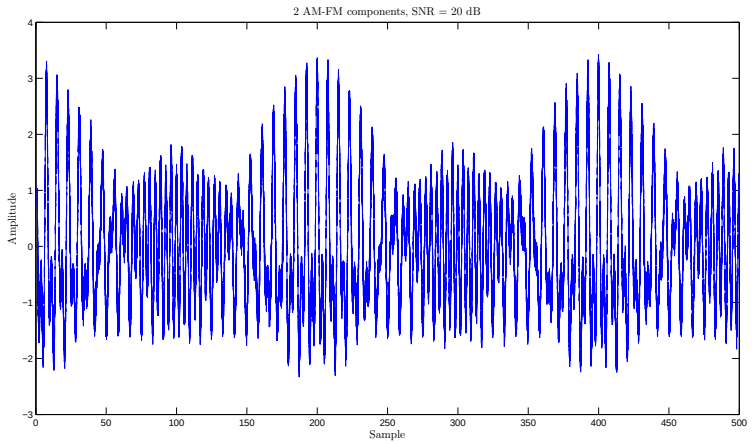

Figure III.1: Two AM-FM components ($M = 2$)

$$s[n] \triangleq \sum_{i=1}^{M} \underbrace{a_i[n]cos(\int_0^n 2\pi f_i[k]dk)}_{s_i[n]}, M \geq 2 \tag{III.3}$$

where $a_i[n]$,$f_i[n]$ are the IF[1] and IA information signals corresponding to the ith component $s_i[n]$.

Parametric modeling estimation is proposed by Jabloun et *al.* [69],[68]. The IA and IF are both approximated by low-order polynomials. The model parameters are estimated via stochastic optimization techniques based on the simulated annealing method. The approach is firstly applied on signals having short-time duration and

[1]It is assumed that signal $\phi[n]$ is a known mathematical function, that can be differentiated or integrated yielding known computable functions. But, as shown in [84] any finite length discrete time signal $\phi[n]$ can be expressed as a linear combination of cosines via the DFT. So, the above restrictive assumption can be removed

nonlinear AM/FM. Then, in [68] an extension of the method for the estimation of highly nonlinear AM/FM signals of long-time duration is proposed. Benidir in [8], the signal is modeled as a higher-order polynomial phase signal. First, an exact decomposition of the derivatives of any polynomial $\phi(t)$ based on shifted versions of this polynomial,i.e., $\phi(t-t_0)$,...,$\phi(t-t_n)$ is proposed in [50, 9, 10]. This decomposition is then applied to construct time-frequency distributions that generalize the classical WVD and Ambiguity Function (AF) [8].

Other techniques do not assume polynomial modeling, where the IF and IA tracking is performed via a combination of the EMD and the HT [64] or the TKEO [19]. Even, the last approach share the assumption of the AM-FM signal model with the parametric modeling approaches, we do not make an other assumption on the models of IAs and IFs.

III.3 ESA or HT ?

Spectral estimation is the second step of the EMD. This consists in computing the IF and IA functions for each IMF by using a demodulation method. An accepted way is to use the Analytic Signal (AS) through the HT. This has made the AS method the most popular method to define both IA and IF functions. A crucial necessary condition for the AS method to give a physical meaningful IF is that the signal will have to be symmetric with respect to the zero mean [64]-[65]. The HT uses the whole signal (theoretically from $-\infty$ to $+\infty$). As we have a finite segment of signal the window effect will distort its spectrum. Furthermore, it is not easy to accept the use of a global operator as basis of a local estimation. An alternative way to estimate IA and IF functions is the ESA [84]. Based on the TKEO, the ESA computes these functions without involving integral transforms as in HT or FT; it is totally based on differentiation. A distinct advantage of the TKEO is its good localization. This property is the consequence of the differentiation based method. Thus, it is natural to use local operator as basis for a local estimation such as IA and IF functions. The advantages of the ESA are efficiency, low computational complexity and excellent time resolution (5-sample window). It has been shown in speech processing that the HT demodulation and the ESA produce similar results for speech resonance demodulation, but HT approach has higher computational complexity [91]. A disadvantage of ESA compared to HT is its sensitivity in very noisy environment. To reduce noise sensitivity, a more systematic approach is to use continuous-time expansions of discrete-time signals to numerically implement the required differentiation

with closed formulas [109]-[38]. A common limit of both HT and ESA is that they can not handle multicomponent signals. Thus, two non-linear and local approaches, ESA and EMD are combined here to track instantaneous features such as IA and IF of a multicomponent AM-FM signal. Associated with the EMD which acts as bandpass filter [116],[49] the ESA can handle multicomponent signals [22],[15]-[19]. Compared to Gabor filtering, EMD is a data driven approach that does not require neither the number of filters and the associated impulse responses, nor the bandwidth parameters [37]-[38]. Since IMFs are represented by spline functions, their smoothed derivatives can be obtained to compute TKEO and then in turn used in ESA to estimate IA and IF functions. Finally, this process adds robustness to ESA. Our contributions for IFs and IAs tracking are :

- Coupling two local and nonlinear approaches namely EMD and ESA (EMD-ESA) as the basis of a multicomponent signal analysis framework. Moreover, we have studied different discrete versions of the EMD-ESA approch, depending on the derivation choice. And then, a continuous version of the approach is finally proposed. This new approach is used for tracking IFs and IAs of multicomponents AM-FM signal with additive white Gaussian Noise.

- Compared to Gabor-ESA approach where bandpass filtering (filterbank of Gabor filters) is determined by a set of parameters, the proposed EMD-ESA requires only one input parameter (SD value). Indeed, each Gabor filter requires two parameters: the central filter frequency and the rms bandwidth. Thus, to analyze a signal of K components the Gabor-ESA necessitates 2K parameters. While Gabor-ESA supposes that K is known, the EMD-ESA determines this value automatically. Compared to Gabor filtering, the EMD is a data driven approach.

III.4 HT demodulation

The IF is obtained from the phase of a complex signal $z(t)$. Gabor introduced the HT to generate an unique complex signal $z(t)$, AS, from real signal $s(t)$ and thus removing ambiguity of the infinitely possible pair combinations of amplitude $a(t)$ and phase $\phi(t)$ functions to represent $s(t)$ [52]. The Analytic Signal (AS) is defined as

$$z(t) = s(t) + i\mathcal{H}[s(t)] = a(t)e^{i\phi(t)} \tag{III.4}$$

Where $i = \sqrt{-1}$ and $\mathcal{H}[s(t)]$ is the HT of any signal $s(t) \in L^2$ class given by

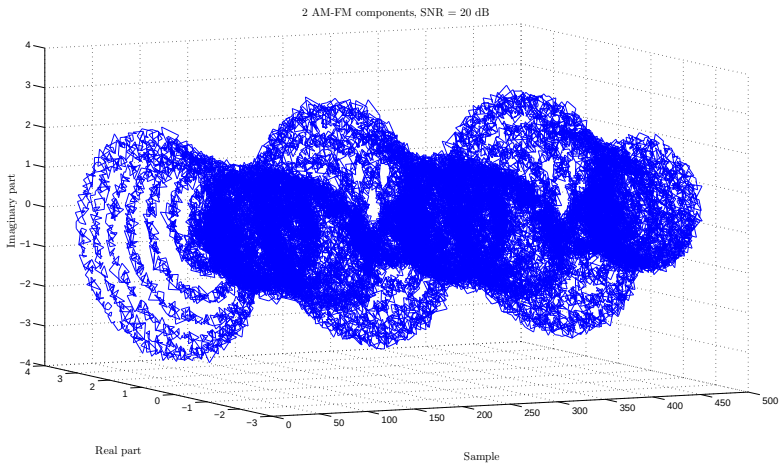

Figure III.2: AS of the two AM-FM components, this representation shows in 3D the complex form of the signal, with their imaginary part and real part. The horizontal axis contain the samples points position. We note that a projection of this signal in the plane (Real part-sample) give the real signal, figure (III.1)

$$\mathcal{H}[s(t)] = \frac{1}{\pi}\mathrm{P}\int_{-\infty}^{\infty}\frac{s(\tau)}{t-\tau}d\tau \tag{III.5}$$

with P indicating the Cauchy principal value of the integral. The canonical pair of IF and IA, $[a(t), f(t)]$, associated with $s(t)$ are derived from the AS as follows:

$$a(t) = \sqrt{[s(t)]^2 + \mathcal{H}[s(t)]^2} \text{ and } \phi(t) = \arctan\left(\frac{\mathcal{H}[s(t)]}{s(t)}\right) \tag{III.6}$$

The IF is simply

$$f(t) = \frac{1}{2\pi}\frac{d\phi(t)}{dt} \tag{III.7}$$

III.5 TKEO

There are apparently more than one way to derive the basic definition of the TKEO (Eq. (III.8)):

$$\Psi(x) = (\dot{x})^2 - x\ddot{x} \tag{III.8}$$

In fact, in the first articles by H. M. Teager [106],[107], no definition was given; only plots forms of the TKEO were shown. The first article by Kaiser [71] also shows traces of this and, only the discrete definition is investigated and explained. This article looks at the process that generated the signal, and shows how we can express the energy from the signal as a simple and elegant (discrete) function. The Teager Operator has since been defined for continuous signals, both real and complex ones.

Kaiser used the following differential equation as a starting point for the operator:

$$\frac{d^2x}{d^2t} + \frac{K}{M}x = 0 \tag{III.9}$$

This second order differential equation describes an object with mass M suspended by a string with constant K. We can regard this as a simple (but incomplete) model of a mechanical-acoustical system, where the object may oscillate, thus creating pressure waves in the surrounding medium [2].

The solution of equation (III.9) is a periodic oscillation given by $x(t) = acos(\omega t + \phi)$ where $x(t)$ is the position of the object at time t, a is the amplitude of the oscillation, $\omega = \sqrt{\frac{K}{M}}$ is the frequency of the oscillation, and ϕ is the initial phase. If $\phi \neq 0$, we have that the object is not initially in equilibrium.

Substituting $\upsilon = \frac{dx}{dt}$, and $x(t) = acos(\omega t + \phi)$, the total energy [3] can be written as,

$$E = \frac{1}{2}M\omega^2a^2 \tag{III.10}$$

From this, we immediately see that the energy of the object is proportional to both a and ω. Note that the energy E is implicitly a function of time.

III.5.1 Discrete energy demodulation

TKEO is a tracking-energy operator introduced by Kaiser [71]. The continuous version of the TKEO, Ψ, when operating on continuous-times signal $s(t)$ is given by,

$$\Psi[s(t)] \triangleq (\dot{s}(t))^2 - s(t)\ddot{s}(t) \tag{III.11}$$

Where $\dot{s}(t) = \frac{\partial s(t)}{\partial t}$. A discrete form of Ψ noted Ψ_d is given by:

$$\Psi_d[s(n)] \triangleq s^2(n) - s(n+1)s(n-1) \tag{III.12}$$

A useful and important property of Ψ operator is its behavior when applied to AM-FM signal $s(t)$ defined by equation (III.1). The output of Ψ of such signal is given by [84]

[2] None of the medium's characteristics are included in the model

[3] The total energy of the object is in Newtonian physics given as the sum of the potential energy of the spring and the kinetic energy of the object, given by: $E = \frac{1}{2}Kx^2 + \frac{1}{2}M\upsilon^2$

$$\Psi[s(t)] \approx a^2(t)\dot{\phi}^2(t) \tag{III.13}$$

The output of Ψ for the derivative of the signal $s(t)$ has the form,

$$\Psi[\dot{s}(t)] \approx a^2(t)\dot{\phi}^4(t) \tag{III.14}$$

Thus, with negligible approximation error under general realistic conditions, equation (III.13) shows that the output of Ψ is the squared product of $a(t)$ and the time-varying phase derivative $\dot{\phi}(t)$. The relation between IF and the phase function is given by in equation (III.7). The ESA demodulation [83] is obtained when we combine relations (III.13) and (III.14) as follows,

$$f(t) \approx \frac{1}{2\pi}\sqrt{\frac{\Psi[\dot{s}(t)]}{\Psi[s(t)]}}, \quad \mid a(t) \mid \approx \frac{\Psi[s(t)]}{\sqrt{\Psi[\dot{s}(t)]}} \tag{III.15}$$

The ESA has found many applications [83],[19] and particularly is speech processing [84]. As indicated, the demodulation (Eqs. (III.15)) is valid provided that narrow-band assumption of signal $s(t)$ holds. By passing the continuous-time derivation in equations (III.13)-(III.14) to discrete differences, one obtains three discrete versions of the ESA [83].

III.5.1.1 DESA-1a

The "1" implies the approximation of derivatives with a single sample difference and "a" refers to the use of asymmetric difference. The IA and IF functions of each IMF (mode k), are approximated as follows [83] :

$$f(n) \approx \arccos\left(1 - \frac{\Psi[s(n) - s(n-1)]}{2\Psi[s(n)]}\right) \tag{III.16}$$

$$|a(n)| \approx \sqrt{\frac{\Psi[s(n)]}{1 - (1 - \frac{\Psi[s(n)-s(n-1)]}{2\Psi[s(n)]})^2}} \tag{III.17}$$

III.5.1.2 DESA-1

In this version the action of Ψ on asymmetric derivatives is partially symmetrized by averaging the action of Ψ on two opposite asymmetric derivatives. The IA and

IF functions are given by the approximation formulas [83], as follows:

$$y(n) = s(n) - s(n-1)$$

$$f(n) \approx \arccos\left(1 - \frac{\Psi[y(n)] + \Psi[y(n+1)]}{4\Psi[y(n)]}\right) \tag{III.18}$$

$$|a(n)| \approx \sqrt{\frac{\Psi[s(n)]}{1 - (1 - \frac{\Psi[y(n)]+\Psi[y(n+1)]}{4\Psi[y(n)]})^2}} \tag{III.19}$$

III.5.1.3 DESA-2

The "2" implies the approximation of first-order derivatives by differences between samples whose time indexes differ by 2. According to [83], like the two previous versions, IA and IF functions are given by following approximations:

$$f(n) \approx \frac{1}{2}\arccos\left(1 - \frac{\Psi[s(n+1) - s(n-1)]}{2\Psi[s(n)]}\right) \tag{III.20}$$

$$|a(n)| \approx \frac{2\Psi[s(n)]}{\sqrt{\Psi[s(n+1) - s(n-1)]}} \tag{III.21}$$

The three algorithms DESA-1a, DESA-1 and DESA-2 should be applied only to monocomponent signal. Thus, $s(t)$ in the formulae of different DESA is considered as monocomponent signal.

III.5.2 Continue energy demodulation

B-splines play an important role in the sifting process as all extracted IMFs of decomposed signal are linear combinations of splines. As can be seen in the EMD diagram (Fig. II.7) the interpolation is integrated at the beginning of the sifting process. Since the sifting is an iterative process, any approximation error will be propagated in the present loop (i) and also to the whole process. To resolve this problem we carefully handle the interpolation step and we propose a new sifting process. For highly oscillating signals, especially noisy data, instead of exact splines we use a smoothing spline interpolation and thus the number of insignificant IMFs is reduced. These representations are used in problems that are best formulated in a continuous rather than in a discrete framework [109]. In sifting process, spline functions are used to interpolate extrema of signal envelopes. As IMFs are represented

by B-splines, it is very natural to perform computational tasks such as differentiation in the B-splines domain [109]. In this respect, B-splines version of the ESA can be derived [91],[37]-[38] and particularly for noisy signals [15]. Thus, with B-splines one has a good equivalence between finite differences and differentiation. The aim is to have an ESA with closed formulae. In general, one may choose between an exact representation which is to be preferred for noise free signals or an approximate representation which is more robust to noisy signals [109]. Note that other approaches such as trigonometric interpolation can be used. Trigonometric interpolation is useful from an analytic point of view, but computationally it is much more expensive than B-splines [110]. In this section both exact and smoothed splines are investigated.

III.5.2.1 Demodulation by exact splines

B-splines are the basic atoms for constructing spline functions. One operation that is essentially simple to manipulate is differentiation. It has the same effect on splines as it has on polynomials. It reduces the degree by one [110]. Thus one can calculate spline derivatives by applying finite differences to the B-splines coefficients of the representation.

Extracted IMF can be written in terms of a B-spline expansions as follows [64]:

$$\mathrm{IMF}_j^n(t) = \sum_{k\in\mathbb{Z}} c_j[k]\beta_j^n(t-k) \tag{III.22}$$

where $\beta_j^n(t)$ and $c_j[k]$ are the Schoenberg's central B-spline of order n [99] and the B-spline coefficients of the jth mode, respectively. The coefficients $c_j[k]$ can be calculated either by solving a linear system, matrix approach [34], or by recurrent filters [109].

The signal $\mathrm{IMF}_j^n(t)$ (Eq. (III.22)) is a continuous-time expansion of an original discrete signal. The head-on idea of the new EMD-ESA-based demodulation is to compute the continuous-time energy operator Ψ and the continuous ESA to the continuous-time signal $\mathrm{IMF}_j^n(t)$, instead of applying the discrete energy operator Ψ_d and the DESA on a discrete signal.

Since IMFs are a narrow band components [64], the ESA can be applied to estimate their IFs and IAs. For sake of clarity $\mathrm{IMF}_j^n(t)$ is replaced by $g_j^n(t)$, then the output of TKEO for $g_j^n(t)$ and $\nabla g_j^n(t)$ are:

$$\Psi[g_j^n(t)] = [\frac{\partial g_j^n(t)}{\partial t}]^2 - g_j^n(t)\frac{\partial^2 g_j^n(t)}{\partial t^2}$$
$$\Psi[\frac{\partial g_j^n(t)}{\partial t}] = [\frac{\partial^2 g_j^n(t)}{\partial t^2}]^2 - \frac{\partial g_j^n(t)}{\partial t}\frac{\partial^3 g_j^n(t)}{\partial t^3} \tag{III.23}$$

The IF, $f_j(t)$, and the IA, $a_j(t)$, of the jth IMF are written as follows [14]:

$$a_j(t) = \frac{\Psi[g_j^n(t)]}{\sqrt{\Psi[\nabla g_j^n(t)]}}$$
$$f_j(t) = \frac{1}{2\pi}\sqrt{\frac{\Psi[\nabla g_j^n(t)]}{\Psi[g_j^n(t)]}} \tag{III.24}$$

where $\nabla(.) \equiv \frac{\partial(.)}{\partial t}$.

In order to formulate the ESA B-Splines (ESA-BS), the first derivatives of IMF are calculated.The closed form of the TKEO for the IMF and their first derivative is given by (Appendix.B):

$$\Psi[g_j^n(t)] = [\frac{\partial g_j^n(t)}{\partial t}]^2 - g_j^n(t)\frac{\partial^2 g_j^n(t)}{\partial t^2}$$

$$\Psi[g_j^n(t)] = [\sum_{l\in\mathbb{Z}}(c_k[l]-c_j[l-1])\beta_j^{n-1}(t-l+\frac{1}{2})]^2-][\sum_{l\in\mathbb{Z}} c_j[l]\beta^n(t-l)[\sum_{l\in\mathbb{Z}}(c_j[l+1]-2c_j[l]+c_j[l-1])\beta_j^{n-2}(t-l)] \tag{III.25}$$

$$\Psi[\nabla g_j^n(t)] = [\frac{\partial^2 g_j^n(t)}{\partial t^2}]^2 - \frac{\partial g_j^n(t)}{\partial t}\frac{\partial^3 g_j^n(t)}{\partial t^3}$$

$$\Psi[\nabla g_j^n(t)] = [\sum_{l\in\mathbb{Z}}(c_j[l+1] - 2c_j[l] + c_j[l-1])\beta_j^{n-2}(t-l)]^2 -$$
$$\sum_{l\in\mathbb{Z}}(c_j[l] - c_j[l-1])\beta_j^{n-1}(t-l+\frac{1}{2})$$

$$\sum_{l\in\mathbb{Z}}(c_j[l+1]-3c_j[l]+3c_j[l-1]-c_j[l-2])\beta_j^{n-3}(t-l+\frac{1}{2}) \tag{III.26}$$

For a cubic-B-splines we give the closed form expressions of the EMD-ESA-BS. Lets the sequence $\{t_i\}_{i=0,1,\ldots,M-1}$ the Knots of the B-Spline; then, in each interval $[t_i, t_{i+1}]$ the signal $g(t)$ (ie., IMF) is approximated by the spline function of third order. Thus we have:

$$g_j^3(t) = c_j[1]t^3 + c_j[2]t^2 + c_j[3]t + c_j[4]$$

then in, $[t_i, t_{i+1}]$ ESA-BS is :

$$a_j(t) = \frac{A(t)+B(t)}{\sqrt{C(t)}} \tag{III.27}$$

$$f_j(t) = \frac{1}{2\pi}\sqrt{\frac{C(t)}{A(t)+B(t)}} \tag{III.28}$$

where,

$$\begin{aligned} A(t) &= 3c_j^2[1]t^4 + 4c_j[1]c_j[2]t^3 + 2c_j^2[2]t^2, \\ B(t) &= (2c_j[2]c_j[3] - 6c_j[1]c_j[4])t + c_j^2[3] - 2c_j[2]c_j[4], \\ C(t) &= 18c_j^2[1]t^2 + 12c_j[1]c_j[2]t + 4c_j^2[2]t - 6c_j[1]c_j[3]. \end{aligned} \tag{III.29}$$

In exact splines, the interpolating polynomial pass exactly through the signal samples. Unfortunately, as will been shown for noisy signals (see Results section) the exact fit may not be even desirable. The obtained results are disappointing. In case of very noisy data, one has to use B-spline approximation functions passing closely but not exactly through the signal samples using smooth splines [110]. To improve the performance of the ESA-BS method in very noisy environment smoothed splines are used. This is done by relaxing the interpolation constraint and to find a function (solution) of order $n = 2r - 1$ that minimize E (Eq. (II.9)).

Once the smooth spline function for each IMF is calculated, the next step is to integrate it to ESA algorithm following the same steps as for the ESA-BS method. The obtained method is termed ESA Regularized B-Splines (ESA-RBS).

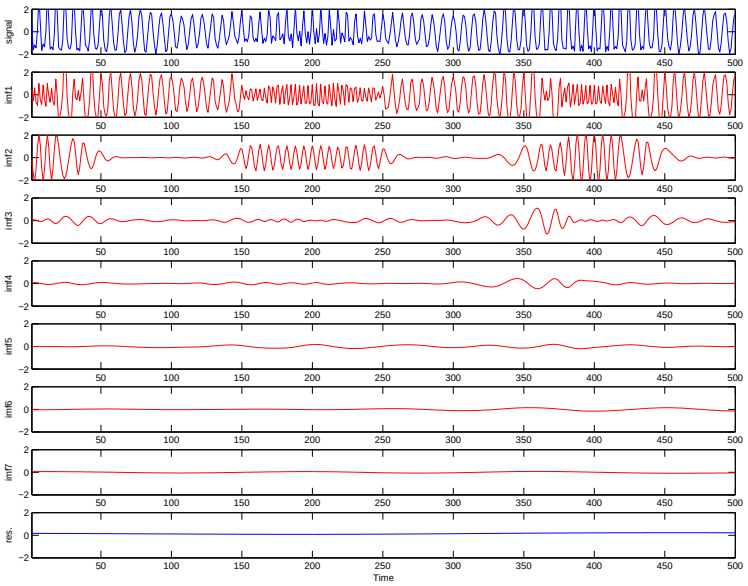

Figure III.3: Decomposition of the noisy AM-FM signal, $s(t)$, (SNR=20 dB) with EMD

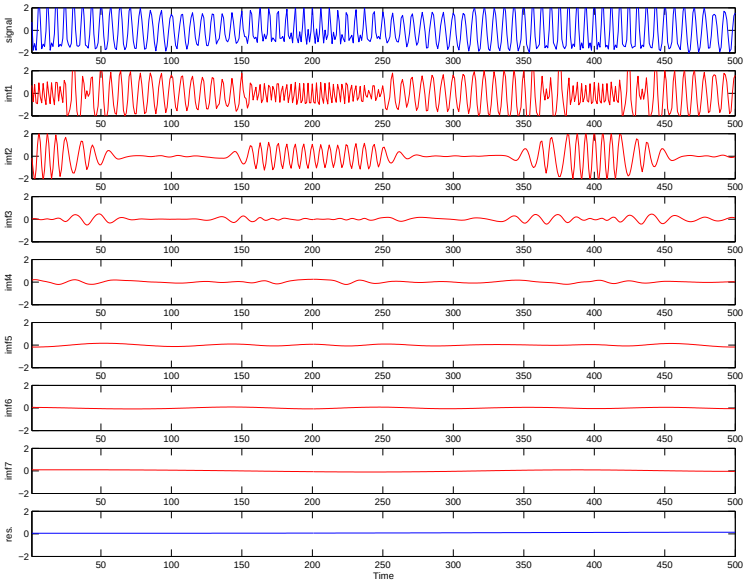

Figure III.4: Decomposition of the noisy AM-FM signal, $s(t)$, (SNR=20 dB) with modified EMD

III.6 Results and Discussion

For the conducted experiments we used parametric AM-FM signals with different levels of white Gaussian noise, the first line in figure (III.3) shows noisy version of the AM-FM signal. Their analytical expression is given by the following equations:

$$s(t) = s_1(t) + s_2(t) + n(t)$$

where $n(t)$ is the added noise.

$$s_i(t) = a(t)\cos[\phi_i(t)] \quad \text{(III.30)}$$
$$a_i(t) = 1 + \kappa_i \cos(\omega_{a_i} t) \quad \text{(III.31)}$$
$$\phi_i(t) = \omega_{c_i} t + \beta_i \sin(\omega_{c_i} t) \quad \text{(III.32)}$$

where, $i = \{1, 2\}$, $\kappa_1 = 0.4$,$\kappa_2 = 0.8$ are the modulation index. The parameters of $s_1(t)$ are: $\omega_{a1} = \pi 0.02$, $\omega_{c1} = 2\pi 0.250$, $\beta_1 = 1.8$ is the depth of modulation. For $s_2(t)$: $\omega_{c2} = 2\pi 0.125$, $\beta_2 = 0.9$.
The signal $s(t)$ is decomposed into a set of IMFs. Most of the experiments give $s_1(t)$ and $s_2(t)$ in first and second IMFs, respectively. Sifting of $s(t)$ at 20dB of the EMD (Fig. III.3) and the EMD-RBS (Fig. III.4) generate both 7 IMF components.

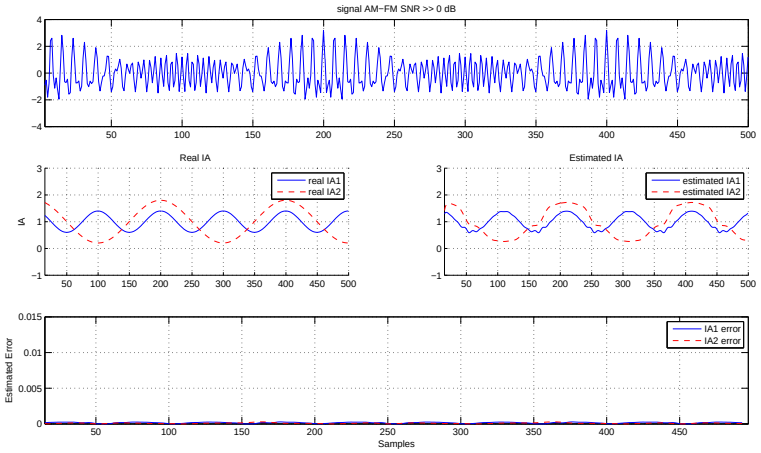

Figure III.5: IAs estimation of noise free signal, $s(t)$, by EMD-ESA-BS

Comparison of the estimated IF and IA functions of the two AM-FM components shows that the EMD-ESA-RBS improves the demodulation results. The performance of the methods are evaluated through MSE and error in IF (IA)

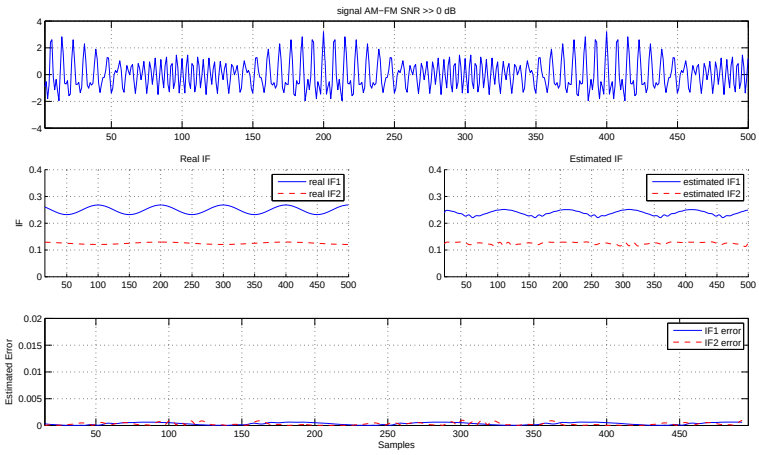

Figure III.6: IFs estimation of noise free signal, $s(t)$, by EMD-ESA-BS

estimation. In each figure, we have depicted the input signal, $s(t)$, the desired IF (IA) components, the associated estimates and the estimation errors. We have first tested the accuracy of the proposed EMD-ESA-BS on noise free signal ($SNR >> 0$). Estimated IF and IA functions of $s(t)$ ($n(t) = 0$) are shown in figures (III.6) and (III.5), respectively. These figures show that the application of the EMD-ESA-BS results in a successful estimation of the IA and IF components with very small errors less than 5.10^{-3}. In both cases we note few small ripples in the estimated components due essentially to the mode mixing phenomenon of the EMD [64].

Results in Table (III.1) present empirical evidence that EMD-EAS-BS performs

Approche	$s_1(t)$	$s_2(t)$
EMD-ESA(Discrete version)	0.002200	0.000103
EMD-ESA-BS(Continuous version)	0.000301	0.000070

Table III.1: Mean Square Error between estimated IFs and real ones for the noise free signal.

better than its discrete version, EMD-ESA, in separating and tracking frequency components.

In the following, we analyze the performance of the EMD-ESA-RBS on the signal $s(t)$ at 20 dB and compare the demodulation results to five established methods, namely EMD-HT, EMD-ESA-BS, EMD-DESA1, EMD-DESA1a and EMD-DESA2. These results are illustrated in figures (III.7)-(III.18). The approaches EMD-EAS-

RBS (Fig. III.10) and EMD-EAS-BS (Fig. III.9) perform better in estimating IF components than other four methods (Figs. III.15, III.16, III.17, III.18) with small errors of 2.10^{-3} and 6.10^{-3} respectively.

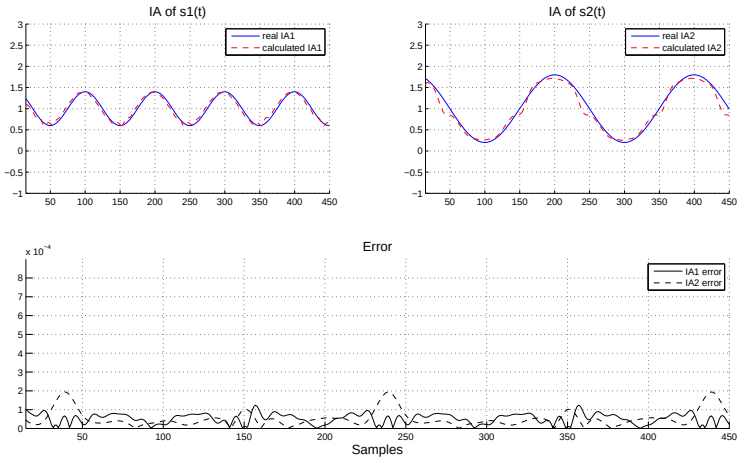

Figure III.7: IA estimation of signal $s(t)$ (SNR= 20dB) by EMD-ESA-BS

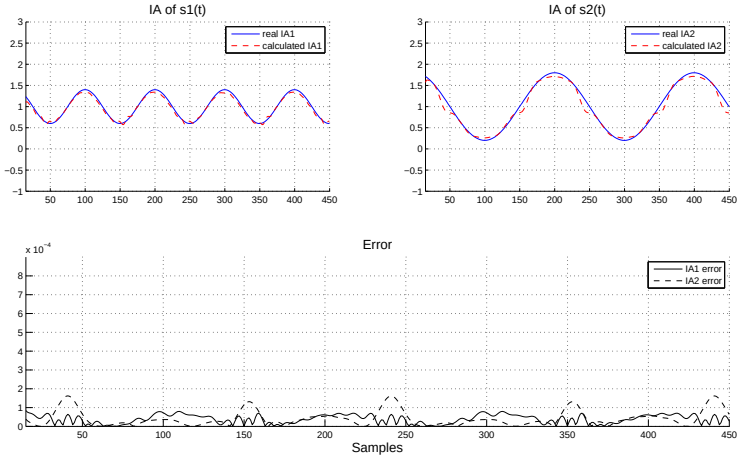

Figure III.8: IA estimation of signal $s(t)$ (SNR= 20dB) by EMD-ESA-RBS

We note that the EMD-DESA1 (Fig. III.16) have better performance than the EMD-HT (Fig. III.15), the EMD-DESA1a (Fig. III.17) and the EMD-DESA2 (Fig. III.18). Except the EMD-EAS-RBS and the EMD-EAS-BS, the other methods show abnormal peaks reaching large amplitudes. This is also confirmed by the results depicting the estimation errors (Figs. III.15, III.16, III.17, III.18).

Furthermore, we see that the DESA1 (Fig. III.16) performs quite well compared

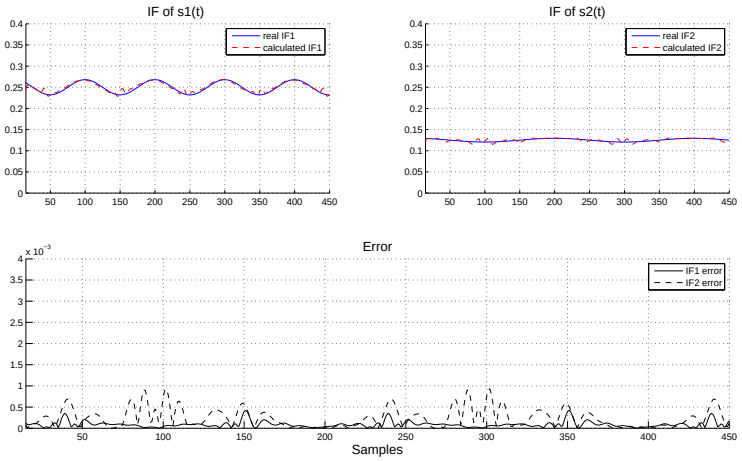

Figure III.9: IF estimation of signal $s(t)$ (SNR= 20dB) by EMD-ESA-BS

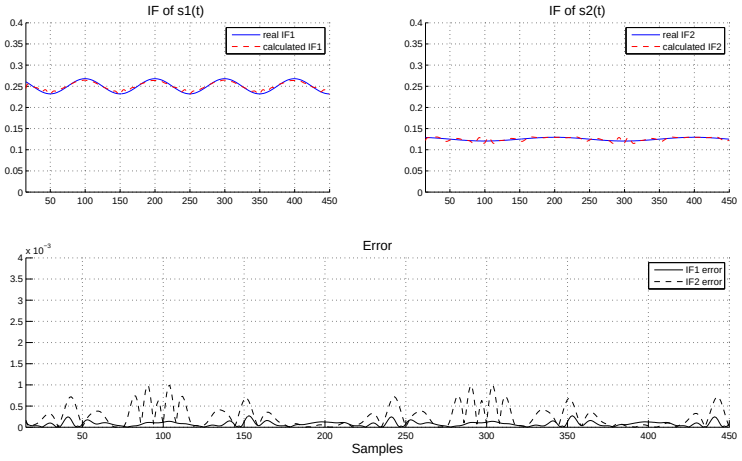

Figure III.10: IF estimation of signal $s(t)$ (SNR= 20dB) by EMD-ESA-RBS

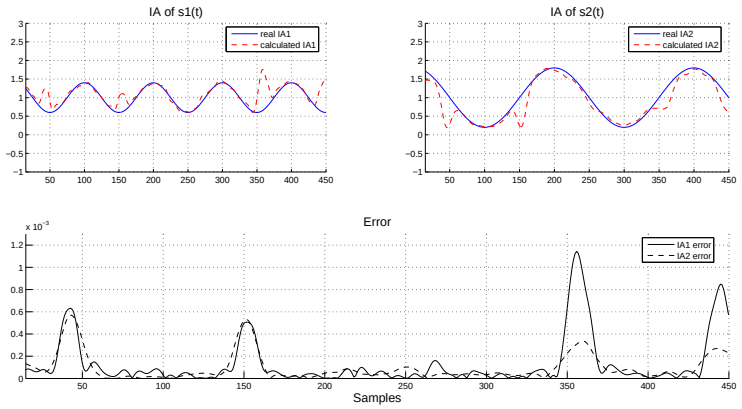

Figure III.11: IA estimation of signal $s(t)$ (SNR= 20dB) by EMD-HT

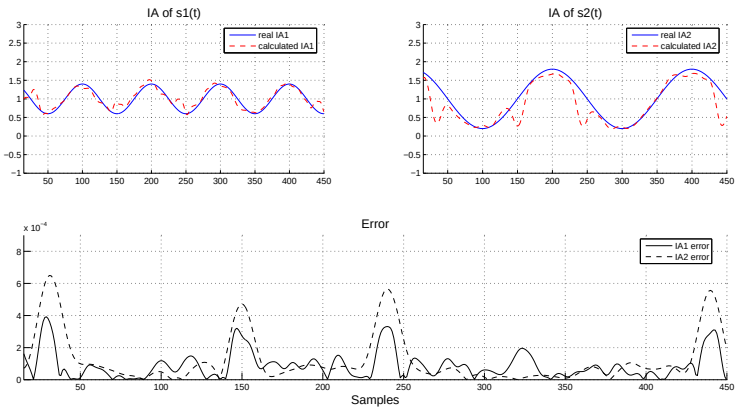

Figure III.12: IA estimation of signal $s(t)$ (SNR= 20dB) by EMD-DESA1

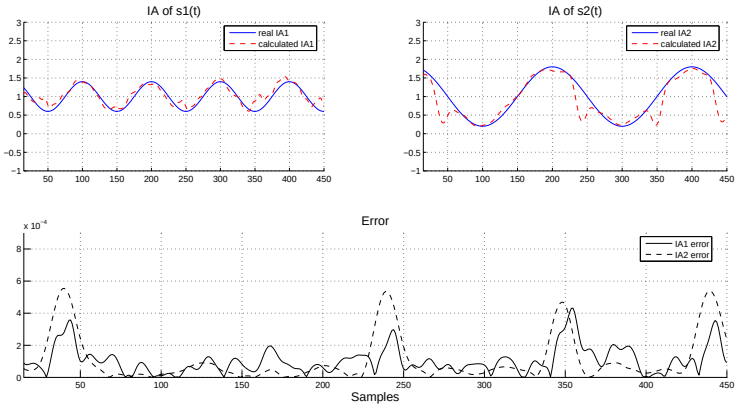

Figure III.13: IA estimation of signal $s(t)$ (SNR= 20dB) by EMD-DESA1a

to DESA1a (Fig. III.17) and DESA2 (Fig. III.18). This is mainly due the fact that the DESA1 uses at each instant three samples while the DESA1a and the DESA2 are limited to two samples. For IA estimation, the performances of the six methods are similar (Figs. III.7, III.8, III.11, III.12, III.13, III.14) but the best result is given by the EMD-ESA-BS (Fig. III.7).

Now, we compare the performance of the six demodulation methods in term of MSE as function of input SNR fixing λ equal to a constant value (Fig. III.19). As can be seen in the range [-10dB, 0dB] except the EMD-ESA-RBS, the MSE of all the methods first increase and decrease. Across the same range the EMD-ESA-RBS decreases rapidly and shows significant performance improvement over the other methods. In noisy environment, signals have large variations and sharp edges and the need of smoothing factor is apparent. Thus, the performance of the EMD-ESA-RBS is expected because the smooth BS gives the method robustness in

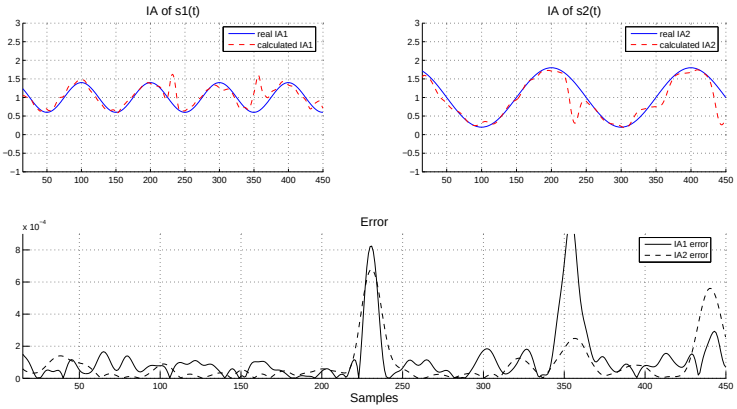

Figure III.14: IA estimation of signal $s(t)$ (SNR= 20dB) by EMD-DESA2

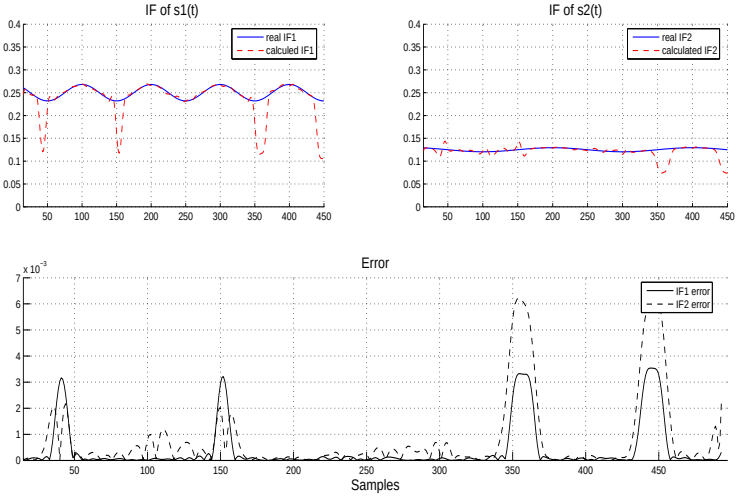

Figure III.15: IF estimation of signal $s(t)$ (SNR= 20dB) by EMD-HT

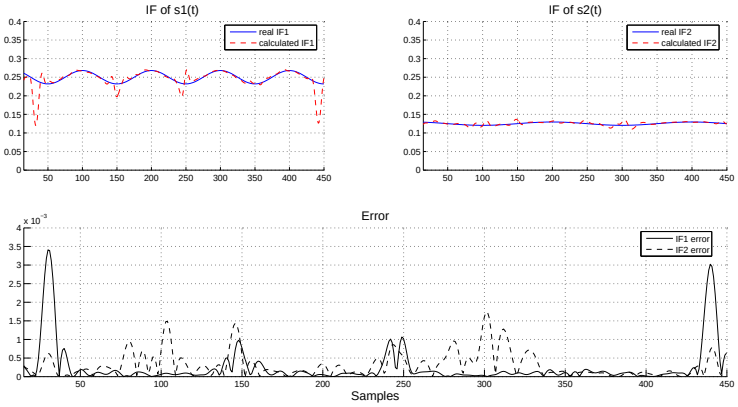

Figure III.16: IF estimation of signal $s(t)$ (SNR= 20dB) by EMD-DESA1

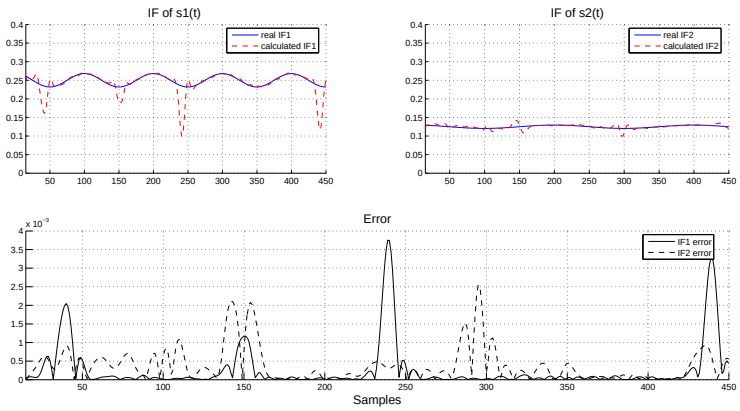

Figure III.17: IF estimation of signal $s(t)$ (SNR= 20dB) by EMD-DESA1a

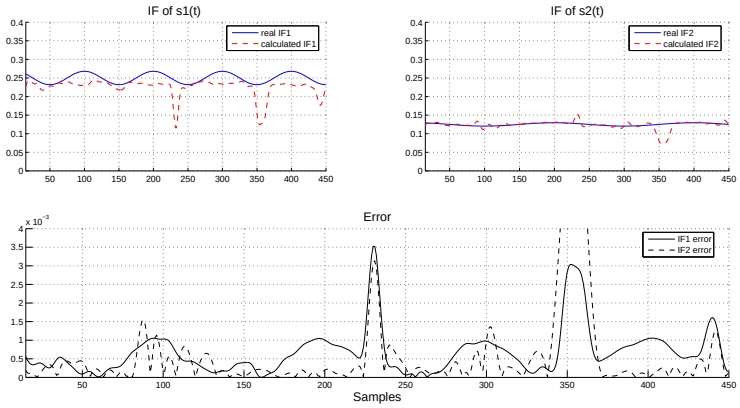

Figure III.18: IF estimation of signal $s(t)$ (SNR= 20dB) by EMD-DESA2

the presence of noise. In the same range, the EMD-ESA-BS performs less than the EMD-ESA-RBS mainly due to exact BS fitting which is responsible of the increase of the MSE, as the noisy samples insert a significant error. However in moderately noisy environment, [0dB, 10dB], the EMD-ESA-BS performs better than the other methods.

In the range [10dB, 17dB] the DESA1 gives the best estimation results in term of MSE. Toward higher SNR values ($\geq$ 20dB), the performance of the six methods become similar and converge, but the best results are given the BS-based methods (Fig. III.19). Figure (III.20) compare the MSE curves of the six methods for IA estimation. As can be seen, the EMD-ESA-RBS performs better than the other methods in the range [-10dB, 5dB]. Note that the EMD-ESA-BS performs less better due to the exact BS fitting. The EMD-DESA2 and the EMD-ESA-BS provide good estimates of IA in the range [5dB, 14dB], while the better estimates

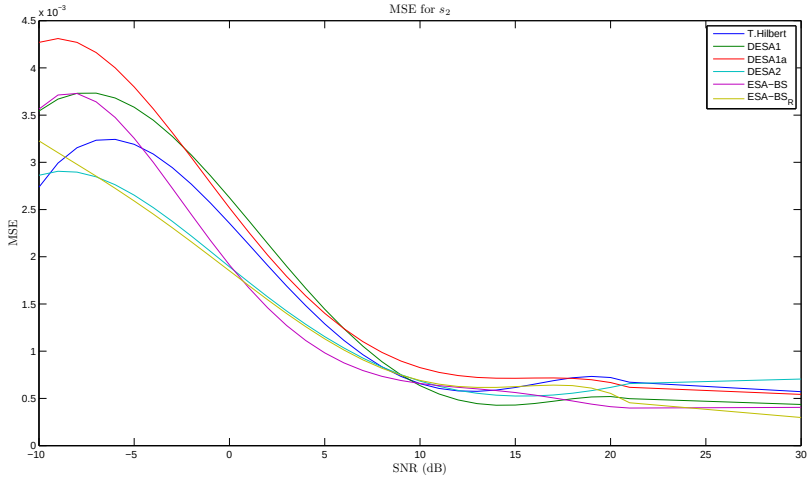

Figure III.19: MSE as function of input SNR for different IF estimations of signal $s_2(t)$

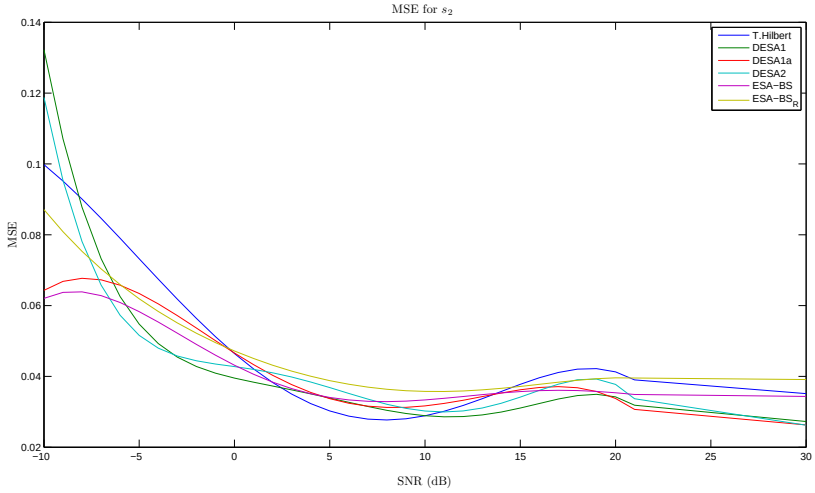

Figure III.20: MSE as function of input SNR for different IA estimations of signal $s_2(t)$

are obtained by the EMD-DESA1 in [14dB, 21dB]. As in figure (III.19) for higher SNR values ($\geq$ 21dB), the performance of all methods become similar (Fig. III.20). Even from low to high SNRs (Figs. III.19, III.20), BS-based methods show significant performance improvement as compared to the other methods, these results are conditioned by the estimation of the optimal value of λ. A careful examination of results depicted in figures (III.19) and (III.20), shows that except for low SNR values ([-10dB, 0dB]) and higher ones ($\geq$ 20dB) the BS-based methods do not provide the better estimates of IF and IA in the same ranges of SNR values. This again shows the difficulty to find an optimal λ value for both IA and IF estimations.

III.7 Summary

In [19],[22] the demodulation using the EMD and the DESA1 has been introduced. Furthermore, we suggest in this thesis to combine also the DESA1a or DESA2 with the EMD as a demodulation approach for estimating IFs and IAs of multicomponents AM-FM signal. Generally DESAs demodulators give comparable performance with regards to the approximation errors for large classes of signals. Since DESA-2 offers the lowest computational complexity, it is the most widely utilized among the three versions [79]. The goal of these combinations is to overcome the narrowband assumption imposed by Maragos [84].

The EMD-DESA works well in free and in moderate noisy environment, but as the EMD-HT it performs poorly for very noisy signals. The EMD-DESA limitation is due to the sensitivity to noise of the TKEO which is based on the differentiation of the signal. Thus, to reduce noise sensitivity a more systematic approach is to use continuous-time expansions of discrete-time signals to numerically implement the required differentiations without approximation. Since IMFs are represented in B-spline expansions [64], a close formulae of the ESA is derived. Also, using a regularized version of B-splines for interpolation in EMD process, more robustness and better estimation of IF and IA functions compared to exact version of B-splines are obtained. In chapter II, we have shown the interest of the new sifting process for IMFs extraction compared to both the conventional EMD and to the EEMD. In this chapter the performances of such sifting are also confirmed for tracking IA and IF functions in noisy environment. Findings of chapters II et III illustrated the interest to use smoothing instead of interpolation in the sifting processing. These results can

be improved by establishing a rigorous strategy to find an optimal regularization parameter for each analyzed signal (data driven parameter).

CHAPTER IV

Teager Huang Transform

Contents

IV.1 Introduction 87

IV.2 Teager-Huang Transform 87

IV.3 Teager-Kaiser spectrum 88

IV.3.1 TKS generation 91

IV.4 Results and discussions 92

IV.4.1 Example 1: Hyperbolic frequencies law 92

IV.4.2 Example 2: Monocomponent FM signal 96

IV.5 Conclusions 98

We introduce here a new TFR named Teager Huang Transform (THT). Unlike the classical approaches the THT dose not need any predefined decomposition basis or parameters. The philosophy of this TFR is the same as the Hilbert Huang Transform (HHT) [62], except that for THT the analyzed signal is demodulated using the ESA instead of HT. The THT is illustrated on synthetic signals with different IF laws. For each signal, the result of the THT is compared to that of the spectrogram, the scalogram, the WVD, the SPWVD, the reassigned SPWVD and the HHT. We analyze the results given by each approach and discuss the limits of each TFR.

IV.1 Introduction

TFRs presented in the first chapter have a common point, they are all Fourier kernel dependent and they provide a TF map of the analyzed signal. The strength of using TFR compared to time or frequency representation, is their capacity to quantitatively resolve changes in the frequency content of nonstationary signal. Their major weaknesses in some cases, is to generate representations that are meaningless or difficult to interpret. For example, the WVD by definition generates added cross terms identifiable some times in the TFR. For others TFRs, finding a decomposition kernel that can optimally represents the original signal is a great challenge: when one is faced to an inexplicable plots resulted by STFT of an analyzed signal, this fact lets us usually suspect the length of the analyzing windows due to the Heisenberg identity. Even the WT for some applications (data coding,...) could perform better than others kernel-based TFRs, the type of the wavelet that one must use for a better data analysis remains a serious issue. We introduce here a TFR named Teager Huang Transform (THT). Unlike the classical approaches, the THT does not need any predefined decomposition basis. The principle of this TFR is the same as that of the HHT [62] except that the analyzed signal is demodulated using the ESA, presented in the previous chapter. Unlike the HHT, the THT is not limited by the Bedrosian theorem. However, until now the THT is still used just as a representation of the signal. No TF attributes or other relevant information (marginals,...) are derived from such representation. We propose in this chapter a mathematical formulation of the TF map of the THT such as some useful definitions or informations such as the marginals or stationarity index can be calculated. Furthermore, this new formulation allows the extension of the application field of the THT (Chapter V). In this chapter, THT is applied to synthetic signals of different frequency laws and to real world signal. In each case, the result of THT is compared to the ones given by the spectrogram, the scalogram, the WVD, SPWVD and the reassigned SPWVD.

IV.2 Teager-Huang Transform

The IFs of the IMFs give sharp identifications of embedded structures of the analyzed signal. Taken collectively, the spectra given by the HT or the ESA of the IMFs yield an energy distribution about the original signal in the TF plane. A common method for displaying the spectra derived from the IMFs is to generate a two-dimensional plot with time and frequency axes. The IA is then plotted as a color spectrogram in the TF plane. In this chapter, the IF and the IA of $s(t)$ are estimated by combining the EMD with the TKEO, which is typically applied to a bandpass signal [19]. As it has

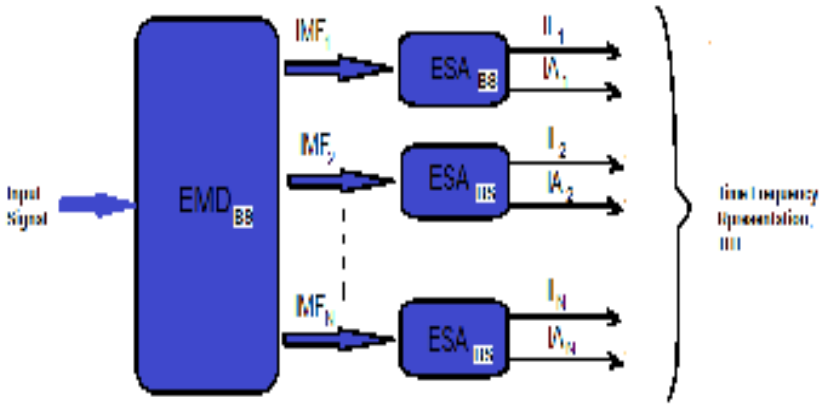

Figure IV.1: IFs and IAs estimating by EMD-ESA

been shown in chapter III and [14],[15]. If $s(t)$ is a multicomponent AM-FM signal, then bandpass filtering is needed to separate each component before applying the ESA. Thus, the EMD is used as a multiband filtering(see Appendix. A) to separate the signal components in the temporal domain and hence reduce multicomponent demodulation to monocomponent one. The conjunction of the EMD with the TKEO methods is designated as THT [24]. The block diagram of THT shown in figure (IV.1), is divided into two parts: separation of the signal into IMFs using the EMD, and demodulation of the separated components (IMFs) into IF and IA signals for each component using the ESA.

IV.3 Teager-Kaiser spectrum

For the AM-FM signal, in the previous chapter (cf, chapter.III), we study the accuracy of different approaches; the components are identified manually. In general with THT, the spectrum of a given signal is resulting from all their IMFs. Generally, it is observed that insignificant IMF has weak amplitude and are dominated by the strong ones [35, 64].

After applying the ESA to each IMF component of $s(t)$, we can express this original signal in the following form:

$$s(t) = \Re\left(\sum_{j=1}^{N} a_j(t) \exp(i \int 2\pi f_j(t) dt)\right) + r_N(t) \qquad \text{(IV.1)}$$

$\Re$ stands for "real part". If we neglect $r_N(t)$, which is either a monotonic function or a constant, relation (IV.1) is reduced to

$$s(t) = \Re\left(\sum_{j=1}^{N} a_j(t) \exp(i \int 2\pi f_j(t)dt)\right) \tag{IV.2}$$

Equation (IV.2) gives both amplitude and frequency of each component as functions of time. If we now expand $s(t)$ in a Fourier representation, we obtain:

$$s(t) = \Re\left(\sum_{j=1}^{\infty} a_j \exp(i2\pi f_j t)\right) \tag{IV.3}$$

where a_j and $_j$ are constants. A comparison of the two representations in equations (IV.2) and (IV.3) suggests that the IMF and the associated DESA outputs can be considered as *generalized Fourier expansion*. The main advantage of this expression over Fourier one is that it accommodates nonstationarity of $s(t)$. Equation (IV.1) enables us to represent IA and IF as functions of time in a three-dimensional plot, in which the amplitude is contoured on TF plane. The weight assigned to each TF cell is the local spectrum amplitude. We interpret the amplitude (or energy) depending on time and frequency as the Teager-Kaiser Spectrum (TKS) denoted by $K(t, f)$. Formally, this is defined as follows.
Let the signal $s(t)$ be represented in the form (IV.1). The TKS (amplitude) is defined as,

$$K(t, f) = K(t, f(t)) := \begin{cases} a_1(t) & \text{on the curve } \{(f_1(t), t);\ t \in \mathbb{R}\} \\ a_2(t) & \text{on the curve } \{(f_2(t), t);\ t \in \mathbb{R}\} \\ \vdots & \\ a_N(t) & \text{on the curve } \{(f_N(t), t);\ t \in \mathbb{R}\} \end{cases} \tag{IV.4}$$

This TFR can also be written as:

$$K(t, f) = \sum_{j=1}^{N} a_j(t, f_j(t)) = \sum_{j=1}^{N} a_j(t, f)\delta(f - f_j(t)) \tag{IV.5}$$

The marginal TKS is defined as

$$k(f) = \int_0^T K(t, f)dt, \tag{IV.6}$$

where T is the time signal duration. Function $k(f)$ measures the total amplitude (or energy) contribution from each frequency value. It represents the cumulated amplitude over the entire signal span in the probabilistic sense. The associated

mean marginal spectrum is given by

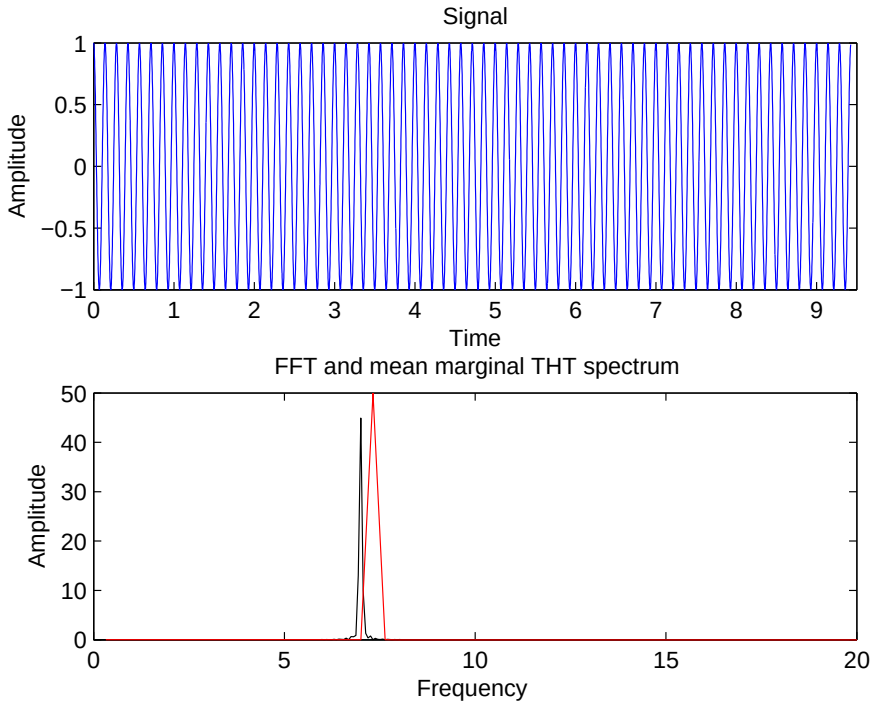

(a)

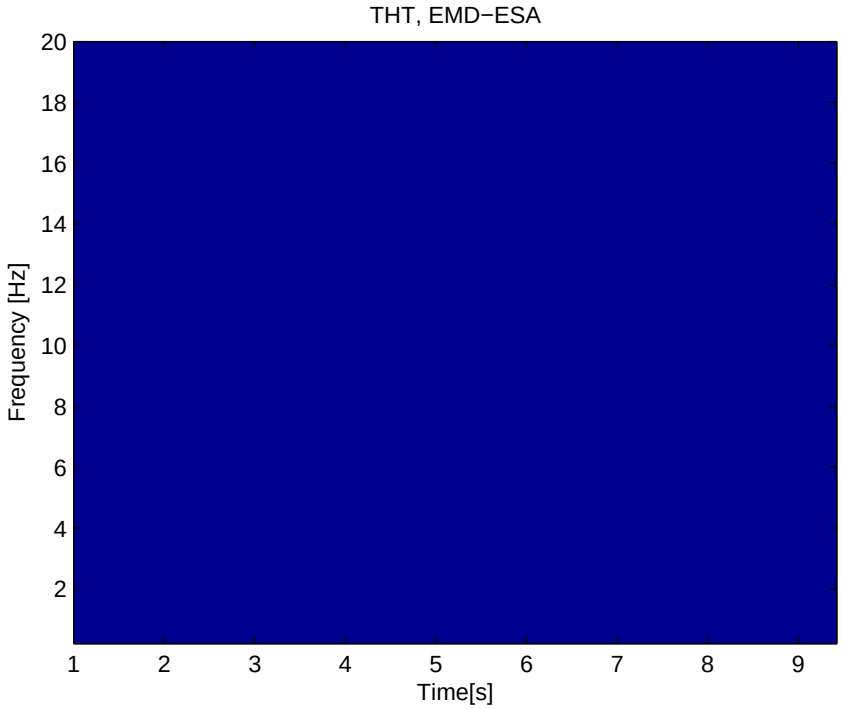

(b)

Figure IV.2: (a) On top a sinusoidal signal, on bottom the corresponding Fourier spectrum and mean marginal TKS in black and red colors, respectively. (b) THT (EMD-ESA) of the signal

$$ms(f) = \frac{1}{T}k(f) \tag{IV.7}$$

We have to note that the Fourier spectrum remains the best way for the extraction and localization of fixed frequencies in case of stationary signal. In figure (IV.2.a), the Fourier spectrum has localized harmonic component better than the marginal TKS. Last, as it has been noticed by Huang et al. [64] for the marginal Hilbert spectrum[1], the marginal spectrum $k(f)$ has a different meaning from the Fourier spectral analysis. In the THT or HHT, the existence of spectrum at a given frequency f means that in the time span of the signal, there is a high likelihood for a component of sinusoidal wave to appear locally.

The degree of stationarity over the whole signal $x(t)$ is given by

$$SD(f) = \frac{1}{T}\int_0^T \left(1 - \frac{K(t,f)}{ms(f)}\right)^2 dt \tag{IV.8}$$

This definition of degree of stationarity is similar to the intermittency used in wavelet analysis [64],[86]. The closer to zero $SD(f)$ is, the more stationary the signal. Stationary signals should have horizontal contours in the TKS. Using the TKS, we can derive the energy fluctuation on the signal $x(t)$, which is given by the Instantaneous Energy (IE) defined by :

$$IE(t) = \int_0^T K^2(t,f)df \tag{IV.9}$$

The function $IE(t)$ is an indication of energy fluctuation with time being weighted by the TKS localized energy over the entire set of sifted IMFs.

IV.3.1 TKS generation

The generation of the TKS could be summarized in two steps. First, the EMD breaks-down the original signal into a set of IMFs, and secondly, these components are used for generation of 3D plot, which is the TKS. The plot represents the variation of frequency and amplitude (or energy) of IMFs over time. Frequency and amplitude of each IMF are obtained by the ESA. Then, the function $K(t,f)$ is generated as follows :

1. Extract IMFs from input signal.
2. Estimate the instantaneous attributes $(a_j(t), f_j(t))$ of j^{th} IMF.

[1]By definition: A time integration of the Hilbert spectrum (HHT) is a reduced frequency-energy representation and is defined as the marginal spectrum [66].

3. Generate a 3D plot, $K(t, f)$, where the amplitude is contoured in the TF plane.

Like the Hilbert spectrum (or HHT), the TKS does not define an explicit equation that maps a 1D signal into a 3D representation that provides information about time, frequency and amplitude (or energy).

IV.4 Results and discussions

The THT is illustrated by two synthetic signals with IFs laws shown in figures with red color. For each signal, the result of the THT is compared to that of the spectrogram, the scalogram, the WVD, the SPWVD, the reassigned SPWVD and the HHT.

IV.4.1 Example 1: Hyperbolic frequencies law

The signals in this section and others signals are generated by the MATLab Toolbox [5]. To compare easily the results given by the TFR, we plot in each one the real frequency laws in red color. The first demonstration is done on FM signal having two hyperbolic frequencies laws, such signal are often used in RADAR and SONAR systems for the detection and localization of targets [56]. One can also use such signals for localizing the position of target [81].

The first TFR applied for analyzing the signal is the spectrogram defined by equation (I.5). The spectrum illustrated in figure (VI.14.a) shows an acceptable fit between the real law and the calculated spectrum, but this one, as it is clear in the plot, lacks accuracy. Even if the calculated spectrogram of the signal includes the real law, and this fact lets one thinks that the spectrogram in this case could localize easily the frequency law. In fact, in practice this task can be more complicated. Indeed, in this example the first attempts to calculate the spectrogram was very disappointing. One has to correctly adjust some parameters. Figure (VI.14.b) shows the spectrogram of the signal where the length of the window (h) is chosen arbitrary, the number of overlaps samples in each segment of signal has not be fixed adequately, and the number of frequency points used to calculate the discrete FT is too large. Here, we point out these technical issues, because these last are usually a source of confusion and lead to a bad interpretation of the resulting spectrum. We can make the same remarks for scalogram, where the Daubechies wavelets used as basis of decomposition are not able to represent the signal. Consequently, the signal spectrum is not well represented (Fig. VI.14.d). To improve the result, instead of

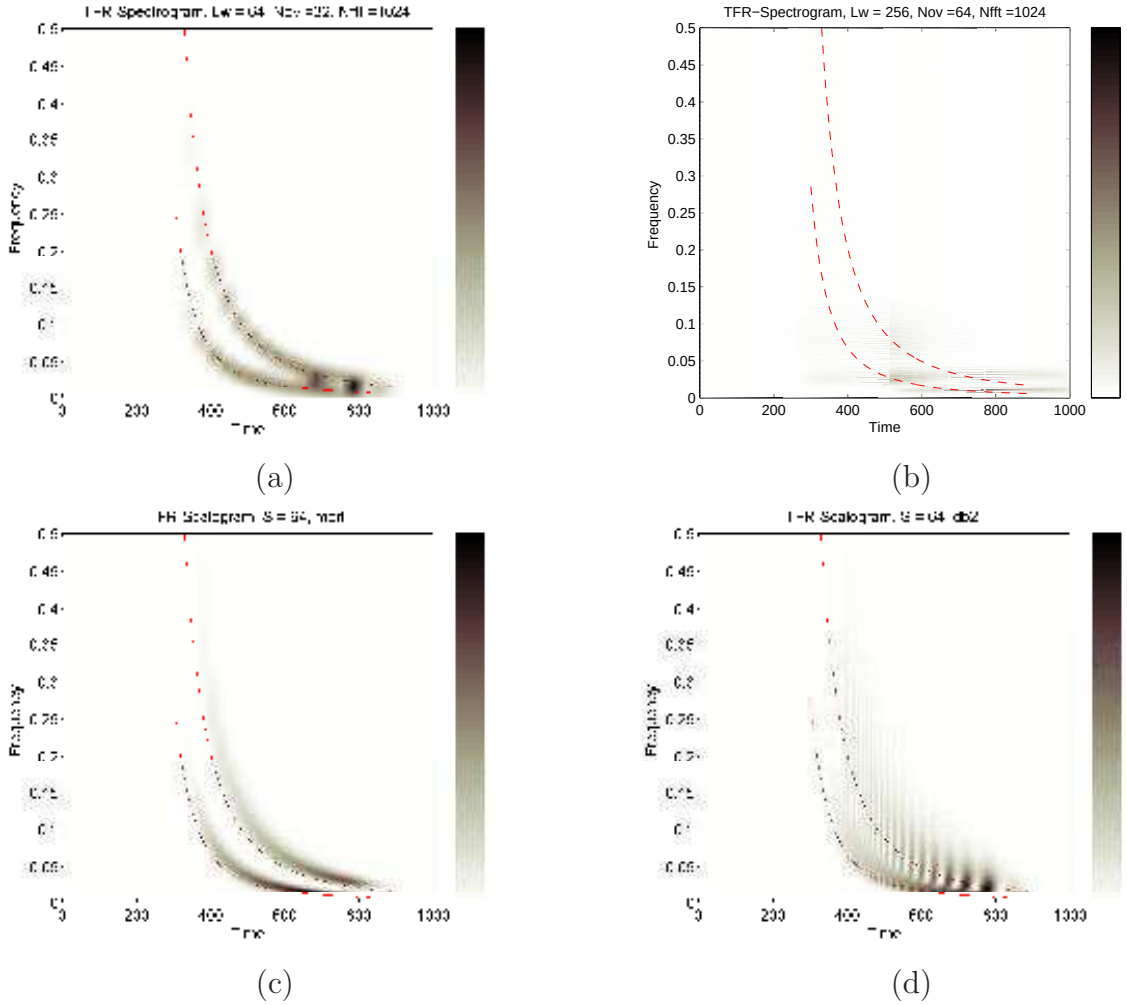

(a) (b)

(c) (d)

Figure IV.3: TFRs of the signal $s_1(t)$. (a) Spectrogram with Length of window ($Lw = 64$), number of overlaps samples in each segment of signal ($Nov = 32$) and number of frequency points ($Nfft = 1024$) (c) Spectrogram ($Lw = 256$, $Nov = 64$, $Nfft = 1024$) (d) Scalogram performed by Daubechies wavelet (db2) and in scales $S = [1 : 64]$ (d) Scalogram (Morlet, $S = [1 : 64]$). The red dashed line corresponds to the real frequency law.

the Daubechies wavelet we use the Morlet wavelet. In figure (VI.14.c) the shape of the frequency law has been smoothed, but the estimated frequency law remains far from the analytic one.

The TFR provided by the WVD (Eq. I.9) is shown in figure (IV.4.a). Except the cross terms, the additional patterns in form of wings observed around the real laws (Fig. IV.4.a), the WVD improves the result given by the spectrogram and the scalogram. Furthermore, the window issue cited above is partially resolved. Moreover after setting some parameters the SPWVD (Eq. I.10) has recovered the frequency law and the cross-terms has been reduced (Fig. IV.4.b). But the choice of the parameters such as time and frequency windows (g,h) and their adequate

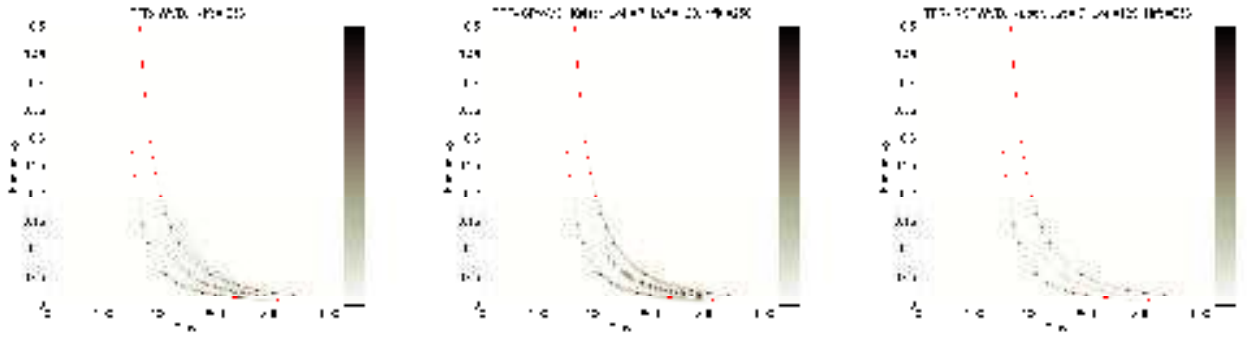

(a) (b) (c)

Figure IV.4: TFRs of the signal $s_1(t)$. (a) WVD. (b) SPWVD. (c) RSPWVD. The red dashed line corresponds to the real frequency law

lengths bring new difficulties. In this example, the Kaiser window among others has sufficiently improved the results but other windows could be used [5]. As a post processing, we can use the RSPWVD (Eq. I.11) to enhance the final results (Fig. IV.4.c).

Even if the results have been improved, neither the SPWVD nor the RSPWVD have been qualified as real TFR, both are postprocessing and are irreversible transforms [32].

The extracted local oscillations (IMFs) of $s_1(t)$ by the EMD are shown in figure (IV.5). IMF1 and IMF8 denote the highest (fast oscillation) and the lowest (slow oscillation) components of $s_1(t)$, respectively. The last component in the figure corresponds to the global trend of $s_1(t)$.

By means of some adjustments, all the previous TFRs could identify frequency components. However, only the HHT (Fig. IV.6.a) and the THT (Fig. IV.6.b) correctly separate the two hyperbolic FM signals. Even the SPWVD and the RSPWVD perform better than the spectrogram, the scalogram and the WVD, in term of separation, show cross-terms around the mean values of the two hyperbola. The cross-terms localization is depending on the frequency components repartition in the TF plane of the analyzed signal. Larger is the cross-term, worst is the resolution. For example, for the WVD, the loss of resolution is visible in time between $t = 870$ and $t = 900$, and in frequency between $f = 0.15$ and $f = 0.5$ for first hyperbola, and between $f = 0.3$ and $f = 0.5$ for second hyperbola. Comparing the THT and the HHT to other TFRs, it is easy to see that for the THT and the HHT both components are well localized with no cross-terms. For the first hyperbola there is a loss of TF resolution between $f = 0.24$ and $f = 0.5$, while no loss of TF resolution cab be found in the second hyperbola.

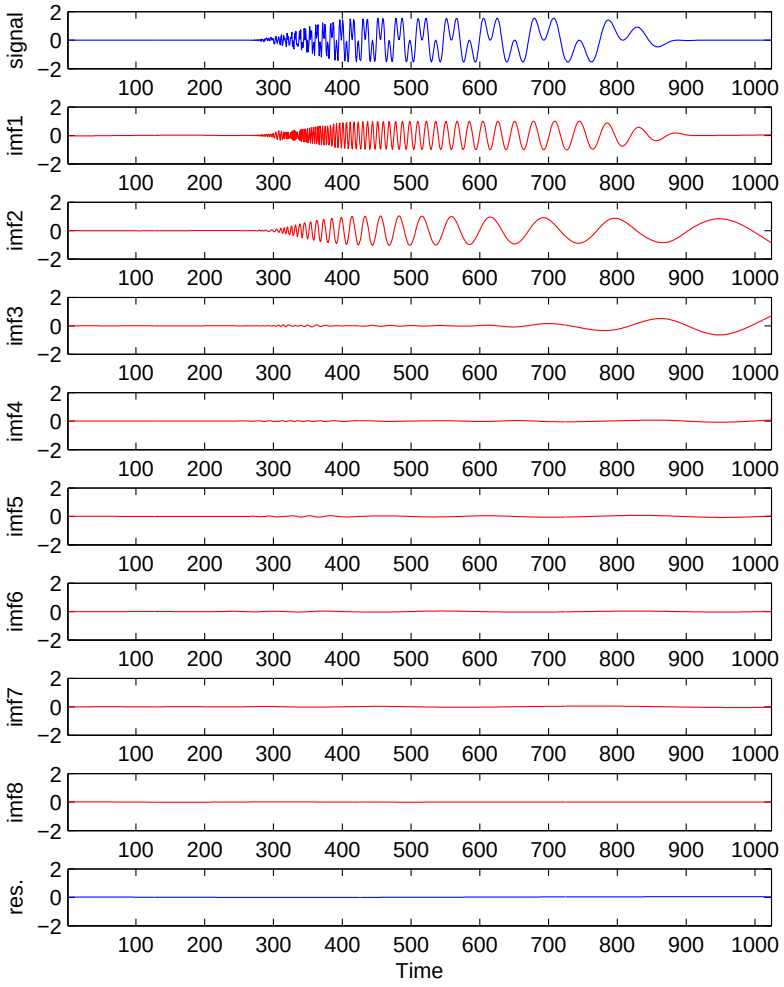

Figure IV.5: Decomposition of the signal $s_1(t)$ by EMD, the signal is plotted in the first row, the IMF1 to IMF8 correspond to the rows 1 to 8, respectively. The last one is the residue.

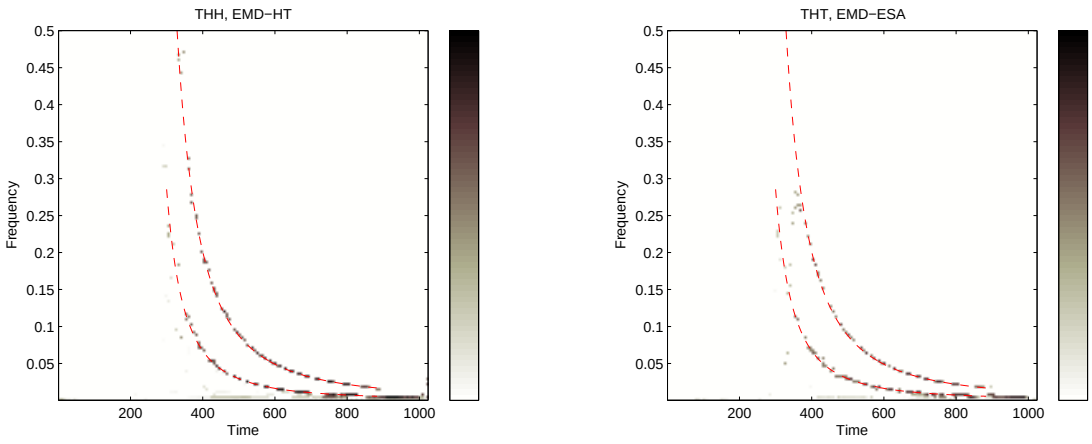

(a) (b)

Figure IV.6: TFRs of the signal $s_1(t)$., (a) EMD-HT. (b) EMD-ESA. The red dashed line correspond to the real frequency law

IV.4.2 Example 2: Monocomponent FM signal

The second study case deals with a moncomponent FM signal. The spectrogram of this signal is shown in figure (IV.7.a), after some parameter adjustments have been done for this signal ($Lw = 32$, $Nov = 16$, $Nfft = 256$), we have finally recovered approximately the real frequency law. We have the same situation with the scalogram (Fig. IV.7.b). The detection of the real frequency law could not be automatically obtained without parameter adjustments; the Morlet Wavelets being chosen for the analysis. The estimated spectrum by the scalogram has bad resolution compared to the spectrogram and lacks of accuracy. The SPWVD (Fig. (IV.7.c)) easily identifies the FM law. Expect at the beginning and at the end, the real and the calculated spectrum are globally similar. The Reassigned version (Fig. IV.7.d) has effectively compensated shortcomings of the SPWVD. The RSPWVD has a smoothing effect on the TF plot and shifted the calculated spectrum to be close to the real FM law.

The HHT tracks directly the frequency component without any parameter adjustments. However, poor resolution is observed in the end points of the signal. Generally, the estimated instantaneous phase by the HT suffers from this problem. Globally the frequency law is correctly identified by the HHT. However, the best result is provided by the THT. The estimated spectrum represents perfectly the real frequency law. This is mainly due to the instantaneous nature of the TKEO that is well dedicated to estimate instantaneous measures such as the IF function.

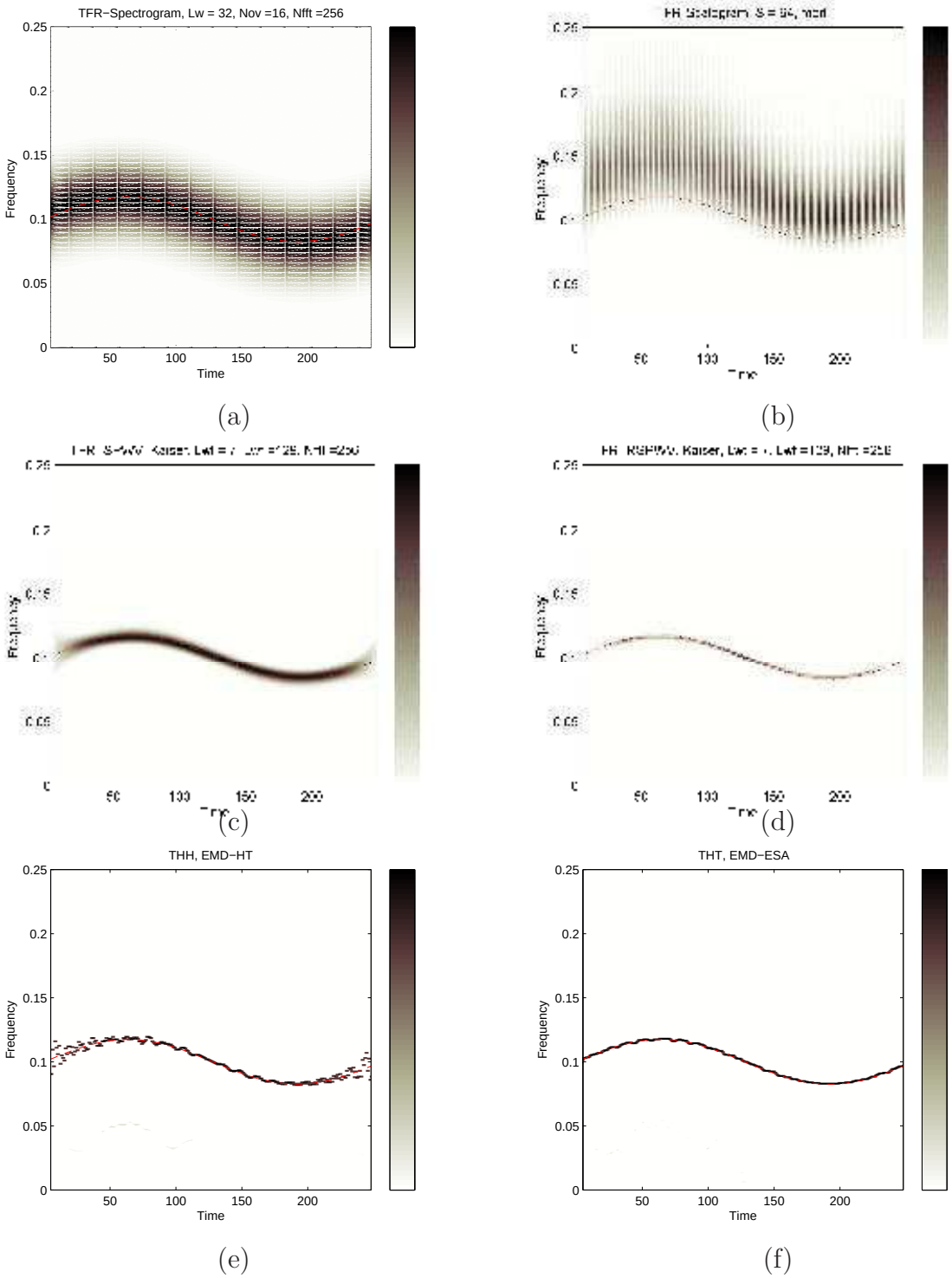

Figure IV.7: Spectrum analysis of $s_2(t)$, (a) Spectrogram. (c) Scalogram. (d) SP-WVD (e). RSPWVD (a) EMD-HT. (c) EMD-ESA. The red dashed line corresponds to the real frequency law

A comparative summary of Fourier analysis, WT and THT analysis is given in table (Tab. IV.1). This table shows that the THT is powerful tool for analyzing nonstationary signals derived from linear or nonlinear systems. The THT is based on adaptive basis (data driven approach) derived from the signal itself. The IF or IA are derived by differentiation rather than convolution and therefore the method is not limited by the uncertainty principle. The results of the THT are presented in time-frequency-energy space for feature extraction.

IV.5 Conclusions

From the obtained resulted we confirm that the STFT, the WT and the WVD are well dedicated for analyzing nonstationary signals. However, both spectrogram and scalogram remain parameters dependent. The quality results of such methods depends on adaptation of the parameters (windows length, nfft, mother wavelet, etc) to each analyzed signal. Thus these methods are not data driven approaches compared to the THT. The obtained results also show the interest of the THT as a TFR. The THT has some shortcomings, like others approaches. First, It can not analyse adequately all type of signal, main problem the number of IMFs extracted by EMD is proportional to the number of the original signal samples, that is mean, if the original signal has not suffisant quantity of samples, the EMD is not able to extract all the components composing the signal. Second, Even if the smoothed B-splines functions have improve the conventional EMD in noisy environment (Gaussian Noise), but we can not confirme this result for other type of noise. So this point can be investigated in future work. However, compared to the WVD and the WT, the THT possesses more traits: fine TF resolution and free of cross disturbance item of WVD. Furthermore, we do not need the model of the narrow-band components (IMFs) and their number. Time resolution of the representation can be as precise as the sampling period. More particularly, results of the THT are not prejudiced by predetermined basis and/or sub-band filtering processes. The THT identifies, in all studied signals, the TF structures with few loss of TF resolution and the obtained spectrum show that the THT is able to track the time-varying characteristic of the signals. Also, the obtained results show the interest to combine two local and nonlinear approaches, the EMD and the TKEO, to process non-stationary signals. However, a large class of synthetic and real signals are necessary to confirm these findings. Based on the EMD, the THT shares the same limits. These shortcomings are essentially due to two factors: a) the EMD is just defined by an algorithm (sifting) and b) the data driven nature of the approach. The sifting depends on the interpolation process and on the size of the standard deviation threshold, SD, which is used to determine the

end of the sifting cycle. As consequence: the modes are not orthogonal but nearly orthogonal and in certain cases the sifting does not produce components that satisfy the requirements of an IMF. B-spline fitting used can create distortion near the end points. Thus, the end effects in splitting need improvements.

	Fourier	RTFs of Cohen class	THT
Basis	a priori	a priori	a posteriori adaptive
Theoretical base	complete mathematical theory	complete mathematical theory	empirical
Frequency resolution	convolution over global domain, uncertainty issue	convolution over global domain, uncertainty issue	instantaneous certainty and physical meaning
Nonlinearity	no	no	yes
Nonstationarity	no	yes	yes
Representation	energy in frequency plane	energy in TF plane	Amplitude or energy in TF plane
Feature extraction	no	discrete, no; continuous, yes	yes

Table IV.1: Proprieties comparison of Fourier analysis, TFRs of Cohen class and THT.

CHAPTER V

Teager Huang Hough Transform

Contents

V.1 Introduction 103

V.2 Hough-Transform 103

V.3 THT and Hough-Transform: THHT 104

V.4 Detection in noise free environment 106

V.4.1 Results 106

V.5 Detection in noisy environment 109

V.5.1 EMD denoising 109

V.5.2 Results 113

V.6 Conclusions 122

In this chapter a formulation of the detection problem of Linear FM (LFM) signals (mono- or multicomponent) in the TF plane of the THT is presented. The detection scheme combining the THT and the Hough Transform ($H_g T$) is termed the Teager-Huang-Hough-Transform (THHT). The input signal is mapped into TF plane using the THT followed by the application of the $H_g T$ to recognize TF components. LFM components are detected and their parameters estimated in terms of peaks and their locations in the parameter space. The advantages of the THHT over the $H_g T$ of the WVD are 1) a detection and estimation free of cross-terms and 2) good time and frequency resolutions. No assumptions are made about the number of components and their models. The THHT is illustrated on multicompoent LFM signals in free and noisy environments and the results compared to WVD-$H_g T$ and the PSWVD-$H_g T$.

V.1 Introduction

Linear Frequency Modulated (LFM) signals or commonly known chirp signals are frequently encountered in many applications such as Radar, Sonar and telecommunications. Thus, the detection and the estimation of such signals are of great importance. Different strategies have proposed for chirp detection. Although, the generalized likelihood ratio test has been reported to be optimal for chirp detection [74], it requires too much computational complexity to support practical applications [51]. Methods based on Maximum Likelihood (ML) estimator [1],[40] are also used but heavy computational complexity is generally needed for high estimation accuracy [80]. TF based methods have been reported to be effective for detecting and estimating LFM signals [6]-[2]. These techniques have attracted considerable attention and prove themselves to be effective among others [112]. The first TF approach involved spectrogram [2]. However, the spectrogram suffers from the fixed time and frequency resolution due to the fixed window length and is not a totally interferences-free representation [54] which limited its application to LFM detection. The WT can also be used for LFM detection because it is not limited by the fixed window constraint. However, it suffers from some interferences and has a poor frequency resolution [54]. Due to its high TF localization, the WV is optimal in the sense of maximum energy concentration about the IF, for LFM signals [54]. For such signals, the VWD detection approach computes the line integral of the WVD along all the lines the TF plane. The line that produces the maximum value corresponds to the ML estimate of the linear IF of the chirp. Thus, the principle of the method is to track straight lines in the TF plane into locating maxima in two-dimensional (initial frequency versus chirp rate) plane [112]. This tracking can be obtained by combining the WVD with $H_g T$ [6] or with Radon transform [114]-[112]. As previously mentioned, the WVD suffers from high interferences (cross terms) which always occur midway between each pair of signal components, whether the auto-WVDs overlap or not.

V.2 Hough-Transform

$H_g T$ is a feature extraction technique essentially used in image processing for detecting geometric curves (lines, circles ...) in binary point images such as object detection [57], [67],[43] and texture analysis [73]. The Cartesian representation $y = ax + b$ of a line is generally clumsy [43] because it has the disadvantage that both the slope and intercept tend to infinity as a line approaches the vertical. For computational reasons, it is therefore better to parameterize the lines in the $H_g T$ with two polar

parameters commonly referred to as ρ and θ [43]. The key idea is to project pixels of a given image into a parametric space where the shapes can be represented in a compact way. In this case, each point (x_i, y_i) in the image plane is transformed into a polar parametrization:

$$H_gT(x_i, y_i) = \rho = x_i \cos\theta + y_i \sin\theta \tag{V.1}$$

This parametrization specifies a straight line by the angle θ of its normal and its algebraic distance ρ from the origin. For each point (x_i, y_i) of an image, the H_gT associates a sinusoid in the plane (ρ, θ), whose points have an amplitude equal to the intensity of the pixel (x_i, y_i). If N points are concentrated along a straight line in the time-frequency domain, they will correspond to N sinusoidal curves intersecting at the same point in the (ρ, θ) domain (Fig. V.1). The integration along the line produces a maximum and its coordinates in the (ρ, θ) domain are directly related to the parameters of the lines. Thus, the H_gT converts a difficult global detection problem in image domain into a more easily solved local peak detection problem in the parameters space. A comprehensive review on the H_gT can be found in [67], [82], [43].

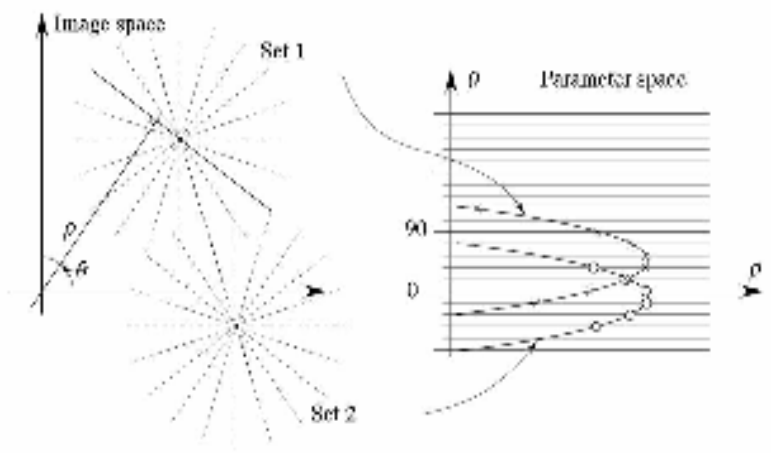

Figure V.1: Illustration of Hough transform

V.3 THT and Hough-Transform: THHT

Different methods have been proposed for LFM component tracking using TFRs [6]-[25]. Thus, TFR is viewed as an image, where the pixel intensity corresponds to the energy presents at a particular time and frequency positions. The combination of the WVD and the H_gT was first presented for chirp identification [6]. The WVD

ideally concentrates the chirp signals in TF plane [32, 25]. FM parameters can be estimated using the $H_g T$ combined with WVD [6], SPWVD [30] or RSPWVD [7]. The principle of the method has been introduced by Kay and Boudreaux-Bartles [75], extended to multicomponent case by Barbarossa [6] and also extended to analysis of constant amplitude signals (the interferences) added to a spread spectrum plus an AWGN by Barbarossa and Scaglione [7]. In general, the detection problem of LFM signal, which is not easy in the time-domain (or frequency domain), is reduced to that of detection of a line in an image. Performing a $H_g T$ in the TF plane, of a signal composed of LFM, gives peaks on the Hough space whose coordinates are directly related to the parameters of the straight lines in the TF image. Although the method is attractive, accurate estimation of FM parameters is not easy due to the cross-terms of the quadratic TFRs (WVD,...), the method has difficulties in practical implementation, and the computational attractiveness of array accumulators of $H_g T$ was not advantageously utilized. The THHT illustrated in figure V.2 is a free of cross-terms TFR and used to detect energy varying linear chirp. When applying the $H_g T$ to the THT of $x(t)$ (Eq. V.2) the output of THHT is an energy TFR:

$$x(t) = e^{2i\pi\left(\nu_0 t + \frac{\beta_0}{2} t^2\right)} \tag{V.2}$$

ν_0 is the start frequency of the linear frequency modulated and β_0 is chirp rate. The comparison of THHT to a threshold is the proposed detection test, and the estimates of the unknown parameters ν_0 and β_0 are given by the coordinates of the peak in the space of the parameters (ρ, θ).

The THHT of a signal $x(t)$ is defined as the line integral through the TK spectrum $K(t, f)$ along the IF model $f(t; \Theta_j)$ where $\Theta_j := (\nu_j, \beta_j)$ is a parameter vector.

$$h(\Theta_j) = \int_{-\infty}^{-\infty} K(t, f(t; \Theta_j)) dt \quad j \in \{0, 1, \ldots N-1\} \tag{V.3}$$

where $f(t; \Theta_j)$ is the parametrized IF and N is the number of components. When dealing with LFM signals, each component gives rise to energy concentration along straight lines in the TF plane of $f(t; \Theta_j) = \alpha_k + \beta_j t$. The integration over all possible lines, obtained by applying the $H_g T$ to the THT gives rise to peaks in the final parameter space. A monocomponent LFM signal corresponds to one peak in the parameter space and a multicomponent LFM signal generates multiple peaks in the parameter space. The THHT $h(\Theta_j)$ is therefore a mapping from the time domain to the parameter space of Θ_j. The detection and parameters estimation is reduced to peaks search in the parameter space. The THHT algorithm involves the following steps:

Step 1) Apply THT to input signal $x(t)$

Step 2) Compute $h(\Theta_j)$ using equation (V.3)

Step 3) Search peaks of $h(\Theta_j)$ which are larger than a predefined threshold.

Step 4) Determine the parameters vectors $h(\Theta_j)$ corresponding to the maxima of $h(\Theta_j)$:

$$(\rho_j, \theta_j) = \underset{\Theta_j}{Arg\,max}\,[h(\Theta_j)]$$

Step 5) Compute the vector parameter Θ_j: $\alpha_j = \dfrac{\rho_j}{\sin\theta_j}$ and $\beta_j = -\cot\theta_j$

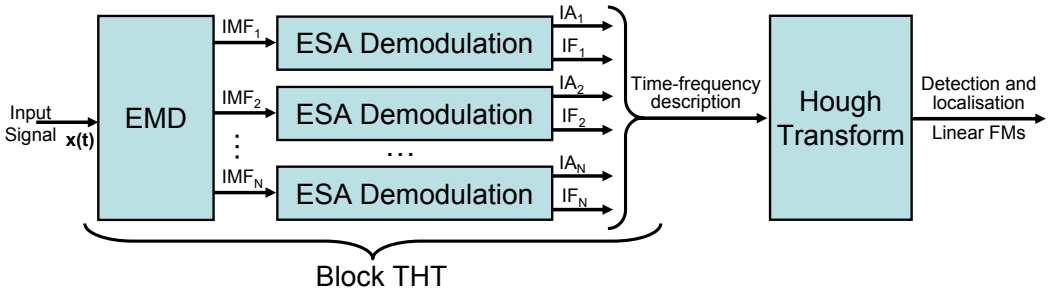

Figure V.2: Block diagram of the THHT.

V.4 Detection in noise free environment

We first test the THHT on free noise signals. THHT is illustrated on two multi-component signals and detection results compared to WVD-H$_g$T and SPWVD-H$_g$T.

V.4.1 Results

The first example is a signal, $x_1(t)$, with four components with observation time $T = 256s$ (Fig. V.3).

The associated THT, WVD and SPWVD are shown respectively in figures V.4(a), V.6(a) and V.8(a). The lines are clearly visible on SPWVD representation and better on THT. For WVD, the detection of the four IFs is not possible due to the interference terms (Fig. V.6(a)). In figure V.8(a), the time smoothing carried out by SPWVD considerably reduces these interferences, but gives the worst resolutions (in time and in frequency). Comparing THT against WVD and SPWVD, the four TF components are well localized with no cross-terms and loss of TF resolution (Fig. V.4(a)). H$_g$T has been applied to these three TFRs. We obtain, in the parameter space (ρ, θ) peaks representing the LFM signals. Both THHT and WVD-H$_g$T show four peaks (Figs. V.5 and V.7). However, the peaks are better highlighted by THHT than by WVD-H$_g$T. A decision test has been

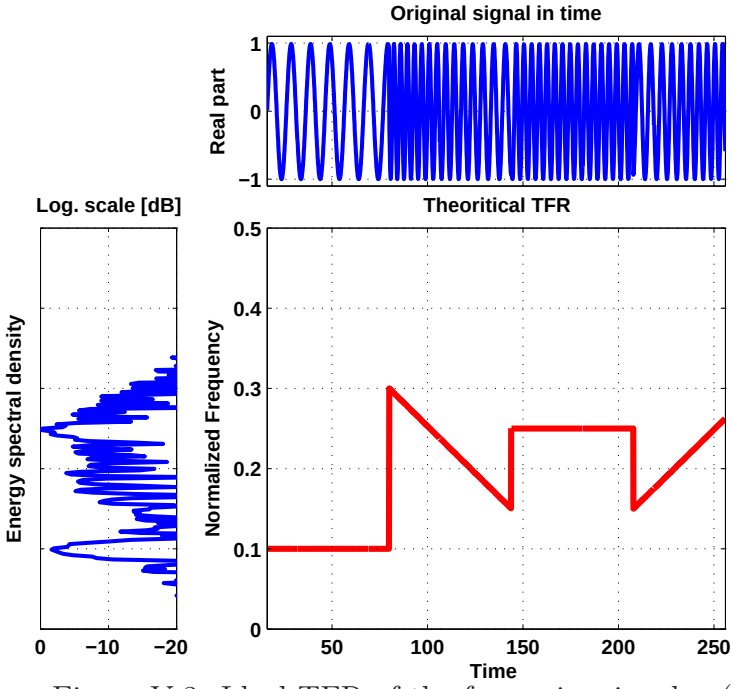

Figure V.3: Ideal TFR of the free noise signal $x_1(t)$.

used : it consists in applying a threshold on this representation; if the peak is higher than the threshold, then the linear chirp is present, and the peak coordinates in accumulation array $(\tilde{\rho},\ \tilde{\theta})$ provide estimates of the IF parameters $(\tilde{\nu},\ \tilde{\beta})$ [43]. The estimation of the IFs by THHT, WVD-H$_g$T and SPWVD-H$_g$T are shown respectively in figures V.4(b), V.6(b) and V.8(b).

Due to the oscillating structures of cross-terms, the detection of peak by H$_g$T on WVD is difficult (Fig.V.6(b)). While SPWVD reduces the cross-terms and gives a better TFR, estimation of different IFs remain difficult (Fig. V.8(b)). For THHT, the TF components are well separated in the parameter space (Fig.V.5). Comparing THHT against WVD-H$_g$T, the four TF components are well detected and estimated (Fig. V.4(b)).

THHT has also been tested on a multi-component signal, $x_2(t)$, of seven linear chirps and sinusoidal chirp in the TF domain (Fig. V.9).

The SPWVD and THT are shown in figures V.10 and V.11. While the different components are hardly readable in the time representation, they appear in SPWVD and are better evidenced in THT. Again, as in the first case the interferences problem is more important as the number of signal components increases and this is well evidenced on the output of SPWVD (Fig. V.11(a)). So, the sinusoidal FM component in SPWVD is represented as a LFM signal (Fig. V.11(b)). Note that

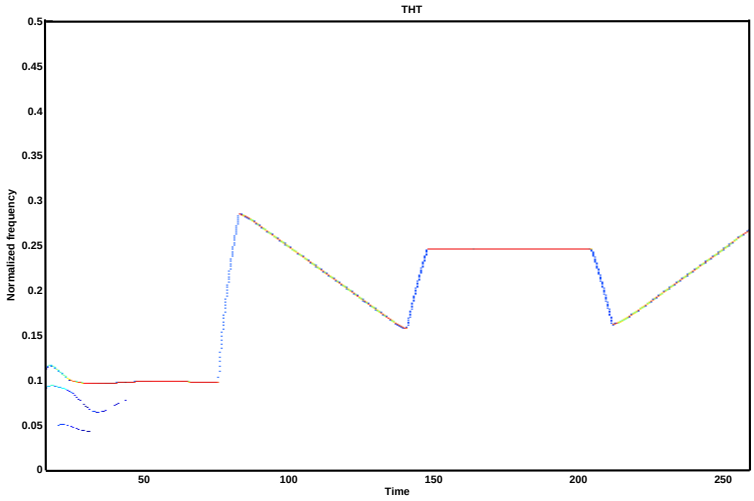

(a) THT of $x_1(t)$

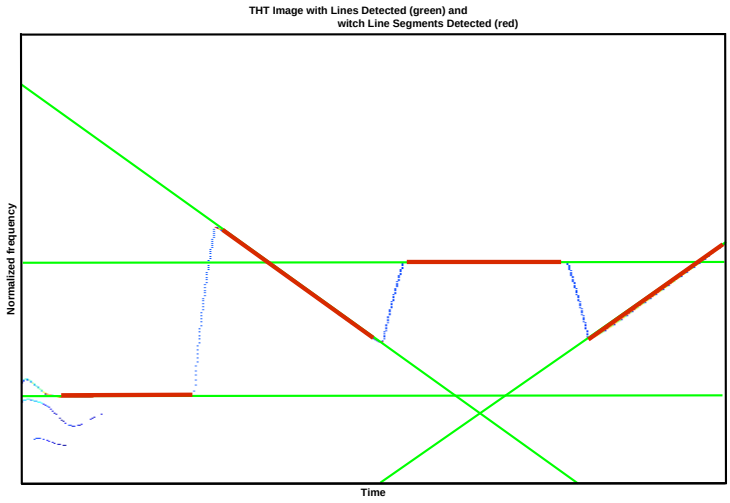

(b) Lines detection on THT.

Figure V.4: Components tracking in THT plane of $x_1(t)$

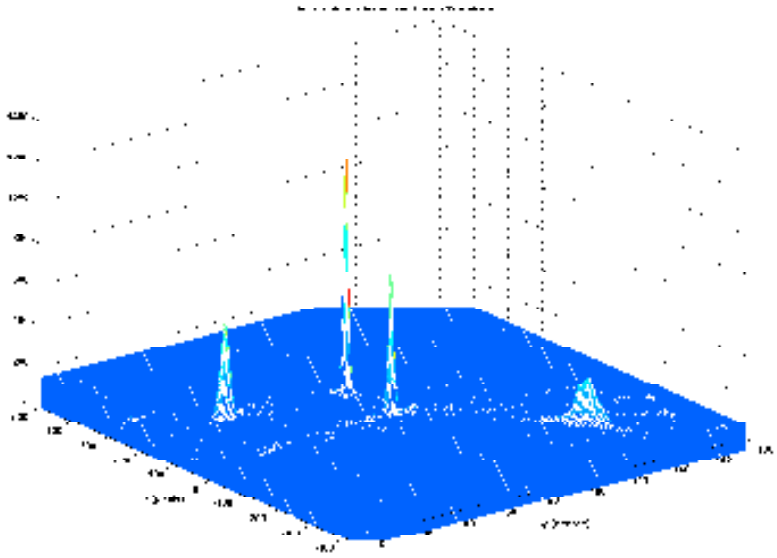

Figure V.5: THHT applied to $x_1(t)$.

THT is devoid of cross-terms effect and all IFs are well localized (Fig. V.10(a). However, SPWVD provides cross-terms and so the detection and estimation of IFs are impossible (Fig. V.11(b)). Comparing THHT against SPWVD-H$_g$T, all linear IFs components are well detected, localized and estimated (Fig. V.10(b)).

V.5 Detection in noisy environment

In many applications, signals enhancement or extraction of signals of interest from noises is necessary. Signals or their components may overlap either in time domain or frequency domain and thus conventional filtering such as time-domain windowing or frequency-domain windowing is not efficient. A solution to this problem is to use a sub-band filtering. In this work we use a data driven time filtering based on EMD where filtering is applied to each IMF extracted from the input signal.

V.5.1 EMD denoising

A denoised version of an input signal can be obtained by filtering each IMF separately followed by signal reconstruction. Let $f_j(t)$ be a clean deterministic IMF. The j^{th} IMF, IMF$_j$, corrupted with additive noise $b_j(t)$ is given by :

$$\text{IMF}_j(t) = f_j(t) + b_j(t)\ , \text{where } j = \{1, \ldots, N\}. \tag{V.4}$$

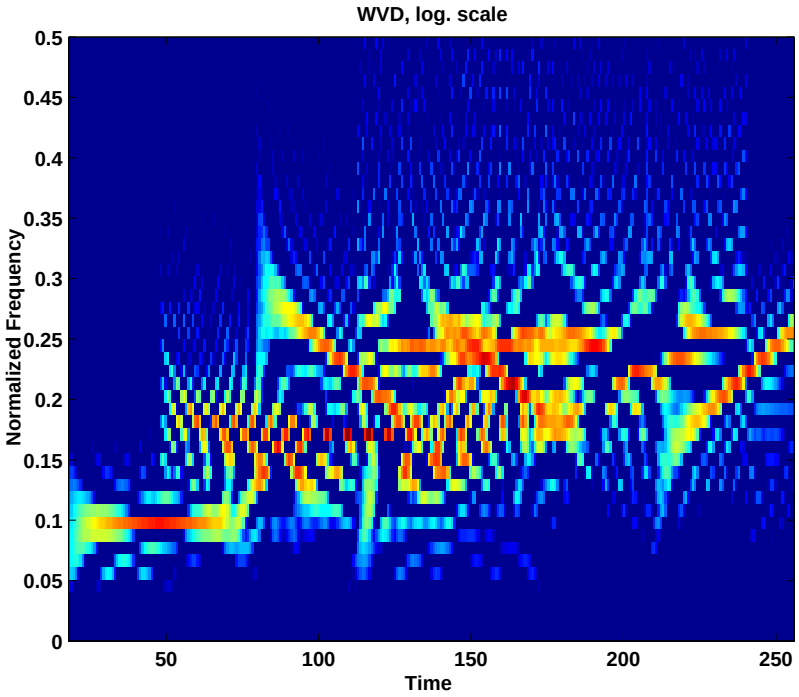

(a) WVD of $x_1(t)$

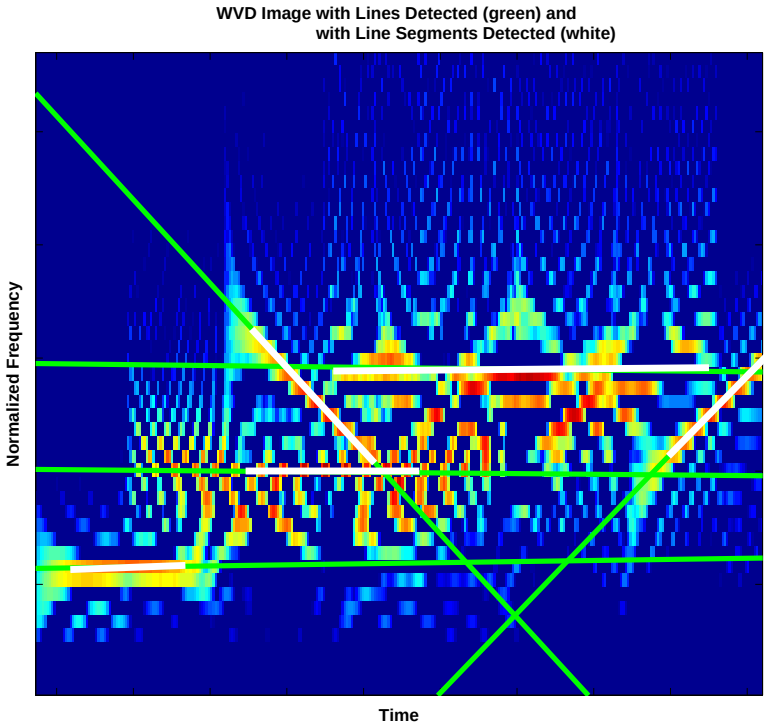

(b) Lines detection on WVD.

Figure V.6: Components tracking in WVD plane of $x_1(t)$

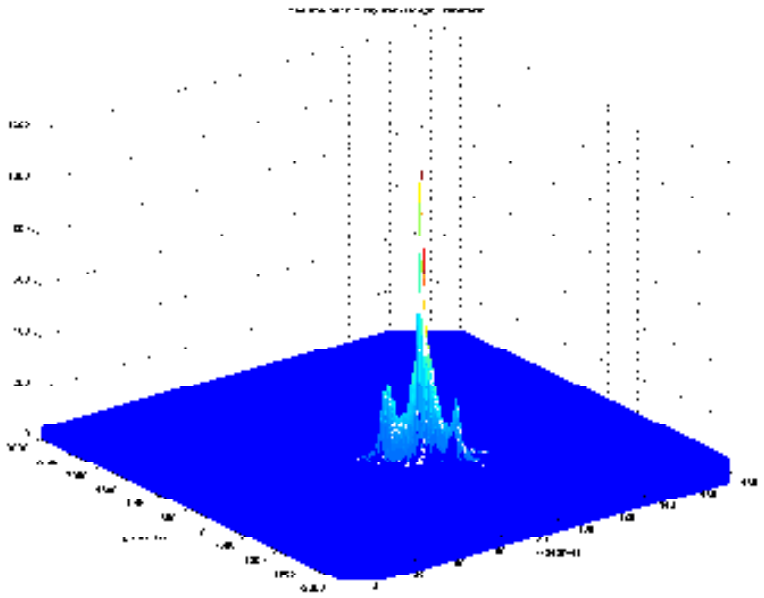

Figure V.7: WVD-H$_g$T applied to $x_1(t)$.

Let $\tilde{f}_j(t)$ be an estimation of $f_j(t)$ based on the noisy observation IMF$_j(t)$. This estimation is given by :

$$\tilde{f}_j(t) = \Gamma[\text{IMF}_j(t), \tau_j] \tag{V.5}$$

where $\Gamma[\text{IMF}_j(t), \tau_j]$ denotes a thresholding or filtering function, defined by parameters τ_j, applied to signal IMF$_j(t)$. The denoised signal $\tilde{x}(t)$ is given by [17] :

$$\tilde{x}(t) = \sum_{j=1}^{N} \tilde{f}_j(t) + r_N(t) \tag{V.6}$$

For noise reduction, the EMD can be combined with a filtering method such as Savitzky-Golay (SG) smoothing (FIR filter) [98] or nonlinear transformation such as the soft-thresholding [41]. If $\Gamma[\text{IMF}_j(t), \tau_j]$ is a filtering method, then τ_j can be the window size of the filter or its kernel used for data smoothing. In this work, we combine the EMD with SG filter which have been shown to be efficient for noise removing [23],[18] (Fig. V.12). SG filter (also called digital smoothing polynomial filter) is time smoothing based on Least Squares (LS) polynomial fitting across a moving window within the data [98]. This filter performs essentially a local polynomial regression on a distribution of a equally spaced points to determine the smoothed value for each data point [98] :

$$\tilde{f}_j(i) = \sum_{m=-M_L}^{m=M_R} \alpha_m.\text{IMF}_j(i+m) \tag{V.7}$$

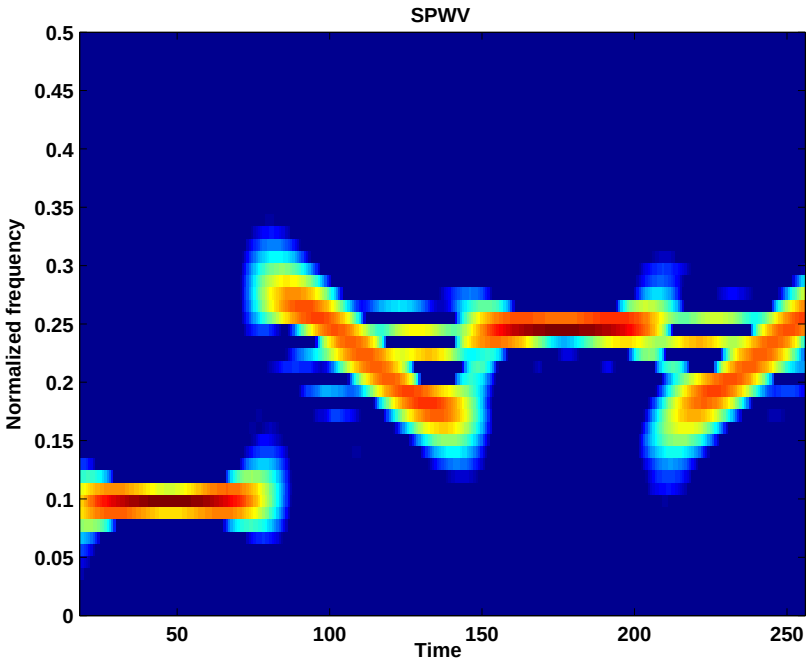

(a) SPWVD of $x_1(t)$

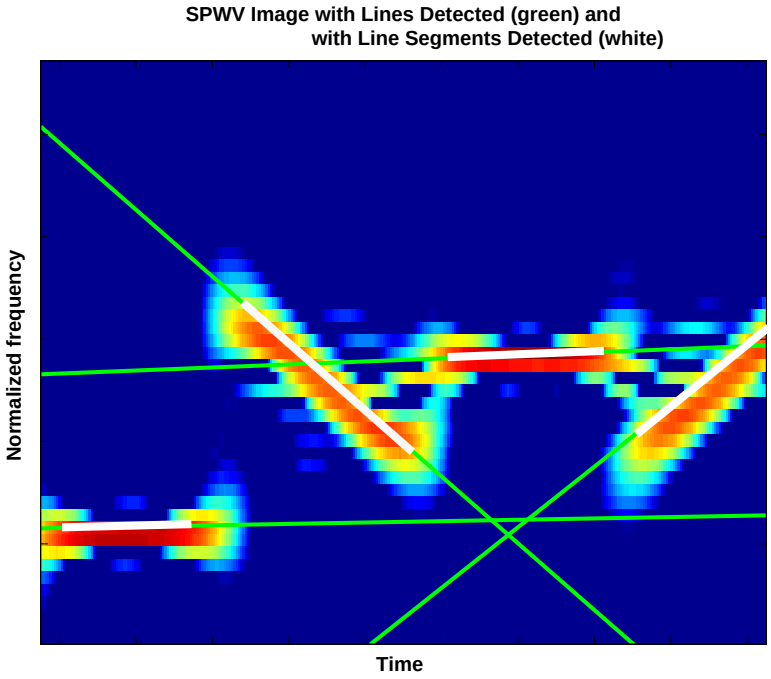

(b) Lines detection on SPWVD.

Figure V.8: Components tracking in SPWVD plane of $x_1(t)$

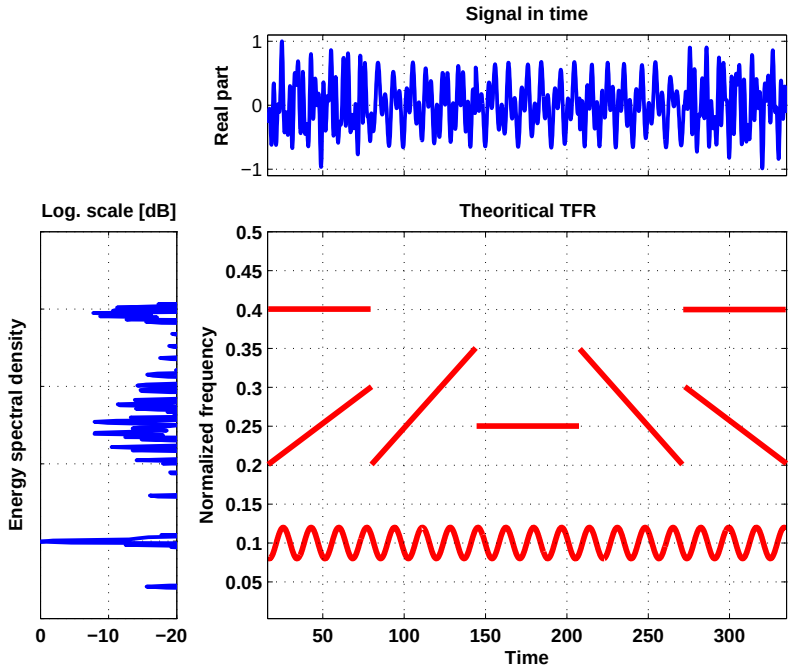

Figure V.9: Ideal TFR of the free noise signal $x_2(t)$.

where $i = \ldots, -2, -1, 0, 1, 2, \ldots$. M_L and M_R is the number of points used to the left and the right of the data point i, respectively. The idea of SG filtering is to find filter coefficients α_m (Eq. V.7) that preserve higher moments within the window of analysis. For each point $\text{IMF}_j(i - M_L), \ldots, \text{IMF}_j(i + M_R)$ are determined by a polynomial of degree p, $\alpha_0 + \alpha_1 i^1 + \alpha_2 i^2 + \ldots + \alpha_p i^p$. The coefficients α_m are given by a LS fit using a shifted windows [98]. SG filter is optimal in the sense that it minimizes the LS error in fitting a polynomial to frames of noisy data. Furthermore, this smoothing filter performs much better than standard averaging FIR filter because it tends to preserve features of the signal such as peak height and high frequency components, which are usually *'flattened'* by other adjacent averaging techniques (like moving averages, for example). SG method was originally designed to preserve the higher moments within time-domain spectral peak data and firstly used for smoothing data in analytical chemistry [98]. In the following, this approach is called EMD_{SG} (Figure. V.12).

V.5.2 Results

We first test the THHT on a simple linear chirp signal $x_2(t)$ (Figure. V.13) embedded in a white Gaussian noise, with a SNR of 30dB with vector parameter $\Theta_0 := (\nu_0 = 0.2, \beta_0 = 0)$ (Eq. V.2). WVD and THT representations are shown in figure (V.14).

Comparing the THT against the WVD, we see that in the THT representation

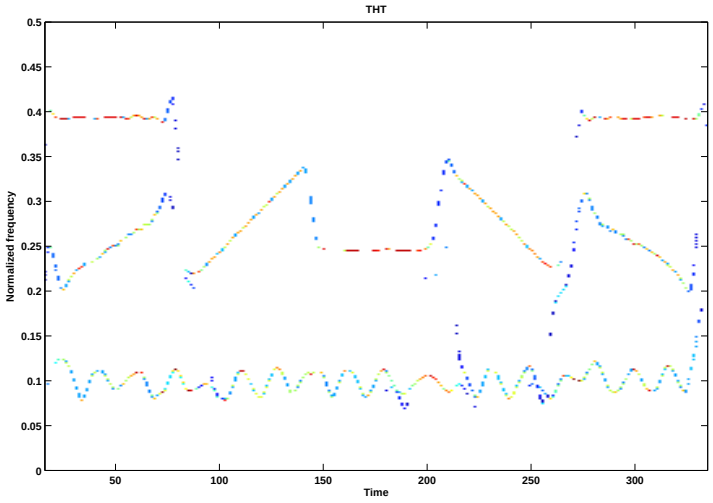

(a) THT of $x_2(t)$

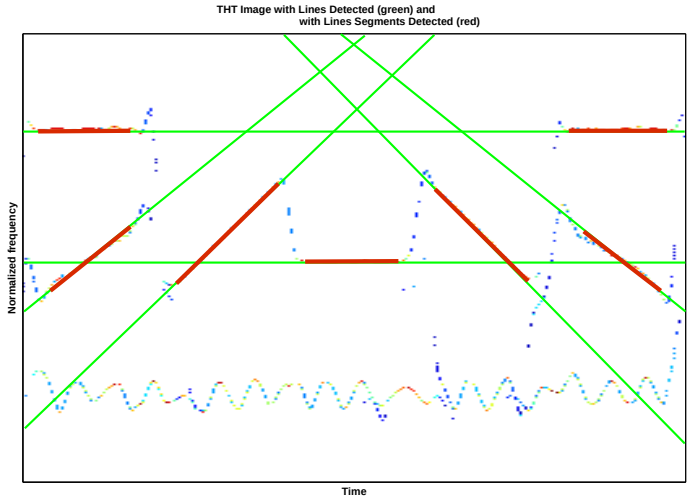

(b) Lines detection on THT.

Figure V.10: Components tracking in THT plane of $x_2(t)$

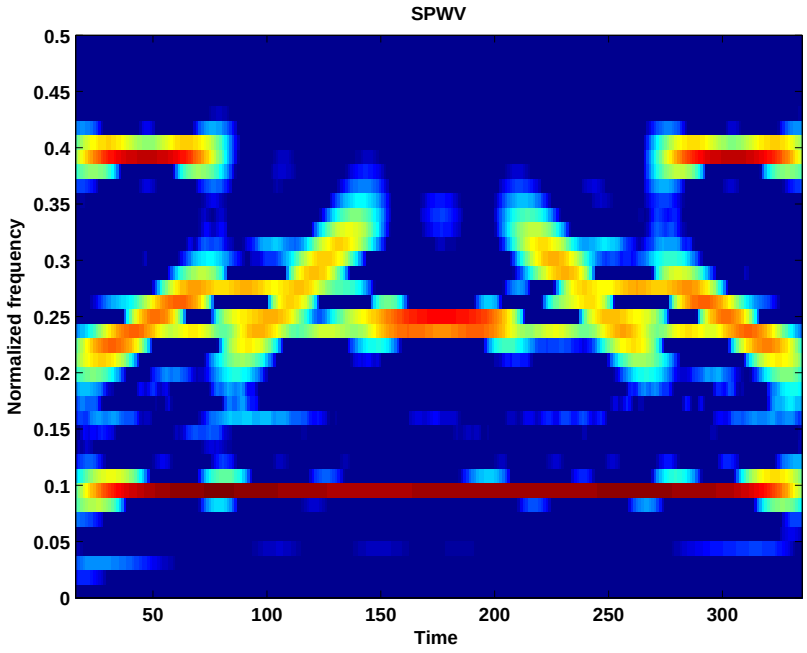

(a) SPWVD of $x_2(t)$

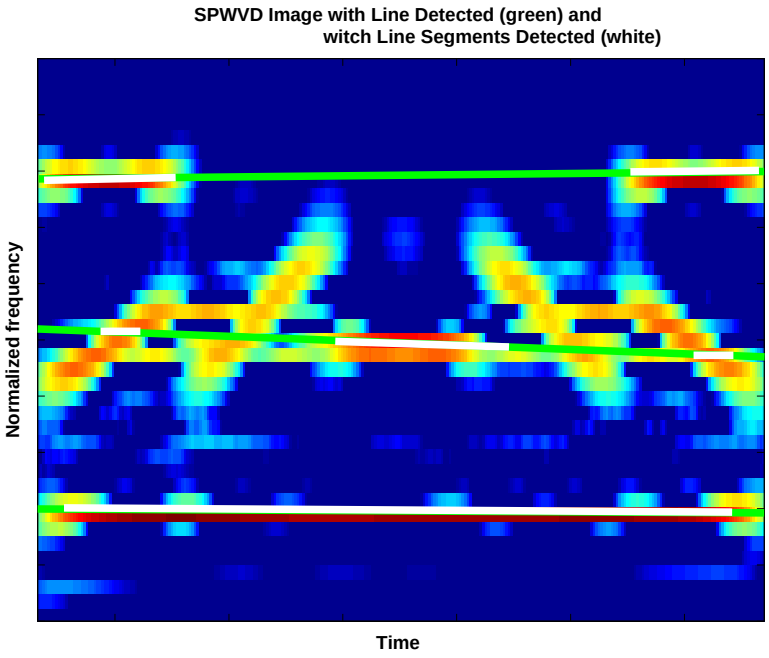

(b) Lines detection on SPWVD.

Figure V.11: Components tracking in SPWVD plane of $x_2(t)$

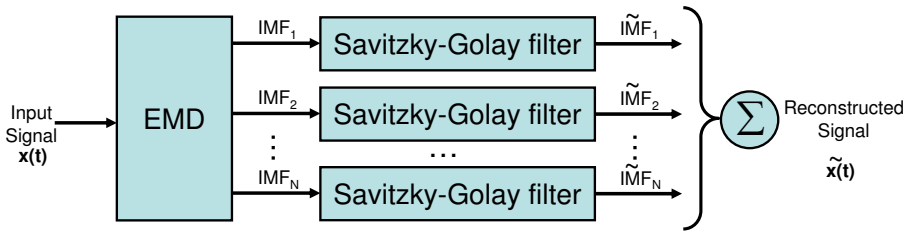

Figure V.12: Block diagram of the $\mathrm{EMD_{SG}}$

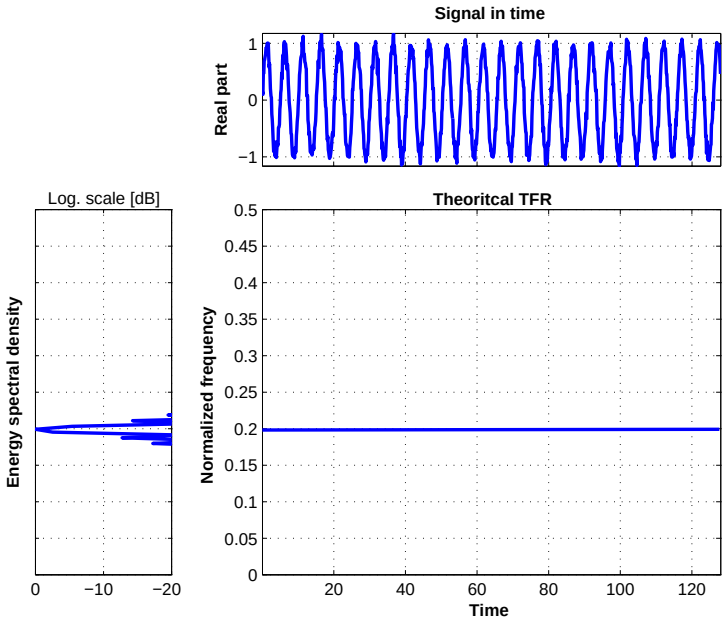

Figure V.13: Ideal TFR of noisy signal $x_2(t)$ (30dB).

the component FI is more localized. The associated $\mathrm{H}_g\mathrm{T}$ applications are shown in figures V.15 and V.16.

The estimation of the IF by THHT and WVD-H_gT are shown in figure V.17. It may be noted that the IF component is very well detected in both representations.

The estimation $(\tilde{\nu}_0, \tilde{\beta}_0)$ of parameter vector $\Theta := (\nu, \beta)$ of signal $x_2(t)$ embedded in a white Gaussian noise is studied with input SNR ranging from 1.5dB to 40dB. We compare the THHT to the WVD-H_gT. For each SNR value, 100 simulations are performed and the average of each parameter calculated (Figures. V.18, V.19). For linear frequency rate $\tilde{\beta}_0$, both methods have the same behavior but the THHT performs slightly better than the WVD-H_gT. The error of estimation is less than 12.10^{-4} and the standard deviations are very low (dot lines in figure V.18). For the start frequency of the parameter $\tilde{\nu}_0$, the THHT gives better result as the SNR increases. Globally, the errors of the THHT and those of the WVD-H_gT have the same magnitudes. Standard deviations of $\tilde{\nu}_0$ are relatively important for THHT

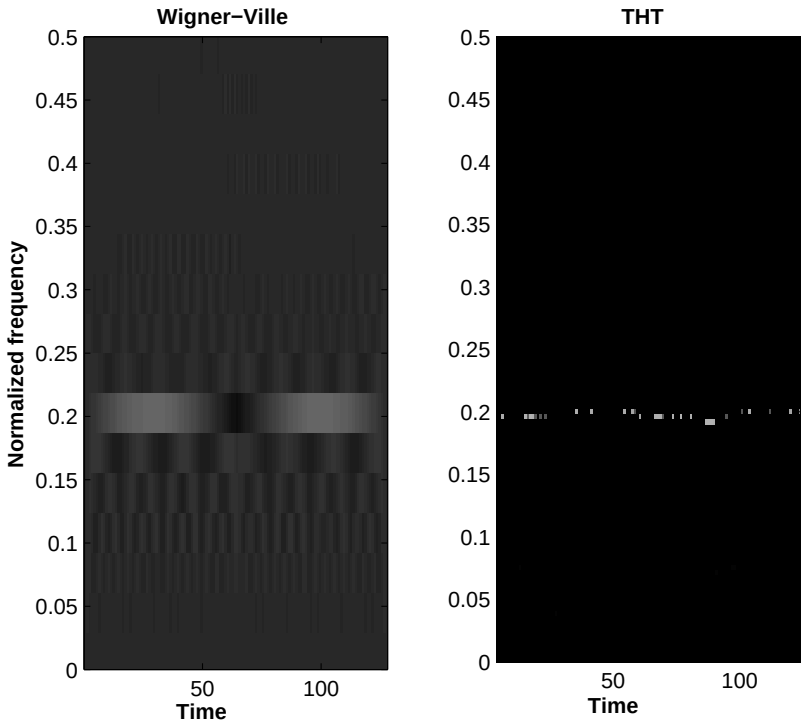

Figure V.14: WVD and THT of $x_2(t)$.

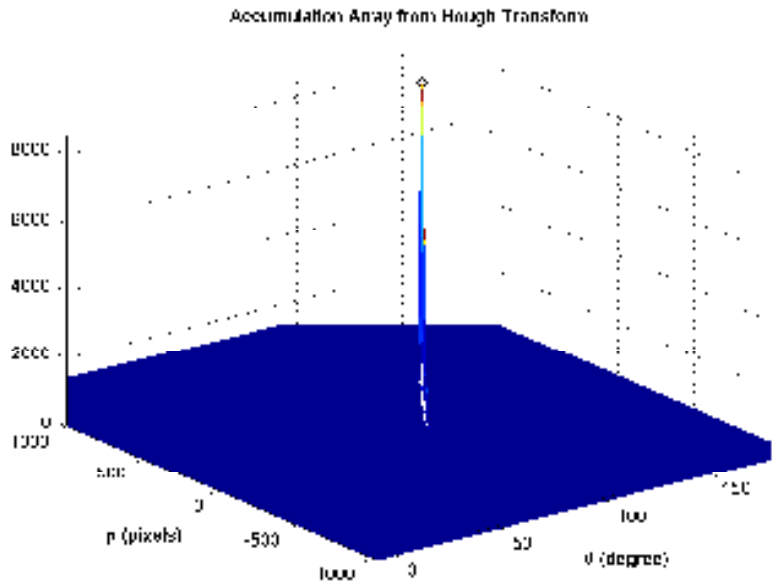

Figure V.15: WVD-H$_g$T applied to $x_2(t)$.

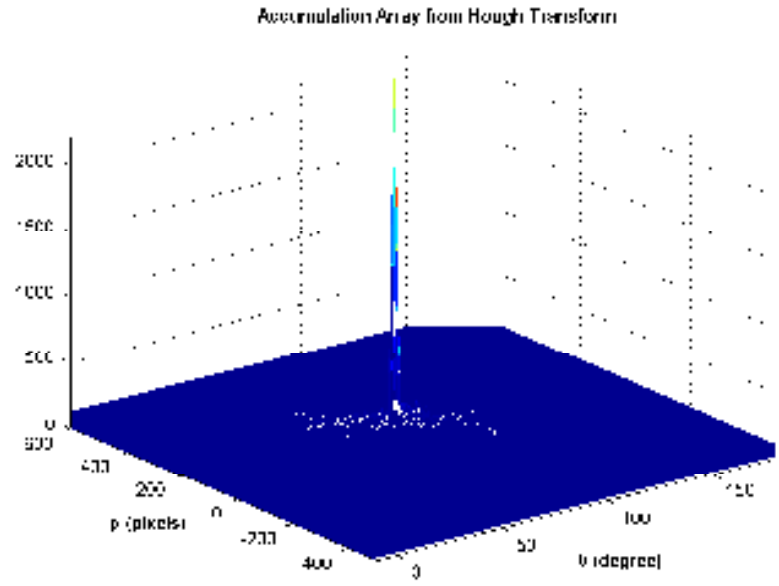

Figure V.16: WVD-H$_g$T applied to $x_2(t)$.

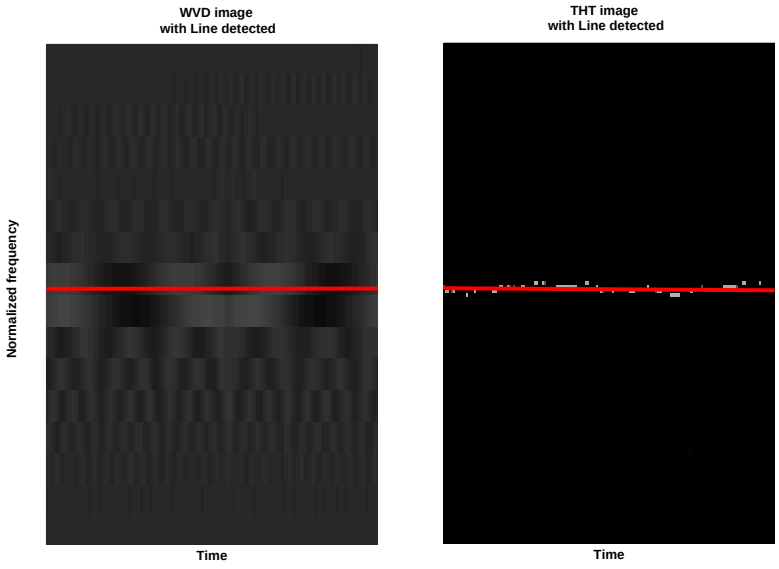

Figure V.17: IF estimation (red) with WVD-H$_g$T (on the left) and THHT (on the right) of $x_2(t)$.

compared to WVD-H$_g$T (dot lines in figure V.19).

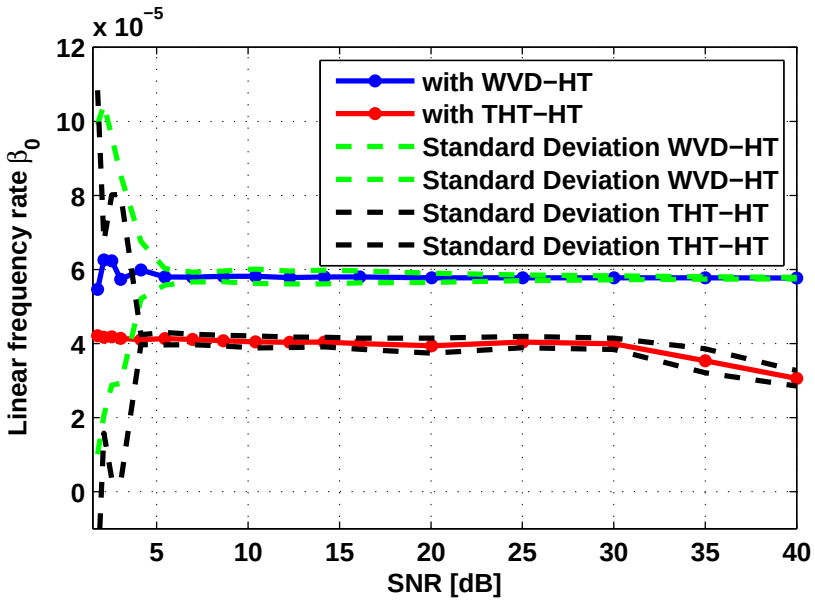

Figure V.18: Estimation of β_0

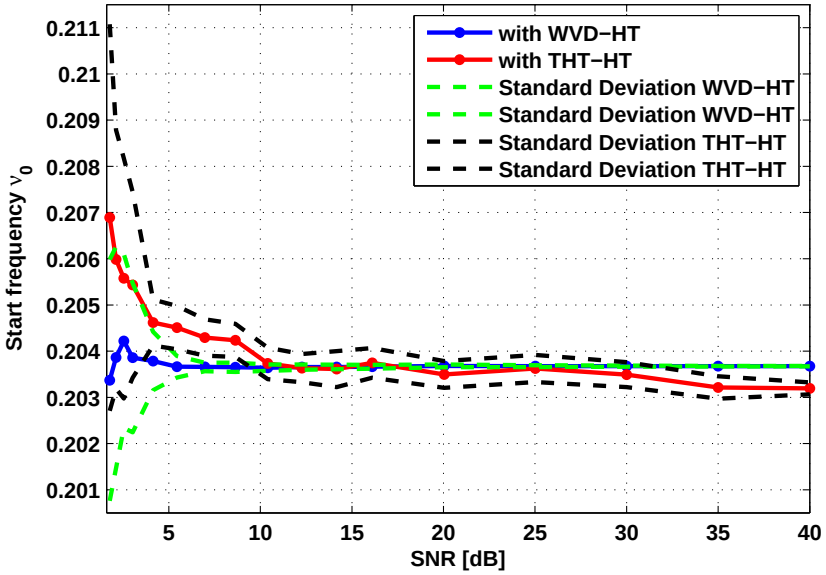

Figure V.19: Estimation of ν_0

The THHT is tested on signal $x_1(t)$ (Fig. V.9) corrupted with additive white Gaussian noise with a SNR of 7dB. The four IFs are evidenced in the two TFRs (Figs. V.20(a) and V.21(a)). The result of detection with the THHT and the SPWVD-H$_g$T are given in figures V.20(b) and V.21(b) respectively. As in the first simulations, the result of the THHT (Fig. V.20(a)) is sharper than that of the SPWVD-H$_g$T (Fig. V.21(a)) which make the detection easier. Both the THHT and the SPWVD-H$_g$T

detect correctly 3 out of 4 of the LFM components (Figs. V.20(b) and V.21(b)). The fourth is no well identified. For THHT, this may be due to estimation of the IF of the IMF by the TEO, which has a moderate sensitivity to noise. For the SPWVD-H$_g$T, despite the smoothing used strong cross-terms persist which degrade the TFR and consequently both detection and estimation with H$_g$T are biased.

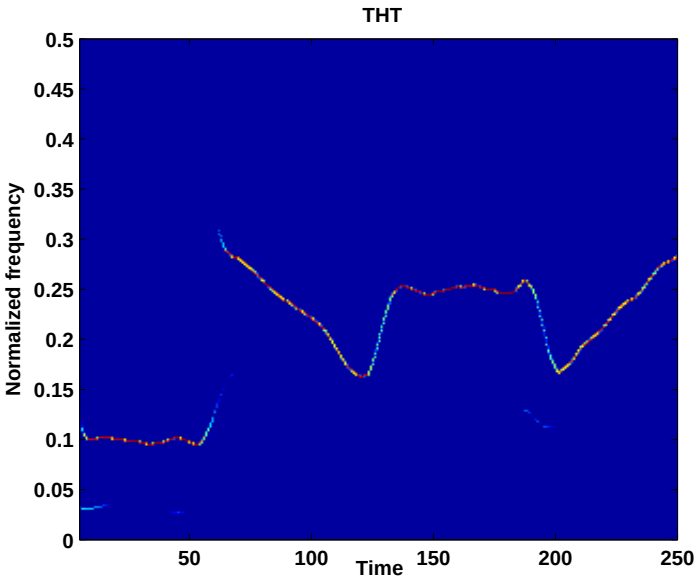

(a) THT of $x_3(t)$

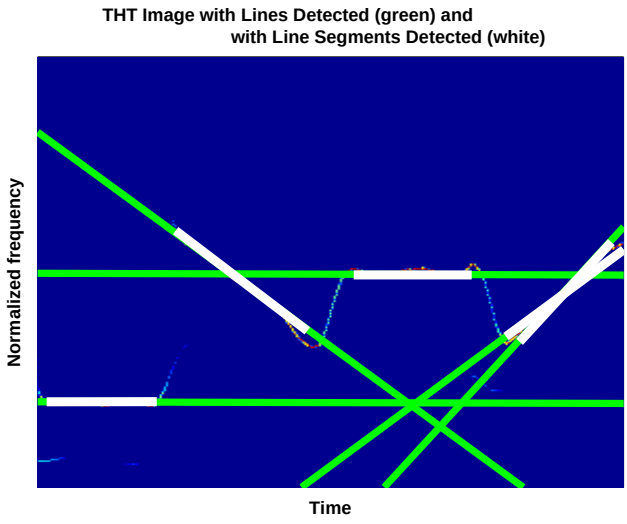

(b) Lines detection on THT

Figure V.20: Components tracking in THT plane of $x_3(t)$ (SNR=7dB)

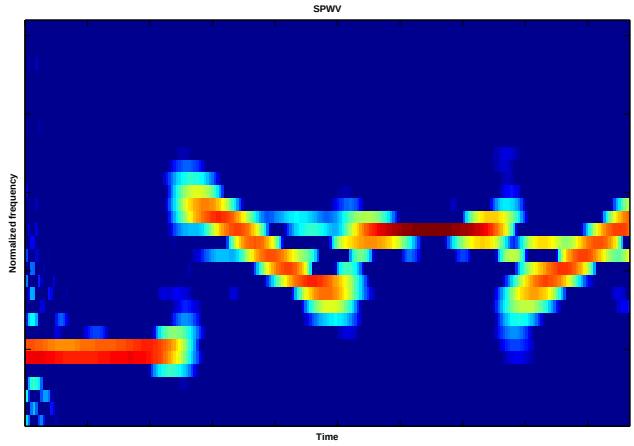

(a) SPWVD of $x_3(t)$

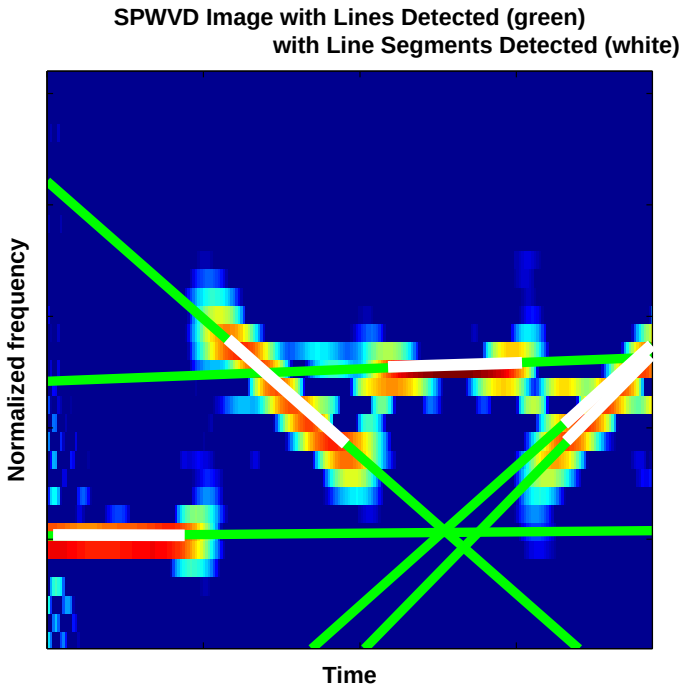

(b) Lines detection on SPWVD.

Figure V.21: Components tracking in SPWVD plane of $x_3(t)$ (SNR=7dB)

V.6 Conclusions

In this chapter a novel detection approach of multicomponent LFM signals in TF domain called THHT is proposed. Preliminary results show the interest and effectiveness of the THHT as tracking method of TF components. The THHT is cross-terms free and does not suffer from the trade-off between time frequency resolution and cross-terms suppression. No assumptions are made about the number of components of the signal nor their amplitude or phase. Numerical examples show that compared to WVD-H_gT and to SPWVD-H_gT, the THHT achieves better performance in terms of TF components tracking of signals in both noise free and noisy environments. Furthermore, the THHT gives results much sharper than those of WVD-H_gT and SPWVD-H_gT. In all presented cases, LFM components are well identified. Since the performance of the THHT has only evaluated by some simulations, a large class of signals (extensive simulations) is necessary to confirm the obtained results. As future work we plan to extend the analysis to more complicated IF laws such as nonlinear FM signals or arbitrary TF shapes. Investigation is in progress to establish a rigorous criterion for thresholding the THHT.

CHAPTER VI

Application to underwater acoustics

Contents

VI.1 Introduction 125

VI.2 IMFs versus physical modes 125

VI.2.1 Physical Modes for a spherical shell 126

VI.2.2 IMFs 128

VI.3 Comparison and discussion 131

VI.4 Backscattering signal analysis 133

Preliminary results of the possibles relationships between the Isolated Modal Resonances (IMRs) of a thin empty spherical shell and the associated extracted IMFs from the acoustic signal backscattered by this spherical shell, are presented. The study is carried out quantitatively and qualitatively. Finally, different TFRs of backscattering signal from simple shells (cylinder) for several physical parameters are analyzed.

VI.1 Introduction

One of the most challenging applications of TFRs deal with the analysis of the underwater acoustic signals. In this work, the THT is illustrated on real world underwater acoustics signals derived from spherical targets which can be viewed as nonlinear systems. Before analyzing the resulted TF maps of backscattering signals by simple shells, we first investigate possibles relationships between Isolated Modal Resonances (IMRs) of a spherical shell and IMFs extracted from the backscattering signal by this shell. Such links between empirical and physical modes, may be useful for Sonar target detection and classification purposes.

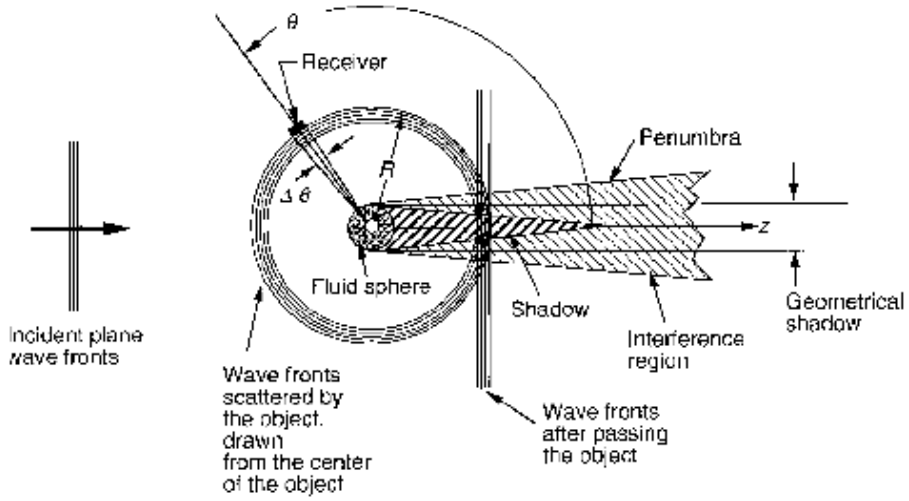

Figure VI.1: Scattering geometry. This cartoon depicts a plane wave, traveling in the z direction, incident upon a fluid sphere (radius a, density ρ_1 and sound velocities c_l c_t), entrained in a second fluid (density ρ, sound speed c). For simplicity, the scattered waves are shown as spherical, which they are in time, although not generally in phase and amplitude. In the forward region, the scattered field and incident field interfere, and may produce a shadow [47].

VI.2 IMFs versus physical modes

The study is conducted using quantitative and qualitative measures. In one hand, it is established that for a single incident pulse, that is short compared to the target physical dimensions, the echo structure of the backscattered acoustic signal from an elastic target consists of multiple periodic pulses [44],[81]. The first pulse is generated by the specular reflection and the subsequent ones are due to the slip and

shock waves corresponding to the creeping and peripheral waves revolving around the target (Fig. VI.2). In the other hand, a new signal processing method, the EMD [64], generates a set of Intrinsic Mode Functions (IMFs) of a signal with separate frequencies components. Even the number of IMFs is a reduced number (Eq. VI.3) and the number of IMRs is an infinite one (Eq. VI.2), the question that can be asked: is there any relationship between IMFs and IMRs?

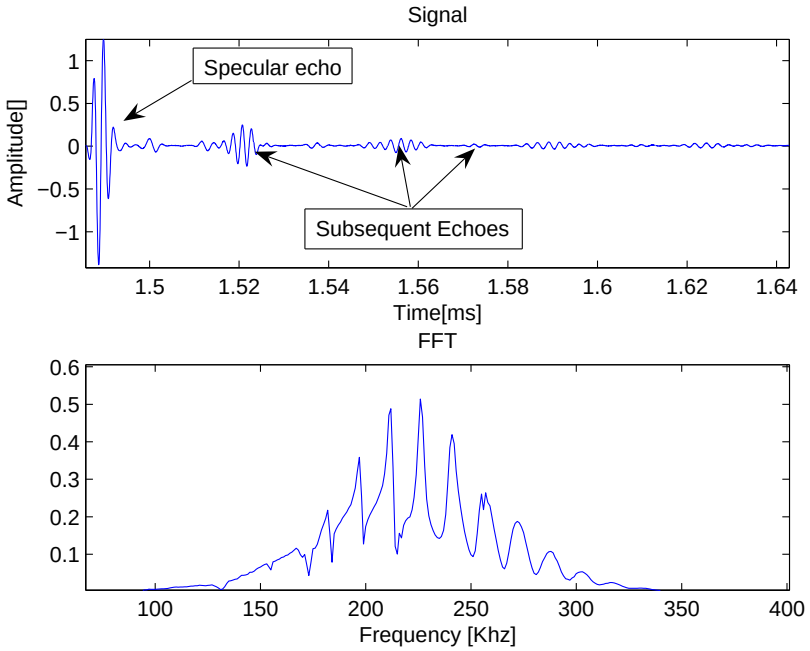

Figure VI.2: 225 kHz echo signal from a spherical shell of radii ratio equal to 0.96.

VI.2.1 Physical Modes for a spherical shell

Resonance scattering theory [44] gives solution to the problem of a plane acoustics wave scattering from a spherical shell. We present in this section, the results in case of radii ratio $b/a = 0.96$ (a: outer radius; b: inner radius). Let us consider a thin empty spherical shell submerged in an unbounded acoustic medium. A plane harmonic pressure wave strikes the shell and is scattered by it. Figure (VI.1) gives a simple idea of some physical phenomena, that are occurring in the moment of the scattering. In reality the waves propagates in all directions with no predetermined order and the received wave is a combination of all and any things. The motion of the shell is described by the equation of linear elasticity theory [104],[78] and that of the liquid is described by the Helmholtz equation [103],[58]. It is a two-dimensional steady-state problem. By means of separation of variables, one can obtain the exact solution in series form [44, 81]. it is valid for arbitrary values of spherical

coordinates R, θ. We shall consider a typical case in hydroelasticity, the case of an aluminum shell immersed in water. The physical parameters of the shell material and the liquid are given by:

Aluminum : $\rho_1 = 2.79X10^3 kg/m^3$, $c_L = 6380m/s$, $c_T = 3100m/s$,
water : $\rho = 1X10^3 kg/m^3$, $c = 1370m/s$.

Here c_L and c_T are the velocities of the longitudinal and transverse waves in the shell material.

Some plots of isolated modal resonances are presented in figure (VI.5). The observation point is situated in the far field. Only the case of backscattering ($\theta = \pi$) is considered (Fig. VI.3). The total function form is computed for the first 10 modes ($n = 10$). The total magnitude of the nth IMR is defined by f_n:

$$f_m(\theta) = \frac{2}{ix}(2m+1)\frac{B_m}{D_m}P_m(\cos(\theta)) \tag{VI.1}$$

where P_m is the Legendre polynomial, and B_m, D_m are 5×5 determinants, we con-

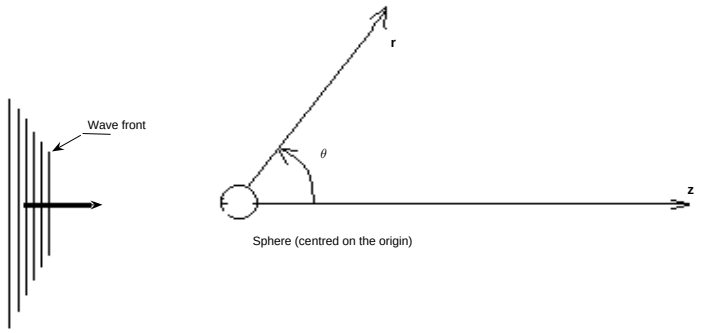

Figure VI.3: Geometry of the scattering calculation. The sphere is centered on the z axis of the plan wave.

sider here the case of a vacuum-filled spherical shell in an unbounded invisible fluid. The elements of the two matrices are given in [44],[72]. Expressions for B_m, D_m are reviewed in appendix (C) for the empty sphere case. These involve spherical Bessel, Neumann, and Hankel functions, j_m, n_m, and $h_m^{(1)}$, and the material properties including the densities of the solid and of water, ρ_1 and ρ, and the longitudinal and transversal wave velocities in the solid, c_l and c_t. The associated time series of the IMRs are computed by means of inverse Fourier transform.
The solution of the scattering problem of acoustic wave by an hollow elastic spherical

shell can be presented in series form as follows:

$$f(\theta) = \sum_{m=0}^{\infty} f_m(\theta) \tag{VI.2}$$

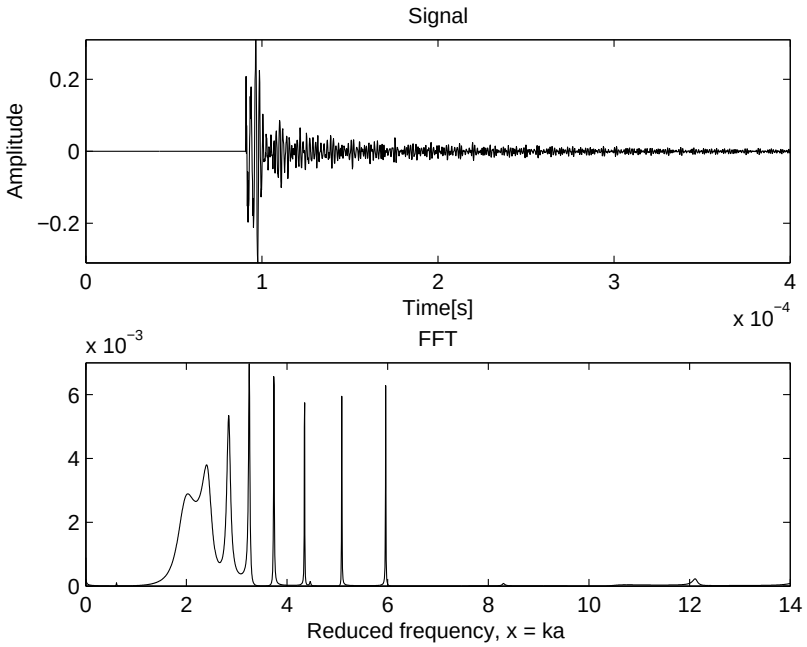

Figure VI.4: On top, filtered time signal (the specular echo is replaced by zeros). The signal is reconstructed from the associated time series of the IMRs of the spherical shell($b/a = 0.94$). On bottom, resonance spectrum

VI.2.2 IMFs

The EMD decomposes any signal $s(t)$ into a series of IMFs through the *sifting* process (Chapter II); each mode (IMF), with distinct time scale [64]. The decomposition is based on the local time scale of $s(t)$, and yields adaptive basis functions. The EMD can be seen as a type of wavelet decomposition, whose sub-bands are built up as needed, to separate the different components of $s(t)$. Thus locally, each IMF contains lower frequency oscillations, than the just extracted one [49]. The result of the *sifting* is that $s(t)$ will be decomposed into $\mathrm{IMF}_j(t), j = 1, \ldots N$ and residual $r_N(t)$:

$$s(t) = \sum_{j=1}^{N} \mathrm{IMF}_j(t) + r_N(t). \tag{VI.3}$$

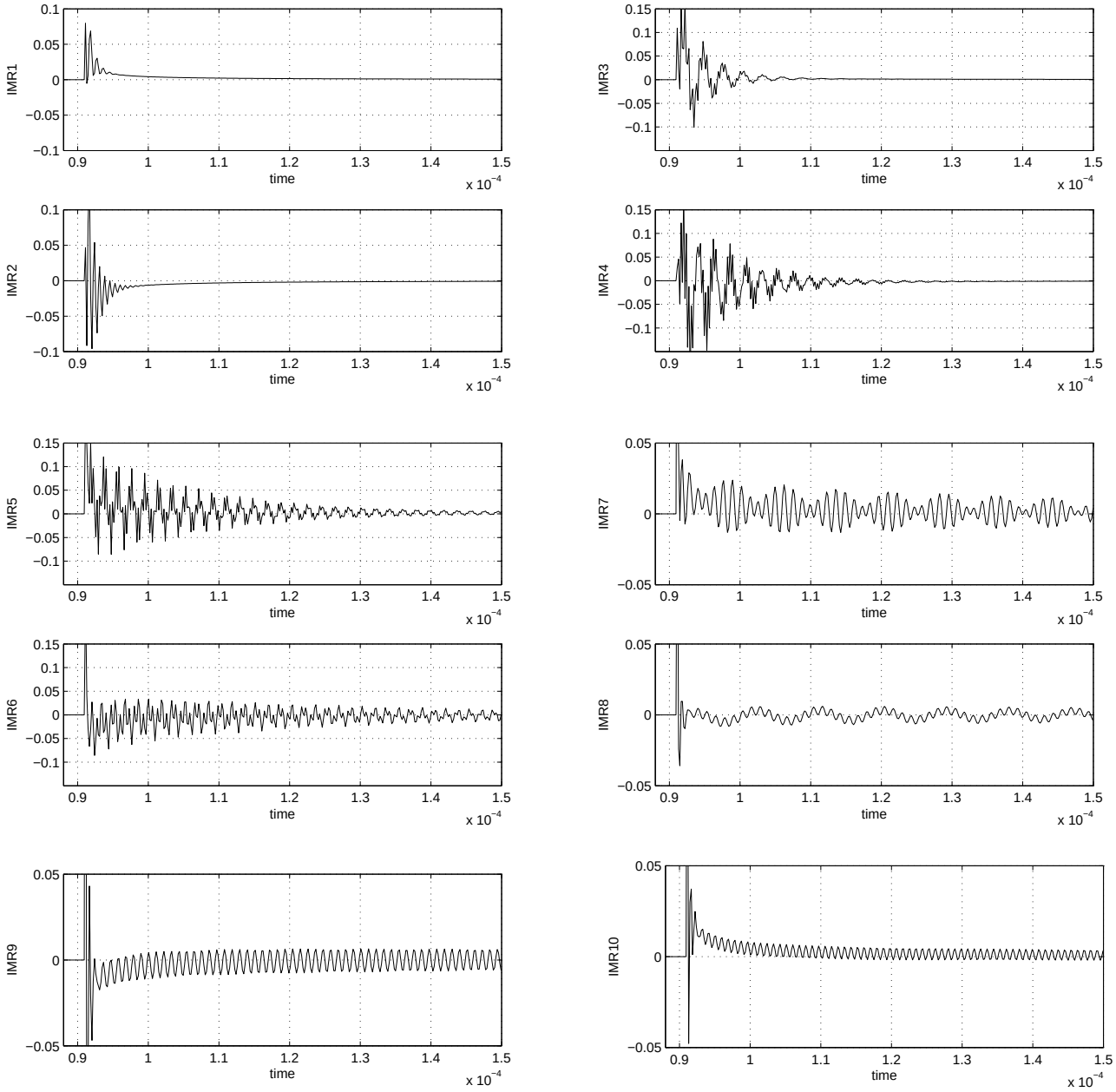

Figure VI.5: Associated time series of the IMRs of a spherical shell, modes 1-10 .

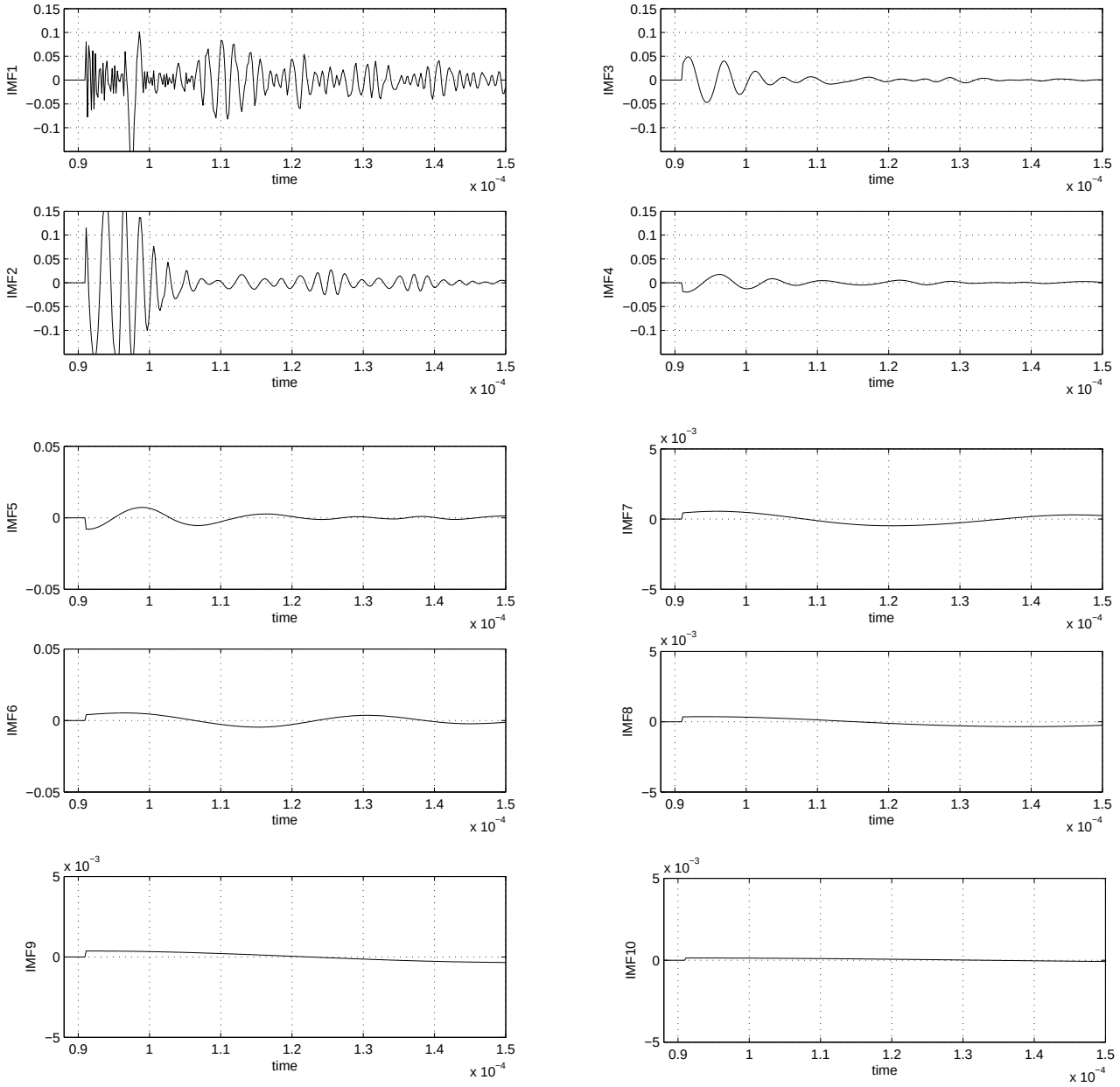

Figure VI.6: IMFs 1-10 extracted from the backscattering signal from a spherical shell.

VI.3 Comparison and discussion

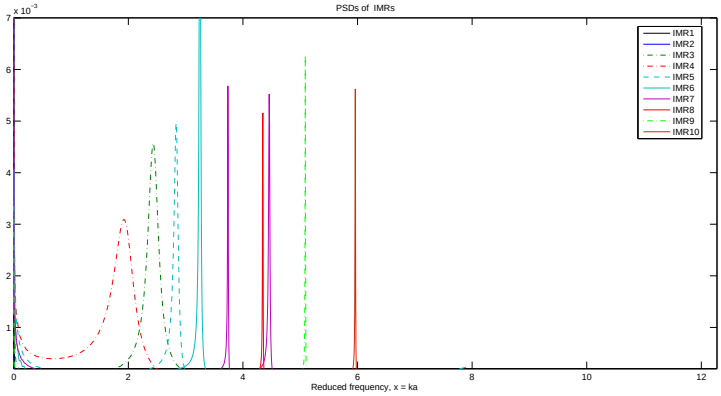

Figure VI.7: PSDs of IMRs

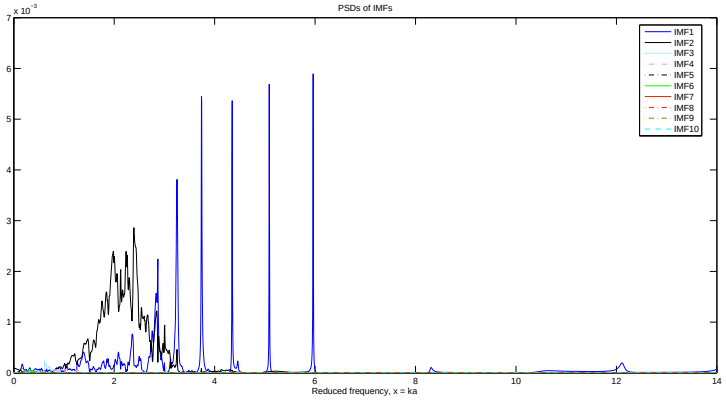

Figure VI.8: PSDs of the IMFs

	μ	E_x	m_3	m_4
IMR1	0	1,00	-0,37	1,00
IMR2	0	0,53	-0,12	0,26
IMR3	0	0,77	-0,22	0,53
IMR4	0	0,17	-0,02	0,02
IMR5	0	0,18	-0,02	0,02
IMR6	0	0,12	-0,01	0,01
IMR7	0	0,12	-0,01	0,01
IMR8	0	0,50	-0,11	0,19
IMR9	0	0,13	-0,01	0,01
IMR10	0	0,43	-0,07	0,10

Table VI.1: Statistical parameters of the IMRs.

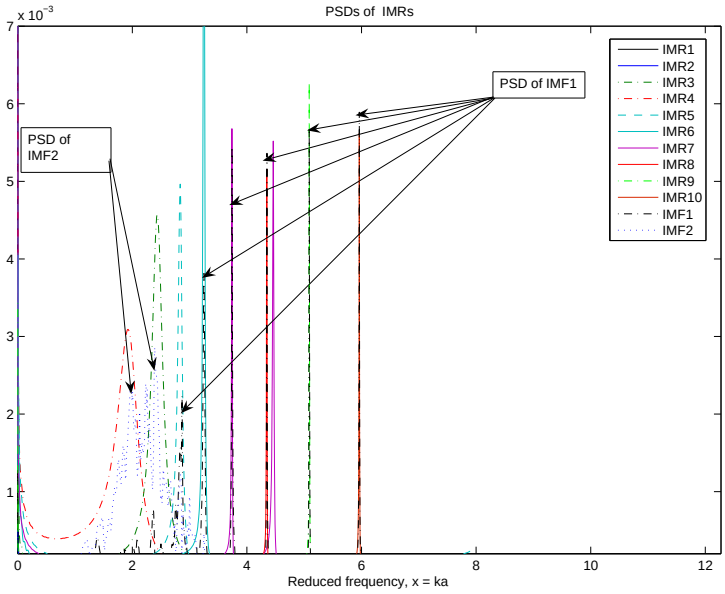

Figure VI.9: superposition of PSDs of the IMRs, IMF1 and IMF2 dark and green dashed lines respectively

	μ	E_x	m_3	m_4
IMF1	0	0,81	1,62	1,00
IMF2	0	0,77	0,17	0,60
IMF3	0	0,63	0,19	0,18
IMF4	0	1,00	-0,1	0,37
IMF5	0	0,17	0,00	0,01
IMF6	0	0,15	0,00	0,00
IMF7	0	0,01	0,00	0,00
IMF8	0	0,00	0,00	0,00
IMF9	0	0,00	0,00	0,00
IMF10	0	0,00	0,00	0,00

Table VI.2: Statistical parameters of the IMFs. Because the amplitudes of IMF8-10 are very small the values of the statistical parameters are considered null with the fixed precision

The backscattering echo signal from a hollow spherical shell is obtained from the contribution of the different propagating elastics waves. Figure (VI.5) shows such waves, noted here as the associated time series of the IMRs. Theses series are obtained one by one by Fourier transforming the physical modes (functions $f_n(\theta)$). In the figure (VI.6) the IMFs extracted from the backscattering signal by EMD are plotted. Comparing one to one the IMFs and the IMRs (see Figs. VI.6 and VI.5), we can not argue that each IMF matches the associated IMR of the same level. However if we superpose the Power Spectral Densities (PSDs) of IMFs and IMRs, respectively (Figs. VI.8 and VI.7) we found that the spectrum of the IMF1 is composed from the spectrums of IMR5, IMR6, IMR7, IMR8, IMR9, and IMR10 and the spectrum of IMF2 is composed from the spectrums of IMR3 and IMR4 (Fig. VI.9). Our investigation is completed by analysis of statistical parameters extracted from the modes. These parameters are calculated for each resulting components. For IMFs and IMRs: the first one is the mean value, as can be seen it is null for both of them. The other parameters are, normalized energy (E_x), and the third moment (m_3), the fourth moment (m_4) known as Skewness and Kurtosis respectively. Results reported in tables 1 and 2, show that these parameters do differ substantially.

VI.4 Backscattering signal analysis

In this section we analyze the TFRs of acoustics signal backscattering by cylindric shells. Each tube is characterized by a material (steel, aluminum) and radii ratio b/a (a: outer radius; b: inner radius). The results of some signals are presented. The experiments were conducted by Professor Gérard MAZE from "Laboratoire Ondes et Milieux Complexes, Université du Havre -France"[16].

Usually the specular echo is a broad band signal, that can not be easily analyzed; If the signal is analyzed with it, the TFRs could not be clearly represented, because the magnitude of the specular echo amplitude is greater than the others subsequent echoes. Consequently, these two type of waves can not be represented at the same scale. In order to analyze the echo signal, we have systematically canceled the specular echo from the backscattering signal.

Signal 1:

The shell is a tube of aluminum immersed in water filled full of air with b/a=0.95 and the material features are given above. The frequency center of the incident beam is situated around 330 KHz. At first observation of the resulting TFRs, one can conclude that the subsequent wave (qualified as Lamb waves in comparison to the resonance modes which lie in the plane [72, 44, 16]) are globally detected, except for

the SPWVD, where the latest waves disparate from the TF plane. The spectrogram and the scalogram depict all the waves but their frequency domain is shifted. We can see for spectrogram, patterns of a large frequency band for each wave packet. For the scalogram, the frequency rang is biased compared to others TFRs. In contrast the HHT and THT give accuracy frequencies values. Moreover, the last TFRs reveal several laws frequency for each wave packet. These ones corresponding to different extracted IMFs from the signal echo.

One can estimate time delay between successive waves packets in all TFRs. HHT and THT give an accuracy information.

Signal 2:

The studied object is a finite cylindrical shell made of stainless steel (density $\rho_1 = 7900kg.m^{-3}$) where longitudinal and transversal sound velocities are, respectively, $C_L = 5790m.s^{-1}$ and $C_T = 3100m.s^{-1}$. The shell is filled with air and radius ratio $b/a = 0.94$. The frequency center of the incident beam is situated around 130 kHz. As it has been mentioned before, the specular echo is canceled from all the following signals.

Signal 3:

The shell is a tube of steel, filled with air $b/a = 97$.The frequency center of the incident beam is situated around 150 kHz

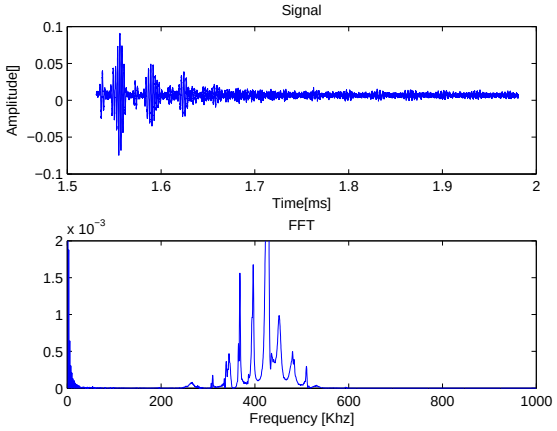

(a)

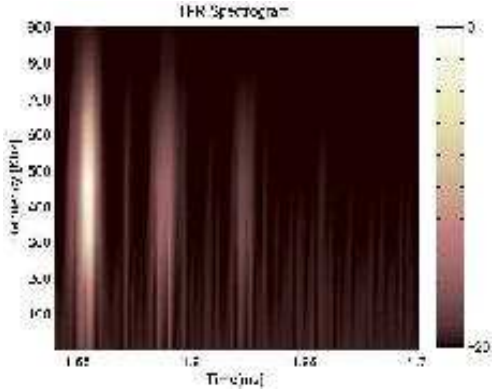

(b)

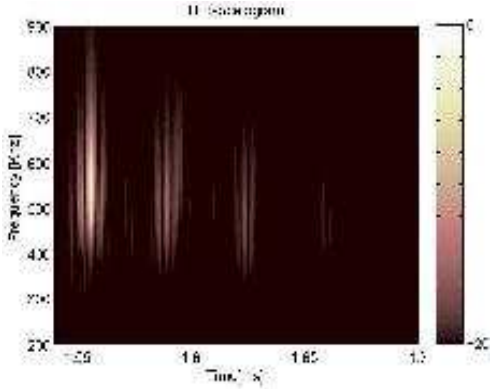

(c)

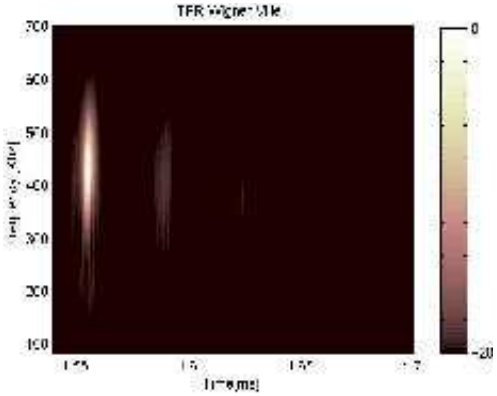

(d)

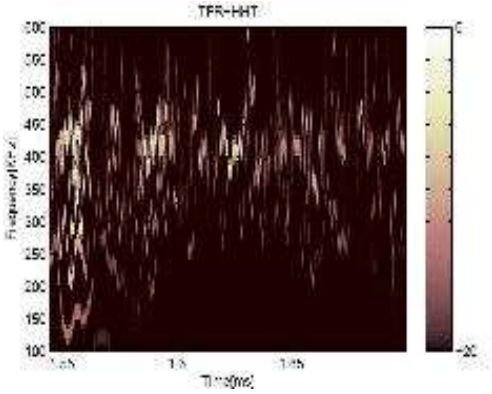

(e)

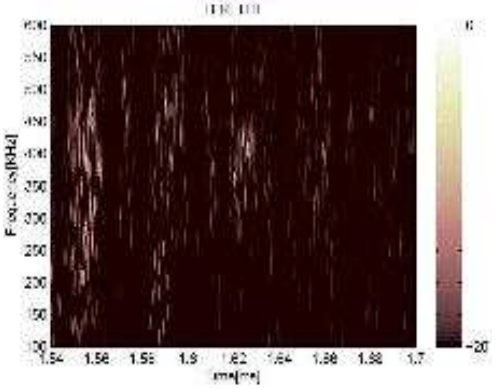

(f)

Figure VI.10: (a) Signal and FFT of signal 1. (b) Spectrogram. (c) Scalogram. (d) SPWVD. (e) HHT. (f) THT.

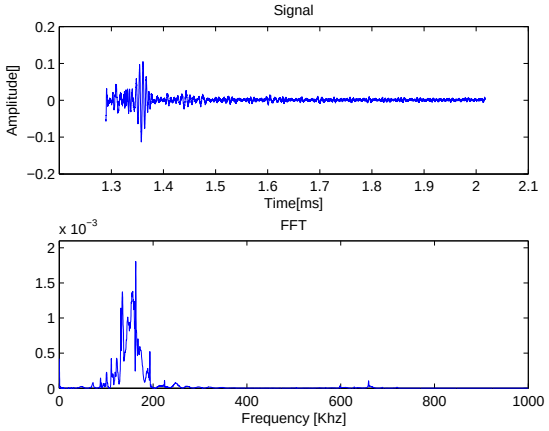

(a)

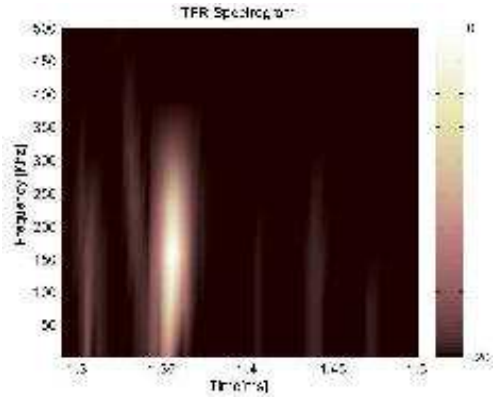

(b)

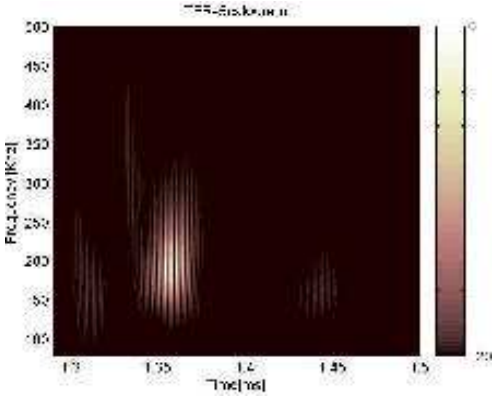

(c)

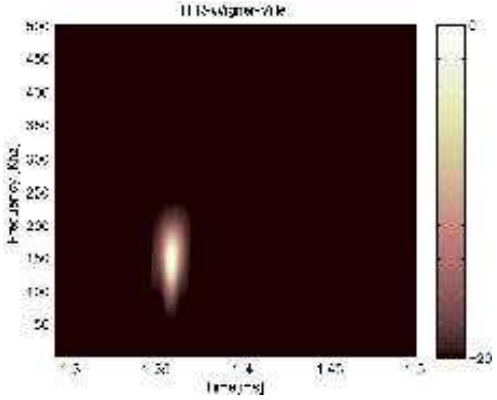

(d)

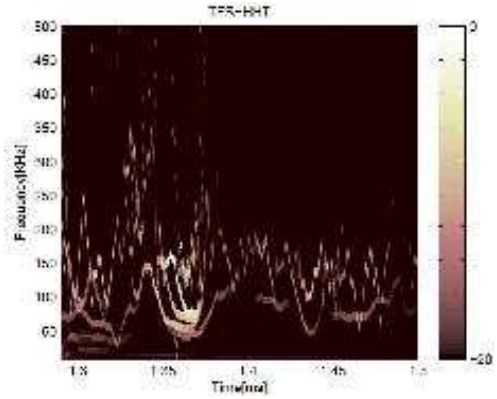

(e)

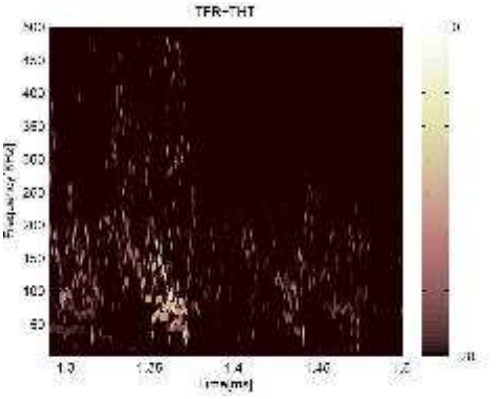

(f)

Figure VI.11: (a) Signal and FFT of signal 2. (b) Spectrogram. (c) Scalogram. (d) SPWVD. (e) HHT. (d) THT.

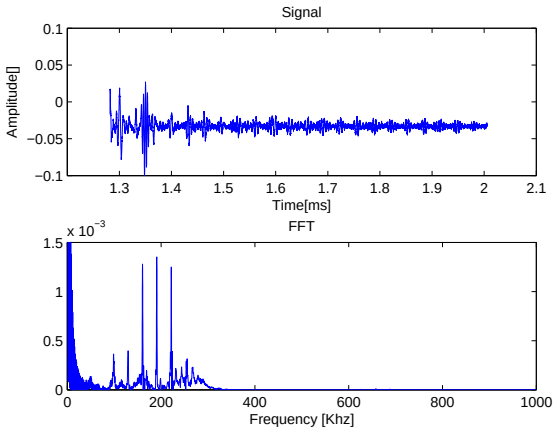
Signal
Amplitude[]
Time[ms]
FFT
x 10^-3
Frequency [Khz]

(a)

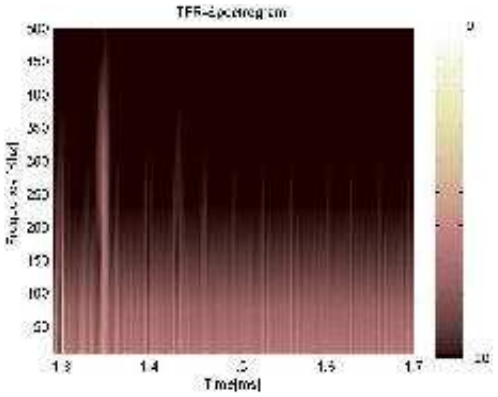
TFR-Spectrogram
Time[ms]

(b)

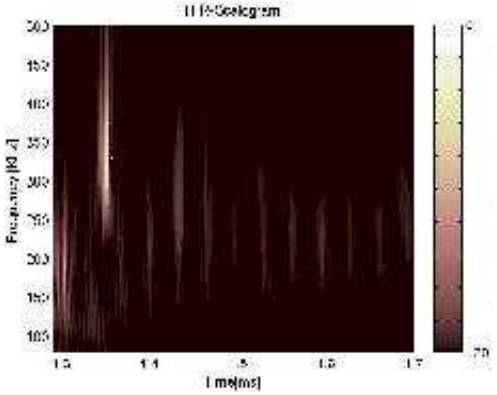
TFR-Spectrogram
Time[ms]

(c)

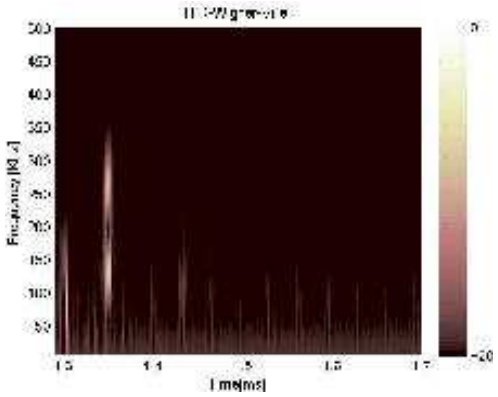
Time[ms]

(d)

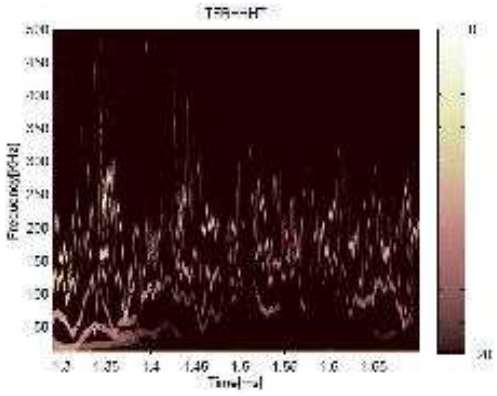
TFR-HT
Frequency[KHz]

(e)

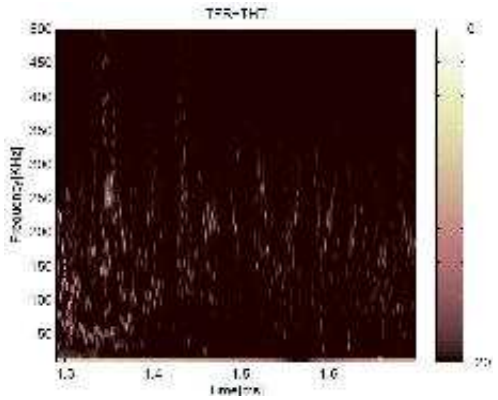
TFR-THT
Frequency[KHz]

(f)

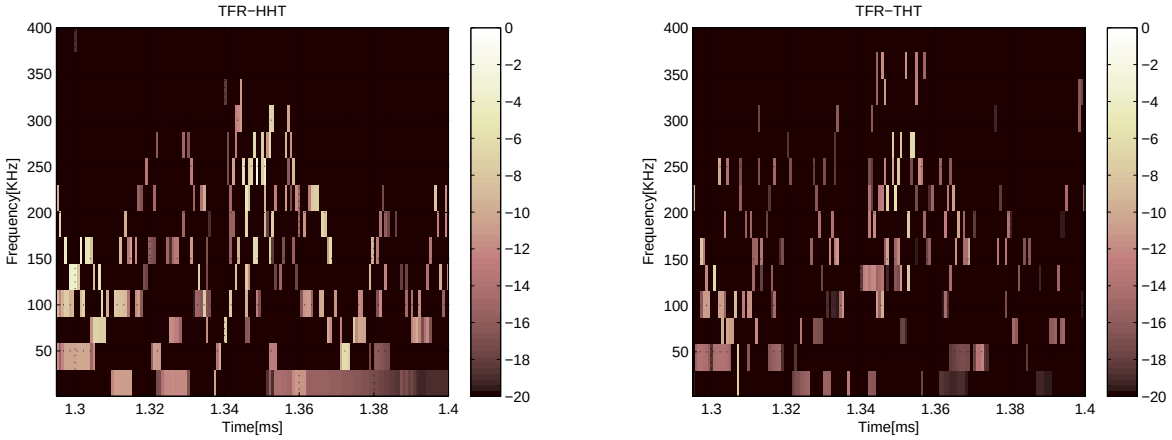

(g) (h)

Figure VI.12: (a) Signal and FFT of signal 3. (b) Spectrogram. (c) Scalogram. (d) SPWVD. (e) HHT. (d) THT. (g) Zooming on HHT, (h) Zooming on THT ($[1.5, 1.55]$ ms).

The acoustics signatures of the wave packets are identified in the TFRs on different patterns .

Signal 4:

The shell is a tube of steel, filled with air $b/a = 95$.

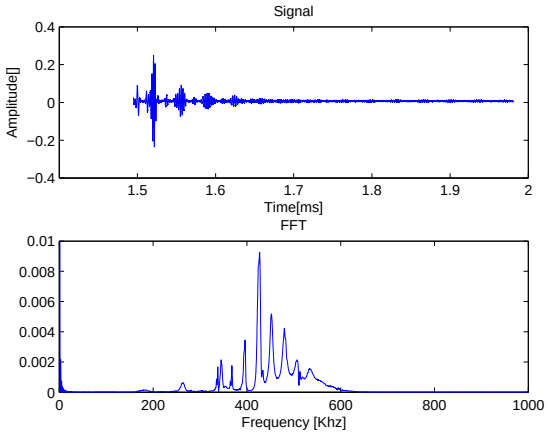
Signal
Amplitude[]
Time[ms]
FFT
Frequency [Khz]

(a)

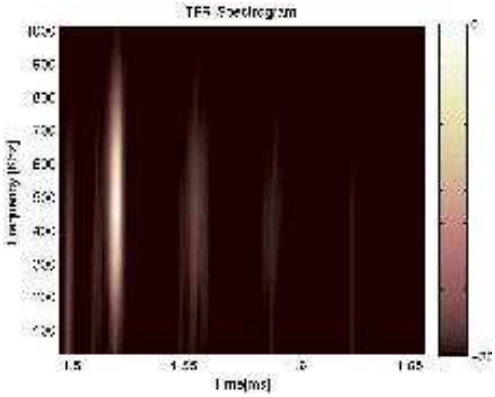
TFR Spectrogram
Time[ms]

(b)

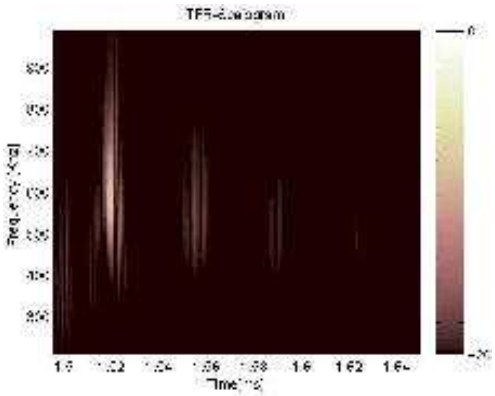
TFR-Spectrogram

(c)

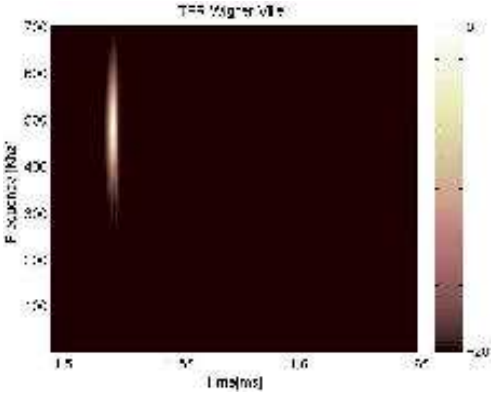
TFR Wigner-Ville
Time[ms]

(d)

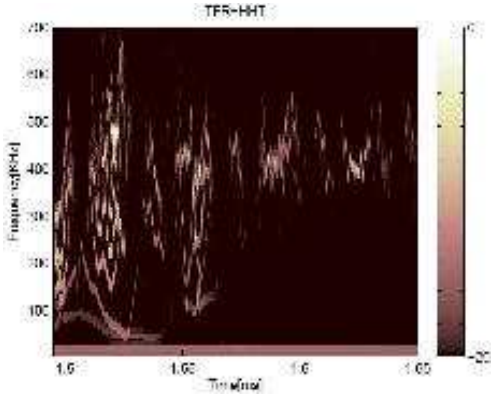
TFR-HHT

(e)

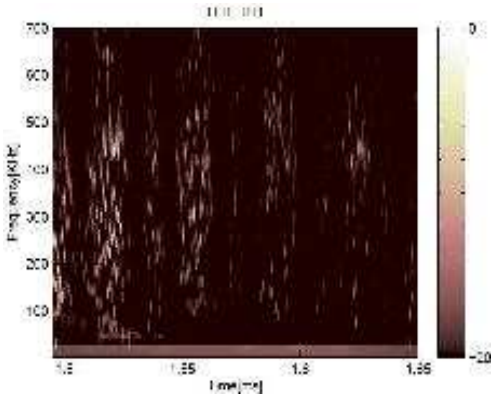

(f)

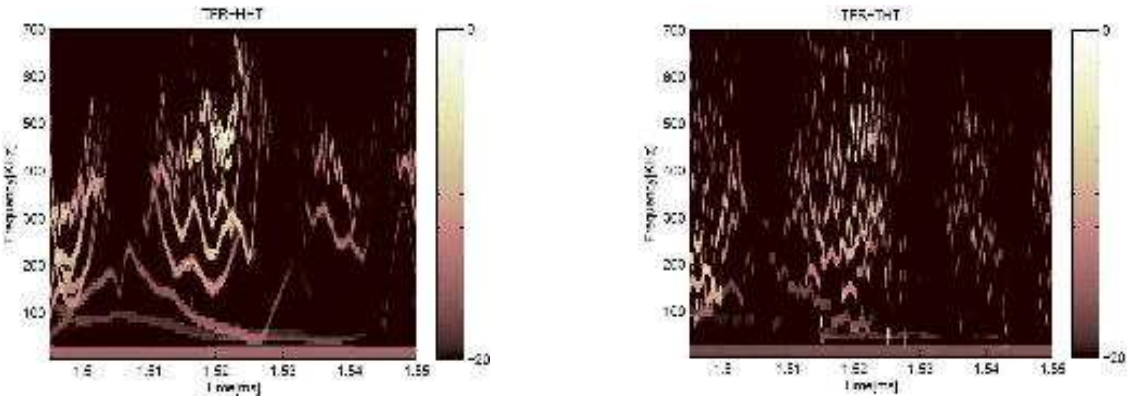

(g) (h)

Figure VI.13: (a) Signal and FFT of signal 4. (b) Spectrogram. (c) Scalogram. (d) SPWVD. (e) HHT. (d) THT. (g) Zooming on HHT, (h) Zooming on THT ($[1.5, 1.55]$ ms).

Signal 5:

The shell is a tube of steel, filled with air $b/a = 95$.

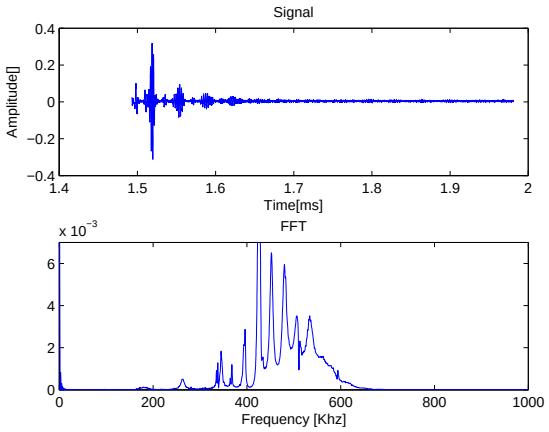
Signal
Amplitude[]
Time[ms]
x 10^-3
FFT
Frequency [Khz]

(a)

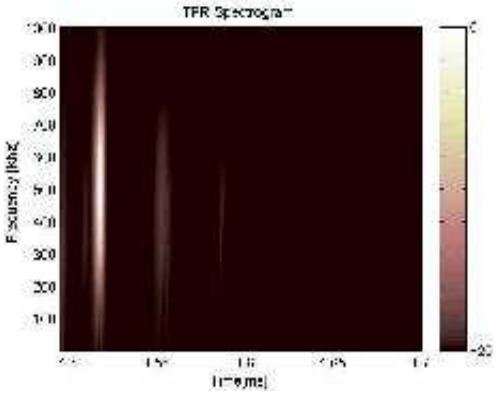
TFR Spectrogram

(b)

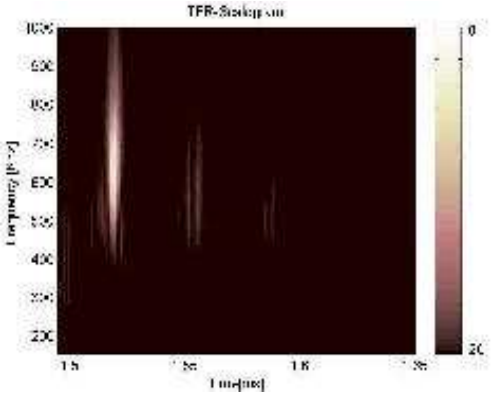

(c)

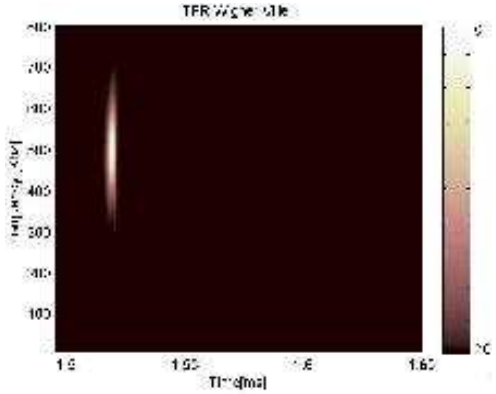

(d)

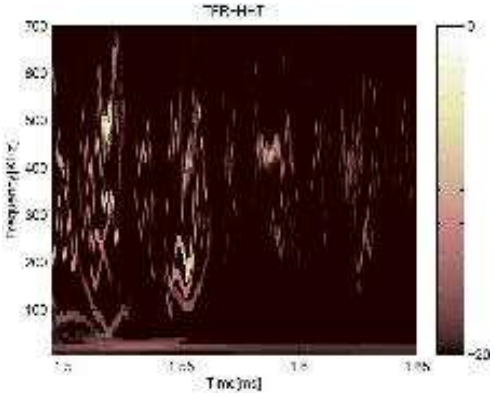
TFR-H-T

(e)

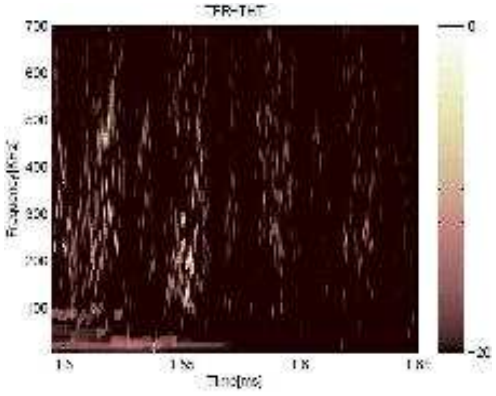
TFR-ThT

(f)

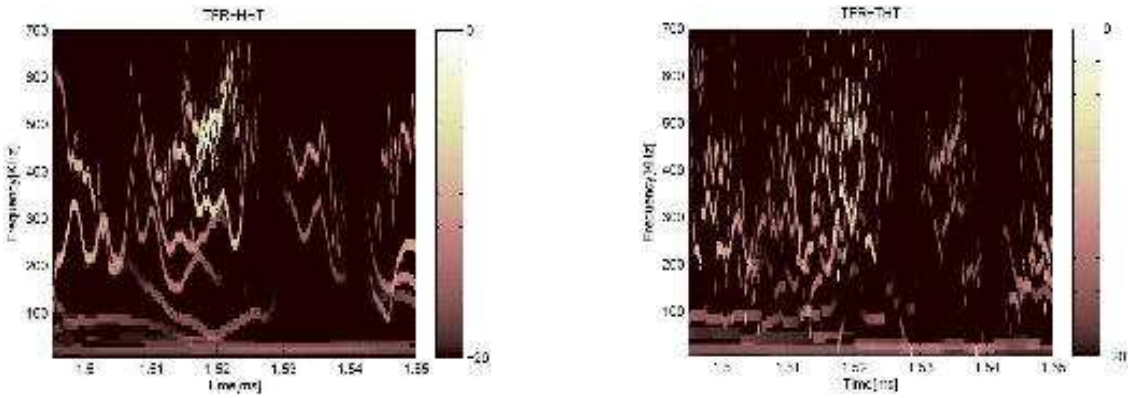

(g) (h)

Figure VI.14: (a) Signal and FFT of signal 5. (b) Spectrogram. (c) Scalogram. (d) SPWVD. (e) HHT. (d) THT. (g) Zooming on HHT, (h) Zooming on THT ($[1.5, 1.55]$ ms).

The analysis of the signals shows that except the SPWVD, the remainder TFRs show the same frequency patterns, the successive wave packets reflected by the object (the Lamb waves [44]), which are pertinent for classification. Both the scalogram and the spectrogram give the same results, but the frequency patterns are better evidenced using the spectrogram. The obtained results show that the SPWVD, the spectrogram and the scalogram are less sensitive to b/a radius ratio and materials of the target, than the HHT and the THT. For all the signals analyzed, only the methods based on the EMD show the frequency patterns of interest. If we compare the resulted THT and HHT on bottom of figures (VI.10, VI.11, VI.12, VI.13, VI.14), we remark that these methods allow the differentiation of objects with similar temporal responses. One can observe for each reflected wave from the shell several frequencies laws. These ones correspond to the IFs of the IMFs extracted from the signal.

The results confirm the interest of the TFRs for the analysis of the echo signals which are nonstationary. Indeed, the obtained TFRs are sensitive to the choice of the material and the radii ration b/a of the target. These results are well evidenced essentially on both the THT and the HHT. Compared to classical methods (SPWVD, scalogram and spectrogram), we notice that only the THT and the HHT are very sensitive to the physical properties of the target. A large class of signals is necessary to confirm these findings. Even both the THT and the HHT, give interesting results, a feature extraction process followed by a classification scheme are necessary to obtain relevant and pertinent information about the targets.

Conclusions and perspectives

In this thesis we have tried to explore some of the potentials of the EMD in signal processing and particularly in TF analysis of nonstationary signals. The first point we have to emphasis in our conclusion is the comparison of the two demodulation methods involved in the thesis: the ESA and the HT. Spectral estimation is the second step of the EMD. This consists in computing the IF and IA functions for each IMF by using a demodulation method. An accepted way is to use the AS through the HT. A necessary condition for the AS method to give a physical meaningful IF is that the signal will have to be symmetric with respect to the zero mean. The HT uses the whole signal. As we have a finite segment of signal the window effect will distort its spectrum. An alternative way to estimate IA and IF functions is the ESA. Based on the TKEO, the ESA computes these functions without involving integral transforms as in HT or FT; it is totally based on differentiation. A distinct advantage of the TKEO is its good localization. This property is the consequence of the differentiation based method. Thus, it is natural to use local operator as basis for a local estimation such as IA and IF functions. This is confirmed by the obtained results. The advantages of the ESA are efficiency, low cost computational complexity and excellent time resolution. A disadvantage of ESA compared to HT is its sensitivity in very noisy environment. To reduce noise sensitivity, a more systematic approach is to use continuous-time expansions of discrete-time signals to numerically implement the required differentiation with closed formulas. To do so, we have proposed the B-spline model. A common limit of both HT and ESA is that they can not handle wide-band signals. Thus one aim of this thesis was to combine two non-linear and local approaches, the ESA and the EMD to track instantaneous features such as IA and IF of a multicomponent AM-FM signal. Associated with the EMD which acts as bandpass filter, the ESA can handle multicomponent signals. Compared to Gabor filtering, the EMD is a data driven approach that does not require neither the number of filters and the associated impulse responses, nor the bandwidth

parameters. Since IMFs are represented by spline functions, we have investigated their smoothed derivatives to compute TKEO and then in turn used in ESA in their continuous form to estimate IA and IF functions. As it has been verified for the case of multicomponent AM-FM signal (Chapter III), this adds robustness to EMD-ESA.

The new sifting introduced in this thesis improves the results of the conventional EMD. As it has been shown on some synthetic signals, our approach extracts correctly the components of the signals and avoid the over-decomposition problem. The decomposition results where interpolations are performed by the B-spline without regularization can generate insignificant IMFs. Furthermore, to improve the performance of the EMD in noisy environment, smoothed splines are used. This is done by relaxing the interpolation constraint. Thus a regularization factor Λ is introduced to measure how smooth the interpolation function will be and how close the data samples the interpolant will pass. Other approaches such as trigonometric interpolation can be used. Trigonometric interpolation is useful from an analytic point of view, but computationally it is much more expensive than B-splines. This why both exact and smoothed splines have been investigated. Even Λ parameter has been found based on simulations with different SNR values, a strategy to find an optimal value adapted to each analyzed signal is necessary. Investigation is in progress to establish a rigorous criterion to select the optimal Λ value. In this thesis six EMD based AM-FM demodulation approaches are studied and their results in terms of IFs and IAs tracking compared. We have limited ourselves to a two-components AM-FM signal embedded in additive white Gaussian noise with varying SNRs. The EMD decomposes this signal into few IMFs, the first and second IMF are identified as the original AM-FM components, the remaining IMFs are mainly due to end side effects and estimation errors of the EMD. The six methods give good results for IFs and IAs estimation for hight SNR values. Whereas, for low SNR up to $5dB$, EMD-HT and EMD-ESA-BSR give better results with 50% less error. Finally, for noise dominated signal, no method can be set as standard as all the compared method fail in tracking one or another components from the set of tested ones.

The first use of the TKEO, especially the ESA in conjunction with the EMD is cited by Huang in a patent published in USA [60]. Huang has identified the TKEO as an extremely local and sharp test for harmonic distortions within any IMF derived from data. Cexus et al [22] are the first who used the EMD and the DESA. Since that, this combination, is named the THT. In this thesis the THT is reviewed, improved and a mathematical formulation of its TF map proposed. Spectrum generated by the THT is a joint distribution of the amplitude and frequency content of the signal as a

function of time often presented as contour of amplitude (or energy) over TF plane. Time resolution of the representation can be as precise as the sampling period. As the HHT, this TFR free of interferences is well suited for processing any data (linear or nonlinear) and stationary or non-stationary signals. No pre or post processing is required. The THT presents little loss of TF resolution and as the HHT, it is very easy to implement. Results of the THT are not prejudiced by predetermined basis and/or sub-band filtering processes. This method is based on an adaptive basis, and there is no uncertainty principle limitation on time or frequency resolution from the convolution pairs based on a priori basis. The effectiveness of THT has been shown on synthetic (with different IF laws) and real signals. Comparison to the HHT and to well established methods such as the spectrogram, the WVD, the SPWVD, the scalogram and the reassigned SPWVD shows that the THT performs better. The obtained results show that the THT identifies in all presented cases the TF structures. A large class of synthetic and real signals are necessary to confirm these findings. The obtained results show the interest to combine two local approaches, the EMD and the TKEO, to process non-stationary signals. Because the THT is based on the EMD consequently it shares the same limits. The shortcomings are essentially due to two factors: a) the EMD is just defined by an algorithm (sifting) and b) the data driven nature of the approach.The B-spline fitting used is computationally intensive and creates distortion near the end points. Thus, the end effects in splitting need improvements. We have shown that the modified THT (EMD-BSR-ESA) is well suited for noisy analyzed signals. The comparison study performed in Chapter III confirms the interest of the continuous version of THT (The interpolation is performed by smooth B-spline model) to represent a signal in TF plane.

Based on the THT and the Hough transform new approach for detecting LFM of multicomponent signals has been introduced in Chapter V. The THHT is obtained based on the new mathematical formulation of the THT (Chapter IV). Preliminary results show the interest and effectiveness of the THHT as tracking method of TF components. The THHT does not suffers from the trade-off between TF resolution and cross-terms suppression. No assumptions are made about the number of components of the signal nor their amplitude or phase. Numerical simulations show that compared to WVD-H_gT and to SPWVD-H_gT, the THHT achieves better performance in terms of TF components tracking of signals in both noise free and noisy environments. Furthermore, the THHT gives results much sharper than those of WVD-H_gT and SPWVD-H_gT. In all presented cases, LFM components are well identified. Since the performance of the THHT has only evaluated by some simulations, a large class of signals (extensive simulations) is

necessary to confirm the obtained results. As future work we plan to extend the analysis to more complicated IF laws such as nonlinear FM signals or arbitrary TF shapes. Investigation is in progress to establish a rigorous threshold criterion for the THHT.

In order to find physical interpretations of the extracted IMFs from scattering signal of simple shells (sphere and cylinder) some simulations are conducted (Chapter VI). The physical modes or the IMRs of these shells are well known, we have synthesized the scattering signals by the shells and extracted the associated IMFs by EMD. Resulting IMFs are in turn compared to IMRs. Preliminary results of this study are encouraging. Based on the comparison of the calculated spectrum of both IMFs and IMRs, preliminary results show that there is a correspondence between these kinds of modes. Even there is no close link between IMFs and IMRs, a mode by mode comparison of the associated statistical parameters shows that there are similarities between these modes. Furthermore, it is found that some IMFs can be obtained by a partial reconstruction of a selected set of IMRs. The present investigation is pursued through the analysis of different target of different physical parameters such as material and dimension, and also velocities of longitudinal and transverse waves.

The analysis of the TFRs of a backscattering signal from simple shells (cylinders having different physical properties), confirm the interest of the TFRs for the analysis of the echo signals which are nonstationary. These results are well evidenced essentially on both the THT and the HHT. Compared to classical methods (SPWVD, scalogram and spectrogram), we have remarked that only the THT and the HHT are very sensitive to the physical properties (the material and the radii ration b/a) of the target. A large class of signals is necessary to confirm these findings. Even both THT and HHT give interesting results, a feature extraction process followed by a classification scheme are necessary to obtain relevant and pertinent information about the targets. For backscattering signal from cylindrical shell, even for the moment we could not conclude about the physical signification of those laws, it is very clear that only HHT and THT give distinct TFR for different backscattering signal. We suggest as future works to use the IFs, IAs and the TKEO of the IMFs as pertinent features for classification process. Furthermore, we suggest to perform the classification of objects using the THT or the HHT as an image where acoustics signatures are the frequencies laws.

APPENDIX A

Analysis of white gaussian Noise by EMD

1. Characteristics of white noise using EMD

The problem of separating noise and signal is complicated and difficult when we do not even know the level of noise in the data. The question then becomes more fundamental: are we looking simply at noise, or are we getting any information in the series of numbers known as data? In this case, knowing the characteristics of the noise is an essential first step before we can attach any significance to the signal eventually extracted from the data. In this subsection , we present the important results of a numerical study on uniformly distributed white noise using EMD[116][49]. Through the work of the last cited references Flandrin and Wu have gotten simultaneously out the same results. We cite here several important fact of those papers :

1. The EMD is effectively a dyadic filter, capable of separating the white noise into IMF components having mean periods twice the value of the previous component, figure.(A.1);

2. The IMF components, except the first IMF, are all normally distributed, figure.(A.3);

3. Based on empirical facts, they found that, the product of the energy density of IMF and its corresponding mean period must be a constant.

4. The energy-density function must be chi-squared distributed, since the IMFs are distributed normally.

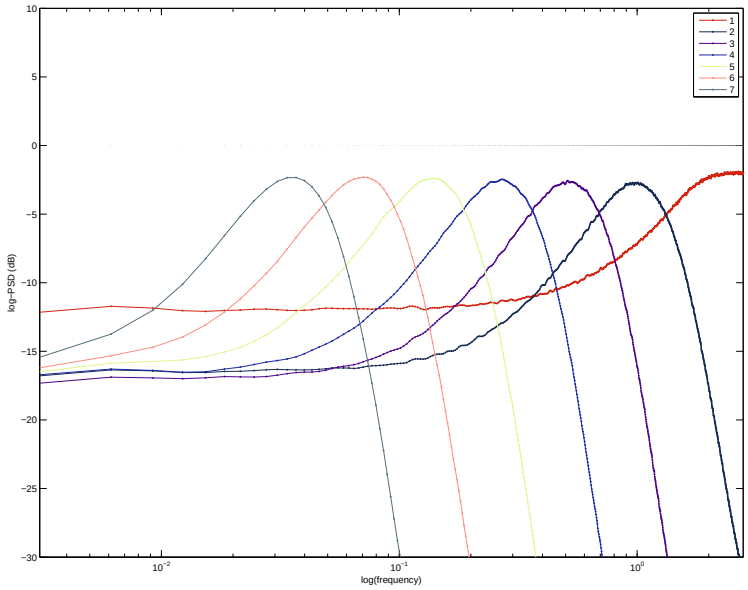

Figure A.1: IMF power spectra in the case of White Gaussian Noise. The spectrum densities (PSD) is plotted as a function of the logarithm of the period for IMFs 1 to 7. The spectral estimates have been computed on the basis of 5000 independent sample paths of 4096 data points

The pertinent results they founded from that study include an analytical expression of the relationship between the energy density and the mean period of the IMF components derived from the white noise through EMD, an analytic expression of the energy-density distribution and its spreading function. All the analytic expressions found are tested against the results produced by Monte Carlo method on a numerically generated random noise.

1.1 The Fourier spectrum of IMFs

Let us consider the general properties of energy density as function of period for the data. For a normalized white noise time series, s_j, for $j = 1, ..., N$, we can express it either in Fourier series components, or IMFs, i.e.

$$s_j = \Re[\sum_{k=1}^{N} S_k exp(i\frac{2\pi jk}{N})] = \sum_n C_n(j) \tag{A.1}$$

where $i = \sqrt{-1}$, $C_n(j)$ is the nth IMF, and

$$S_k = \sum_{j=1}^{N} s_j exp(-i\frac{2\pi jk}{N}) \tag{A.2}$$

Then , the energy density of the nth IMF can be defined as

$$E_n = \frac{1}{N}\sum_{j=1}^{N}[C_n(j)]^2 \tag{A.3}$$

Theoretically, the Fourier spectrum of a white noise series should be a perfect constant, indicating that the contribution to the total spectrum energy comes from each Fourier component uniformly and equally. The Fourier pectra for the IMFs, however, are not a constant white spectrum, for the decomposition through EMD has the effect of subjecting the data to a dyadic filter bank. Therefore, the IMFs are band passed as discussed by Flandrin et al.[49].

Now, let us examine the Fourier spectral shape for each IMF. To this end, the Fourier spectrum for 5000 independent segments of 4048 data points each of all the IMFs are calculated. The individually averaged Fourier spectra for all the IMF are plotted, figure (A.2). We can see that all the Fourier spectrum, except the first one, have identical shapes in terms of ln T axis, where T is the period of a Fourier component. From these figures, it is obvious that the ratios of the neighboring spectra are almost identically equal approximately 2,which is consistent with the doubling of averaged periods of neighboring IMFs. Except for the first IMF, based on what is obviously observed and empirically validated, one can have an integral expression to represent, to the first order of approximation, the functional form of Fourier spectrum for any IMF as

$$\int F_{lnT,n} dlnT = const., \tag{A.4}$$

Where $F_{lnT,n}$ is the Fourier spectrum of the nth IMF as a function of lnT and the subscript n representing the nth IMF. similarly in frequency domain (in this case we scale the spectrum to respect the Energy conservation principal). Then, the energy of the nth IMF is written as

$$NE_n = \int F_{\omega,n} d\omega, \tag{A.5}$$

Where $F_{\omega,n}$ is the Fourier spectrum of the nth IMF in terms of frequency, ω. After

some mathematics the last equation is written as

$$NE_n = \int F_{\omega,n} d\omega = \int F_{T,n} \frac{dT}{T^2} = \int F_{lnT,n} \frac{dlnT}{T} = \frac{\int F_{lnT,n} dlnT}{\overline{T}_n} \tag{A.6}$$

Where $F_{T,n}$ is the Fourier spectrum of the nth IMF in terms of period,T, and $\overline{T}_n$ is defined by

$$\overline{T}_n = \int F_{lnT,n} dlnT (\int F_{lnT,n} \frac{dlnT}{T})^{-1} \tag{A.7}$$

Substituting Eq.(A) into Eq.(A), we find the equation that relates the energy density, E_n, and the averaged period $\overline{T}_n$, i.e.

$$E_n \overline{T}_n = const., \tag{A.8}$$

$$lnE_n + ln\overline{T}_n = const. \tag{A.9}$$

Assuming that the const in Eq.(A) equal to one, because of the normalization of the white gaussian noise, the Eq.(A) became,

$$ln\overline{E}_n + ln\overline{T}_n = 0. \tag{A.10}$$

where $\overline{E}_n$ is $E_n$when N approaches infinity

1.2 Energy distribution

Examining the probability of an individual IMF in figure (A.3)we can argue that is approximately normal, which is evident from the superimposed fitted normal distribution function (the black line). In high frequency, the first IMFs, the data and the fitted normal distribution function are on a good concordance. For the last IMFs, when the oscillations decease the number of events deceases and the deviation from the normal distribution function grows; Such a time-series,its energy, given in Eq.(A) should have a χ^2 distribution, with the mean of the energy token as the degree of freedom of the χ^2 distribution, $r_n = N$

$$\rho(NE_n) = (NE_n)^{N\bar{E}_n/2-1} e^{-NE_n/2} \tag{A.11}$$

Therefore, the probability distribution of E_n is given by

$$\rho(E_n) = N(NE_n)^{N\bar{E}_n/2-1} e^{-NE_n/2} \tag{A.12}$$

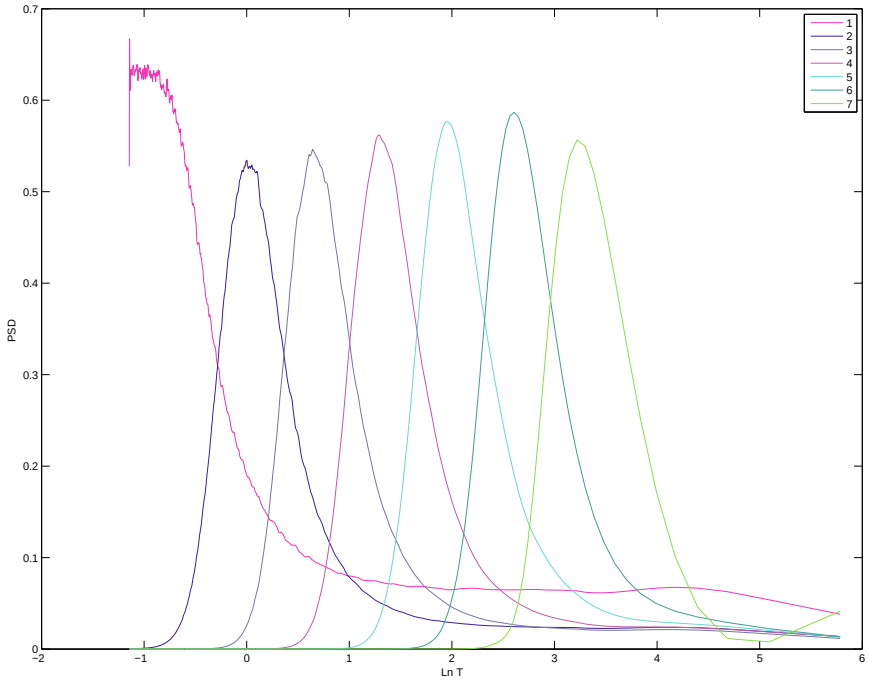

Figure A.2: IMF power spectra in the case of White Gaussian Noise. The spectrum densities (PSD) is plotted as a function of the logarithm of the periode for IMFs 1 to 7. The spectral estimtes have been computed on the basis of 5000 independent sample paths of 4096 data points

The speared of the energy of white-noise samples of a certain length N.For simplicity, we use the variable $y = lnE$ and we omitt the subscript n. The distribution of y is therefore

$$\begin{aligned}\rho(y) &= N(Ne^y)^{N\bar{E}/2-1}e^{-NE/2} \\ &= Kexp(\frac{1}{2}yN\bar{E} - \frac{1}{2}NE) \\ &= Kexp(-\frac{N\bar{E}}{2}(\frac{E}{\bar{E}} - y)\end{aligned} \tag{A.13}$$

Where $K = N^{N\bar{E}/2}$

$$\frac{E}{\bar{E}} = e^{y-\bar{y}} = 1 + y - \bar{y} + \frac{y-\bar{y}^2}{2!} + \frac{y-\bar{y}^3}{3!} + \cdots . \tag{A.14}$$

Substituting the Eq.(A) into Eq.(A), we find

$$\rho(y) = Kexp-\frac{N\bar{E}}{2}[1 - \bar{y} + \frac{y-\bar{y}^2}{2!} + \frac{y-\bar{y}^3}{3!} + \cdots]$$

$$= K' exp - \frac{N\bar{E}}{2}[\frac{y-\bar{y}^2}{2!} + \frac{y-\bar{y}^3}{3!} + \cdots], \tag{A.15}$$

Where $K' = Kexp[-\frac{1}{2}N\bar{E}(1-\bar{y}]$. When $|y-\bar{y}| << 1$, the distribution of $\bar{E}_n(\bar{E})$ is approximately a Gaussian with a standard deviation

$$\sigma^2 = \frac{2}{N\bar{E}_n} = \frac{2\bar{T}_n}{N}. \tag{A.16}$$

$$\rho(y) = Kexp - \frac{N\bar{E}}{2}[\frac{1-\bar{y}^2}{2!}] = K' exp[-\frac{N\bar{E}(y-\bar{y}^2)}{4}] \tag{A.17}$$

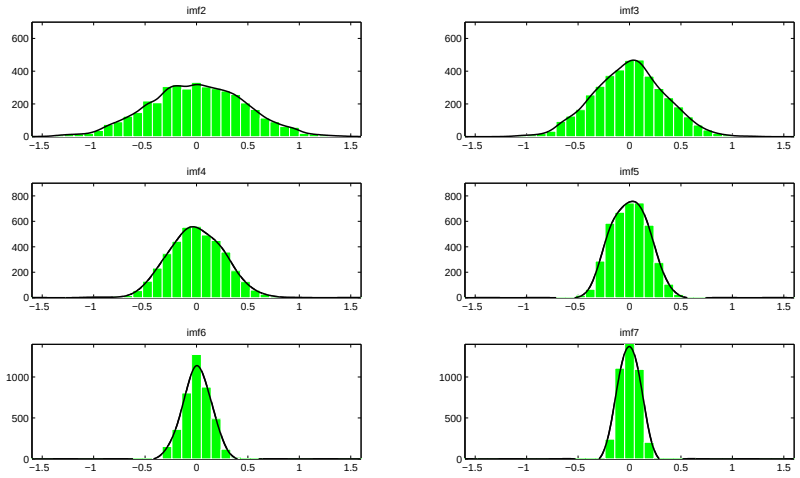

Figure A.3: Histograms of IMFs from 2 to 7 for a WGN sample with 4096 data points.The superimposed black lines are the Gaussian fits for each IMF, except IMF3

APPENDIX B

The first derivatives of IMF in B-Spline space

1. B-Spline functions

The basis functions $\beta_j^n(t)$ can be generated iteratively by repeated convolution of a B-spline of order 0:

$$\beta_j^n(t) = \beta_j^0(t) * \beta_j^{n-1}(t) \tag{B.1}$$

where $\beta_j^0(t)$, $\forall k \in \mathbb{N}$, is the indicator function in the interval $[-\frac{1}{2}, \frac{1}{2})$

$$\beta_j^0(t) = \begin{cases} 1 & t \in [-\frac{1}{2}, \frac{1}{2}) \\ 0 & \text{otherwise} \end{cases}$$

An interesting property of B-spline functions is their compact support (Eq. (B.1)), this is very important because it limit the propagation of approximation errors from a Box to an other. The p derivative of spline of order n is obtained by applying the p order central difference operator. The result of this calculation is a spline of order $(n-p)$ [99]. For example, the first and the second derivatives of B-splines of order n are given by:

$$\begin{aligned} \frac{\partial \beta_j^n(t)}{\partial t} &= \beta_j^{n-1}(t+\frac{1}{2}) - \beta_j^{n-1}(t-\frac{1}{2}) \\ \frac{d^2\beta_j^n(t)}{\partial t^2} &= \beta_j^{n-2}(t+1) - 2\beta_j^{n-2}(t) + \beta_j^{n-2}(t-1) \end{aligned} \tag{B.2}$$

An interesting feature of B-spline forms is given by equation (B.3) and equation (B.2). Using these relations, closed-form expressions for the derivatives involving only the coefficients $c_l[n]$ and the B-spline function are derived.

2. First derivatives of IMF based on B-Spline functions

To calculate the continuous ESA (Eq. (III.24)), we have to compute the first-, second- and third-order derivatives of the IMFs.

In order to calculate the derivatives of IMFs, we propose to use their continuous forms instead of the discrete ones. Indeed, each extracted IMF is represented by a B-spline signal [64]. An IMF in splines domain is rewritten as:

$$g_j^n(t) = \sum_{l\in\mathbb{Z}} c_j[l]\beta_j^n(t-l) \tag{B.3}$$

First derivative:

$$\frac{\partial g_j^n(t)}{\partial t} = \sum_{l\in\mathbb{Z}} c_j[l]\frac{\partial \beta_j^n(t-l)}{\partial t} \tag{B.4}$$

Using the following propriety:

$$\frac{\partial \beta_j^n(t)}{\partial t} = \beta_j^{n-1}(t+\frac{1}{2}) - \beta_j^{n-1}(t-\frac{1}{2}) \tag{B.5}$$

the first derivative is given by,

$$\frac{\partial g_j^n(t)}{\partial t} = \sum_{l\in\mathbb{Z}} c_j[l][\beta_j^{n-1}(t-l+\frac{1}{2}) - \beta_j^{n-1}(t-l-\frac{1}{2})] \tag{B.6}$$

$$= \sum_{l\in\mathbb{Z}} c_j[l]\beta_j^{n-1}(t-l+\frac{1}{2}) - \sum_{l\in\mathbb{Z}} c_j[l]\beta_j^{n-1}(t-l-\frac{1}{2}) \tag{B.7}$$

Let, $-l-\frac{1}{2} = -l'+\frac{1}{2}$
$l = l'-1$

$$\frac{\partial g_j^n(t)}{\partial t} = \sum_{n} c_j[n]\beta_j^{n-1}(t-l+\frac{1}{2}) - \sum_{l'\in\mathbb{Z}} c_j[l'-1]\beta_j^{n-1}(t-l'+\frac{1}{2}) \tag{B.8}$$

$$= \sum_{l}(c_j[l] - C_j[l-1])\beta_j^{n-1}(t-l+\frac{1}{2}) \tag{B.9}$$

Second derivative :

$$\frac{\partial^2 g_j^n(t)}{\partial t^2} = \sum_{l\in\mathbb{Z}} c_j[k]\frac{\partial^2 \beta^{jn(t-l)}}{\partial t^2} \tag{B.10}$$

Using the following propriety:

$$\frac{\partial^2 \beta_j^n(t)}{\partial t^2} = \beta_j^{n-2}(t+1) - 2\beta_j^{n-2}(t) + \beta_j^{n-2}(t-1) \tag{B.11}$$

We replace in Eq. (B.2), we have:

$$\frac{\partial^2 g_j^n(t)}{\partial t^2} = \sum_{l\in\mathbb{Z}} c_j[l][\beta_j^{n-2}(t-l+1) - 2\beta_j^{n-2}(t-l) + \beta_j^{n-2}(t-l-1)] \tag{B.12}$$

Let $l+1 = l_1$ for first B-Spline and $l-1 = l_2$ for the third B-spline in the previous equation, then:

$$\frac{\partial^2 g_j^n(t)}{\partial t^2} = \sum_{l_1\in\mathbb{Z}} c_j[l_1 - 1]\beta_j^{n-2}(t-l_1)$$

$$-2\sum_{l\in\mathbb{Z}} c_j[l]\beta_j^{n-2}(t-l) - \sum_{l_2\in\mathbb{Z}} c_j[l_2+1]\beta_j^{n-2}(t-l_2)$$

$$\frac{\partial^2 g_j^n(t)}{\partial t^2} = \sum_{l\in\mathbb{Z}} [c_j[l+1] - 2c_j[n] + c_j[l-1]]\beta_j^{n-2}(t-l) \tag{B.13}$$

For third derivative we obtain:

$$\frac{\partial^3 g_j^n(t)}{\partial t^3} = \sum_{l\in\mathbb{Z}} c_j[l]\frac{\partial^3 \beta^n(t-l)}{\partial t^3} \tag{B.14}$$

$$\frac{\partial^3 g_j^n(t)}{\partial t^3} = \sum_{l\in\mathbb{Z}} c_j[l][\beta_j^{n-3}(t-l+\frac{3}{2}) - 3\beta_j^{n-3}(t-l+\frac{1}{2})$$

$$+3\beta_j^{n-3}(t-l-\frac{1}{2}) - \beta_j^{n-3}(t-l-\frac{3}{2})] \tag{B.15}$$

Instead of three B-spline form in the last equation, we keep only $\beta_j^{n-3}(t-l+\frac{1}{2})$,

$$\frac{\partial^3 g_j^n(t)}{\partial t^3} = \sum_{l\in\mathbb{Z}} (c_j[l+1] - 3c_j[l] + 3c_j[l-1] - c_j[l-2])\beta_j^{n-3}(t-l+\frac{1}{2}) \tag{B.16}$$

APPENDIX C

Determinant for an empty shell

Let a and b denote the outer and inner radius of the shell. Letting $X = ka$, $Y = (c/c_L)X$, $Z = (c/c_T)X$, and $N = n(n+1)$, and using primes to denote differentiation, $U = (c/c_L)kb$ and $W = (c/c_T)kb$ the elements are. For an evacuated shell D_n is the determinant of the 5-by-5 matrix with elements given by [85]:

$$
\begin{aligned}
d_{11} &= (\rho/\rho_1)Z.^2 h_n^{(1)}(X),\\
d_{12} &= (2N - Z^2)j_n(Y) - 4Y j_n(Y)',\\
d_{13} &= 2N[Z j_n(Z)' - j_n(Z)],\\
d_{21} &= -X h_n^1(X)',\\
d_{22} &= Y j_n(Y)',\\
d_{23} &= N j_n(Z),\\
d_{31} &= 0,\\
d_{32} &= 2[j_n(Y) - Y j_n(Y)'],\\
d_{33} &= 2Z j_n(Z)' + [Z^2 - 2N + 2]j_n(Z)\\
d_{14} &= (2N - Z^2)n_n(Y) - 4Y n_n(Y)',\\
d_{15} &= 2N[Z n_n(Z)' - n_n(Z)],\\
d_{24} &= Y n_n(Y)',\\
d_{25} &= N n_n(Z),\\
d_{34} &= 2[n_n(Y) - Y n_n(Y)'],\\
d_{35} &= 2Z n_n(Z)_{'} + [Z^2 - 2N + 2]n_n(Z),\\
d_{41} &= 0,\\
d_{42} &= (2N - W^2)j_n(U) - 4U j_n(U)',\\
d_{43} &= 2N[W j_n(W)' - j_n(W)],\\
d_{44} &= (2N - W^2)n_n(U) - 4U n_n(U)',\\
d_{45} &= 2N[W n_n(W)' - n_n(W)],\\
d_{51} &= 0,\\
d_{52} &= j_n(U) - U j_n(U)',\\
d_{53} &= 2W j_n(W)' + [W^2 - 2N + 2]j_n(W),
\end{aligned}
$$

$d_{54} = 2[n_n(U) - Un_n(U)']$,
$d_{55} = 2Wn_n(W)' + [W^2 - 2N + 2]n_n(W)$.

Where j_n, n_n and $h_n^{(1)}$ are spherical Bessel, Neumann, and Hankel functions, respectively. The material properties include the densities of solid and water, $_1$ and , and the longitudinal and transverse wave velocities in solid, c_L, c_T. Primes denotes differentiation with respect to the indicated argument. Also B_n is found by taking $b_{ij} = d_{ij}$ except for the elements $b_{11} = -\rho/\rho_1 x_s^2 j_n(x)$ and $b_{21} = Zj_n^{'}(x)$

Bibliography

[1] T. Abatzoglou. Fast maximum likelihood joint estimation of frequency and frequency rate. *IEEE Trans. on Aerospace and Electronic Systems*, 22(6):708–715, 1986.

[2] R. Altes. Detection, estimation and classification with spectrograms. *J. Acoust. Soc. Amer.*, 67, no. 4:1232–1246, 1980.

[3] W.W.L. Au. Comparison of sonar discrimination: Dolphin and artificial neural network. *J. Acoust. Soc. Am*, 1994:2728–2735, 1994.

[4] F. Auger and P. Flandrin. Improving the readability of time-frequency and time-scale representations by the reassignment method. *IEEE Trans. SP*, 43, no. 5:10681089, 1995.

[5] F. Auger, P. Flandrin, P. Goncalvès, and O. Lemoine. Time-frequency toolbox for matlab, users guide and reference guide„ 1995.

[6] S. Barbarossa. Analysis of multicomponent lfm signals by a combined wigner-hough transform. *IEEE Trans. Sig. Process*, 43, no. 6:1511–1515, 1995.

[7] S. Barbarossa and O. Lemoine. Analysis of nonlinear fm signals by pattern recognition of their timefrequency representation. *IEEE Signal Process. Lett*, 3, no. 4:112115, 1996.

[8] M. Benidir. *Design of time-frequency distributions using polynomials and applications, Time-frequency signal analysis and processing*, chapter V, pages 193–201. Prentice-Hall, 2003.

[9] M. Benidir. Characterization of polynomial functions and application to time-frequency analysis. *IEEE, Trans. SP*, 45:549–552, May, 1997.

[10] M. Benidir and A. Ouldali. Polynomial phase signal analysis based on the polynomial derivatives decompositions. *IEEE Trans. Signal Processing*, 47:1954–1965, July, 1999.

[11] B. Boashash. *Time-Frequency Signal Analysis Methods Applications*. Longman-Cheshire, 1992.

[12] B. Boashash. Time frequency signal analysis and processing: A comprehensive reference. In *Elsevier, Oxford, UK*, 2003.

[13] B. Boashash. Note on the use of the wigner distribution for time frequency signal analysis. *IEEE Transactions on Acoustics, Speech, and Signal Processing*, 36, no. 9:15181521, Sept, 1988.

[14] A. Bouchikhi and A.O. Boudraa. If estimation of multicomponent signal by empirical mode decomposition and b-spline version of teager-kaiser energy operators. *GRETSI*, Troyes. France:817–820, 2007.

[15] A. Bouchikhi, A.O. Boudraa, S. Benramdane, and E.H.S. Diop. Empirical mode decomposition and some operators to estimate instantaneous frequency: A comparative study. *Proc. IEEE ISCCSP*, Saint Julia, Malta.:608–613, 2008.

[16] A. Bouchikhi, A.O. Boudraa, and G. Maze. Analysis of acoustics signals echos from cylindrical elastic shells by hht and tht. *Proc. International Conference in Underwater Measurements*, Nafplion, Greece:1455–1460, 2009.

[17] A.O. Boudraa and J.C. Cexus. Denoising via empirical mode decomposition. In *IEEE-ISCCSP*, pages 1–4, Marrakech, Maroc, Mars 2006.

[18] A.O. Boudraa and J.C. Cexus. Denoising via empirical mode decomposition. In *Proc. IEEE ISCCSP, 4 pages, Marrakech, Morocco.*, 2006.

[19] A.O. Boudraa, J.C. Cexus, F. Salzenstein, and L. Guillon. If estimation using empirical mode decomposition and nonlinear teager energy operator. *IEEE ISCCSP*, Hammamet, Tunisia:45–48, 2004.

[20] E. O. Brigham. *The Fast Fourier Transform and Applications*. Englewood Cliffs, 1988.

[21] D.C. Cassidy. Answer to the question: When did the indeterminacy principle become the uncertainty principle? *American Journal of Physics*, 66:278–279, 1998.

[22] J. C. Cexus and A.O. Boudraa. Nonstationary signals analysis by teager-hunag transform (tht). In *Proc. EUSIPCO*, Florence, Italy, 2006.

[23] J.C. Cexus, A.O Boudraa, and S. Benramdane. Débruitage des signaux par approche emd : Multi-emd$_s g. GRETSI, Troyes, France : 421 - -424, 2007$.

[24] J.C. Cexus, A.O. Boudraa, A. Bouchikhi, and A. Khenchaf. "analyse des échos de cibles sonar par transformation de huang-teager (tht)". *Traitement du Signal*, 24, no. 1-2,:119–129, 2008.

[25] E. Chassande-Mottin and P. Flandrin. On the time-frequency detection of chirps. *Appl. Comput. Harmon. Anal.*, 6(2):252–281, 1999.

[26] P.C. Chesnut and R.W. Floydvol. An aspect independent sonar target recognition method. *J. Acoust. Soc. Am*, 70:772–734, 1981.

[27] P. Chevet, N. Gache, and V. Zimpfer. Time-frequency filters for target classification. *J. Acoust. Soc. Am*, 106, no. 4:1829–1837, 1999.

[28] P. Chevret, F. Magand, and L. Besacier. Time-frequency analysis of circumferential wave energy distribution for spherical shells. application to sonar recognition. *Appl. Sig. Process*, 3:136–142, 1996.

[29] H. Choi and W. J. Williams. Improved time-frequency representation of multicomponent signals using exponential kernels. *IEEE. Trans. Acoustics, Speech, Signal Processing*, 37, no. 6:862 871, Jun, 1989.

[30] L. Cirillo, A. Zoubir, and M. Amin. Parameter estimation for locally linear fm signals using a time-frequency hough transform. *IEEE Trans. Sig. Process*, 56, no. 9:4162–4175, 2008.

[31] L. Cohen. Time-frequency distributions. *A Review. Proceedings of the IEEE*, 77, no 7:941–980, 1989.

[32] L. Cohen. *Time-Frequency Analysis*. Prentice-Hall, 1995.

[33] I. Daubechies. Orthonormal bases of compactly supported wavelets. *Comm. Pure Appl. Math*, 41:906–966, 1988.

[34] C. de Boor. *A practical guide to splines*. Sring-Verlag, New York, 1978.

[35] Delechelle, E. Lemoine, and J. Oumar Niang. Empirical mode decomposition: an analytical approach for sifting process. *Signal Processing Letters, IEEE*, 12:764 – 767, 2005.

[36] J. Dhombres and J-B. Robert. *Fourier, créateur de la physique mathématique*. collection « Un savant, une époque » Belin, 1998.

[37] D. Dimitriadis and P. Maragos. An improved energy demodulation algorithm using splines. *ICASSP*, Salt Lake, Utah, USA:1–4, 2001.

[38] D. Dimitriadis and P. Maragos. Continuous energy demodulation and application to speech analysis. *Speech Comm*, 48:819–937, 2006.

[39] E. S. Diop, R. Alexandre, and A.O. Boudraa. Analysis of intrinsic mode functions: a pde approach. *IEEE signal processing letters*, 17, no. 4:398–401, 2010.

[40] P. Djuric and S. Kay. Parameter estimation of chirp signal. *IEEE Trans. on Acoustics, Speech and Signal Processing*, 38(12):2118–2126, 1990.

[41] D.L. Donoho. De-noising by soft-thresholding. *IEEE Trans. Inform. Theory*, 41(3):613–627, 1995.

[42] D.M. Drumheller, D.H. Hughes, B.T. O'Connor, and C.F. Gaumond. Identification and synthesis of acoustic scattering components via the wavelet transform. *J. Acoust. Soc. Am*, 97:3649–3656, 1995.

[43] R.O. Duda and P.E. Hart. Use of the hough transformation to detect lines and curves in pictures. *Commun. ACM*, 15, no. 1:11–15, 1972.

[44] N. D.Veksler. *Resonance Acoustic Spectroscopy*. Springer-Verlag Berlin, 1993.

[45] B. Escudié, C. Gazanhes, H. Tachoire, and V. Torra. *Des Cordes aux Ondelettes*. Publication De lUniversité de Provence, 2001.

[46] M. Feder and E. Weinstein. Parameter estimation of superimposed signals using the em algorithm. *IEEE Trans. Sig. Process*, 36, No 4:477 489, April, 1988.

[47] C. Feuillade and C.S. Clay. Anderson (1950) revisited. *J. Acoust. Soc. Am.*, 106, no. 2:553–564, 1999.

[48] P. Flandrin. *Time-frequency/time-scale analysis*. Academic Press., 1998.

[49] P. Flandrin, G. Rilling, and P. Goncalves. Empirical mode decomposition as a filter bank. *IEEE Sig. Proc. Lett*, 11, no. 2:112–114, 2004.

[50] B. Friedlander. Parametric signal analysis using the polynomial phase transform. *Proc. IEEE Workshop Higher-Order Statistics*, 1:151–159, 1993.

[51] X. Li G. Bi and C.M.S. See. Lfm signal detection using lpp-hough transform. *Signal Processing*, 27:1–11, 2010.

[52] D. Gabor. Theory of communication. *J. IEE*, 93:426–457, 1946.

[53] P. Gibbins. A note on quantum logic and the uncertainty principle. *Philosophy of Science*, 48, No 1:122–126., 1981.

[54] F. Hlawatsch and G.F. Boudreaux-Bartels. Linear and quadratic time-frequency signal representations. *IEEE Signal Processing Magazine*, 9, No 2:21–67, April 1992.

[55] F. Hlawatsch and W. Kozek. Time frequency projection filters and time-frequency signal expansions. *IEEE Trans. Sig. Process*, 42:3321–3334, 1994.

[56] J.F. Hoffman. Classification of spherical targets using likelihood and quadrature components. *J. Acoust. Soc. Am*, 49:23–30, 1971.

[57] P. Hough. Hough, method and means for recognizing complex patterns, 1962.

[58] M. S. Howe. *Acoustics of fluid-structure interactions*. Cambridge, New York, 1998.

[59] H.Roitblat, P.W. Moore, P.E. Nachtigall, R.H. Penner, and W.W.L. Au. Natural echolocation with an artificial neural network. *Int. J. Neural Networks*, 1:707–716, 1989.

[60] Huang. Normalized hilbert transform and instantaneous frequency. *Patent, number: GSC 14,673-1*, 2003.

[61] N. Huang and Z. Shen. A new view of water waves- the hilbert spectrum. *Ann, Rev. fluid Mech*, 31:417–475, 2006.

[62] N. E. Huang and S.P. Shen. *The Hilbert-Huang transform and its applications*. Interdisciplinary mathematical sciences; V.5 ISBN 981-256-376-8, 2005.

[63] N. E. Huang and Z. Wu. A review on hilbert-huang transform: Method and its application, to geophysics studies. *Rev. Geophys*, 46, No. 2:RG2006, 2008.

[64] N. E. Huang, Z.Shen, S. R. Long, M.C. Wu, H. H. Shih, Q. Zheng, N. C. Yen, C. C. Tung, and H. H. Liu. The empirical mode decomposition and hilbert spectrum for nonlinear and non-stationary time series analysis. *Proc. Royal Society*, 454, no. 1971:903–995, 1998.

[65] N.E. Huang, Z. Wu, S.R. Long, K.C. Arnold, X. Chen, and K. Blank. On instantaneous frequency. *Advances in Adaptive Data Analysis*, 1 no. 2:177–229, 2009.

[66] N.E. Huang, Z.H. Wu, and S.R. Long. On instantaneous frequency. In *in: Workshop on the Recent Developments of the HilbertHuang Transform Methodology and Its Applications, Taipei, China,*, 2006.

[67] J. Illingworth and J. Kittler. A survey of the hough transform. *Computer Vision, Graphics, and Image Processing*, 44, No. 1:87–116, 1988.

[68] M. JABLOUN, F. LEONARD, M. VIEIRA, and N. MARTIN. A new flexible approach to estimate highly nonstationary signals of long time duration. *IEEE Transactions on Signal Processing*, 55, No.7:3633–3644, July 2007.

[69] M. Jabloun, M. Vieira, F. Leonard, and N. Martin. Local orthonormal decomposition for both instantaneous amplitude and frequency of highly nonstationary discrete signals. In *IMA: The Institute of Mathematics and Its Applications, Cirencester, U.K, pp. 107110.*, Dec. 2004.

[70] J. Jeong and W.Williams. Kernel design for reduced interference distributions. *IEEE Trans. Signal Process*, 40, No.2:402412, 1992.

[71] J.J. Kaiser. On a simple algorithm to calculate the energy of a signal. *ICASSP*, Albuquerque, NM, USA:381–384, 1990.

[72] S. G. Kargl and P.L Marston. Observations and modeling of the backscattering of short tone bursts from a spherical shell: Lamb wave echos, glory and axial reverberations. *J. Acoust. Soc. Am.*, 85, No 3:1014–1028, March, 1989.

[73] A.A. Kassim, Z. Mian, and M.A. Mannan. Connectivity oriented fast hough transform for tool wear monitoring. *Pattern Recognition*, 37, no. 9:1925–1933, 2004.

[74] S. Kay. *Fundamentals of statistical signal processing: Detection theory.* Prentice Hall, NJ, 1988.

[75] S.M. Kay and G.F. Boudreaux-Bartles. On the optimality of the wigner distribution for detection. In *ICASSP*, pages 1017–1020, March 1985.

[76] K.Kodera, R. Gendrin, and C. de Villedary. Analysis of time-varying signals with small bt values. *IEEE Transactions on Acoustics, Speech and Signal Processing ASSP*, 26(1):64–76, 1978.

[77] P.K. Kumar and K.M.M. Prabhu. Classification of radar returns using wigner-ville distribution. *Acoustics, Speech, and Signal Processing, IEEE International Conference*, 6:3105–3108, 1996.

[78] L.D. Landau and E. M. Lifshitz. *Theory of Elasticity (3rd ed.).* Oxford, 1986.

[79] M.J. Lipsey and J.P. Havlicek. On the teager-kaiser energy operator "low frequency error". *Midwest Symp. Circuits, Syst*, 3:53–56, Tulsa, OK, USA, 2002.

[80] X. Lv, M. Xing, S. Zhang, and Z. Bao. Keystone transformation of the wigner-ville distribution of multicomponent lfm signals. *Signal Processing*, 89, No 5:791–806, 2009.

[81] F. Magand. *Reconaissance de cibles par Sonar actif large bande. Application à des coques de formes simples et à la classification des espèces de poissons en mer*. PhD thesis, Thèse de Doctorat, INSA-Lyon, N° d'ordre 96 ISAL 0040, 1996.

[82] H. Maitre. Un panorama de la transformation de hough. a review on hough transform. *Traitement du Signal*, 2(4):305–317, 1985.

[83] P. Maragos, J.F. Kaiser, and T.F. Quatieri. On amplitude and frequency demodulation using energy operators. *IEEE Trans. Sig. Process*, 41:1532–1550, 1993.

[84] P. Maragos, T. F. Quatieri, and J. F.Kaiser. Energy separaton in signal modulations with applications to speech analysis. *IEEE, Trans. Sig. Proc*, 41:3024–3051, 1993.

[85] P. L. Marston. Acoustic beam scattering and excitation of sophere resonance: Bessel beam example. *J Acoust Soc Am*, 122 (1):247–252, Jul, 2007.

[86] Mertins, Alfred, Mertins, and Dr Alfred. *Signal Analysis: Wavelets, Filter Banks, Time-Frequency Transforms and Applications*. John Wiley & Sons, Inc., New York, NY, USA, 1999.

[87] M. Neithamer, L.J. Jacobs, J. Qu, and J. Jarzynski. Time-frequency representations of lamb waves. *J. Acoust. Soc. Am*, 109, no. 5:1841–1847, 2001.

[88] E. CHASSANDE-MOTTIN P. Flandrin, F. AUGER. *Applications in Time-Frequency Signal Processing*, chapter Chap. 5, pages 179–203. CRC Press LLC, 2003.

[89] G. G. S. Pegram, M. C. Peel, and T. A. Mcmahoun. Empirical mode decomposition using rational splines: application to rainfall time series. *Proc. R. Soc. A*, 464:1483–1501, 2008.

[90] T. Poggio, V. Torre, and C. Koch. Computational vision and regularization theory. *Nature*, 317:314–319, 1985.

[91] A. Potamianos and P. Maragos. A comparison of the energy operator and the hilbert transform approach to signal and speech demodulation. *Signal Process*, 37:95–120, 1994.

[92] A.D. Poularikas. *The Handbook of formulas and tables for signal processing*. CRC Press LLC, 1999.

[93] T. Prosen and M. Robnik. Energy transport and detailed verification of fourier heat law in a chain of colliding harmonic oscillators. *J. Phys. A: Math. Gen*, 25:3449, 1992.

[94] S. BEN RAMDANE. *Analyse du champ de pression pariétale des surfaces portantes en mouvements instationnaires forcés par décomposition modale empirique*. PhD thesis, Ecole Centrale de Nantes, No B.U. : 498-026, 2008.

[95] G. Rilling. *Décompositions Modales Empiriques Contributions à théorie, l'algorithmie et l'analyse de performances*. PhD thesis, l'Université de Lyon - École Normale Sup'erieure de Lyon, Laboratoire de Physique École doctorale de Physique, 2007.

[96] G. Rilling, P. Flandrin, and P. Conçalvès. On empirical mode decomposition and its algorithms. In *IEEE EURASIP Work-shop Nonlinear Signal Image Processing*, Grado, Italy, 2003.

[97] G. Rilling, P. Flandrin, P. Goncalves, and J.M. Lilly. Bivariate empirical mode decomposition. *IEEE Sig. Proc. Lett*, 14, No. 12:936–939, 2007.

[98] A. Savitzky and M.J.E. Golay. Smoothing and differentiation of data by simplified least squares procedures. *Analytical Chemistry*, 36:1627–1639, 1964.

[99] I.J. Schoenberg. Contribution to the problem of approximation of equidistant data by analytic functions. *Quart. Appl. Math*, 4:45–99, 1946.

[100] M. Schwartz, W.R. Bennett, and S.Stein. Communication systems and techniques. Technical report, NewYork: McGraw-Hill, 1966.

[101] R.C. Sharpley and V. Vatchev. Analysis of the intrinsic mode functions. Technical report, Department of Mathematics University of South Carolina, 2004.

[102] K.M. Snopek. New insights into wigner distributions of deterministic and random analytic signals. *International Symposium on Signal Processing and Information Technology*, 0:374–379, 2006.

[103] A. Sommerfeld. *Partial Differential Equations in Physics*. New York, 1949.

[104] A. Sommerfeld. *Mechanics of Deformable Bodies*. New York, 1964.

[105] N. Stevenson, M. Mesbah, and B. Boashash. A sampling limit for the empirical mode decomposition. *Proceedings of the Eighth International Symposium on In Signal Processing and Its Applications*, 2:647–650, 2005.

[106] H. M. Teager and S. M. Teager. *A Phenomenological Model for Vowel Production in the Vocal Tract*, chapter III, pages 73–109. San Diego, CA: College-Hill Press, 1983.

[107] H. M. Teager and S. M. Teager. Evidence for nonlinear sound production mechanisms in the vocal tract. *France: Kluwer Acad. Publ.*, 55 of D:241–261, 1990.

[108] M. Tria, J.P. Ovarlez, L. Vignaud, J.C. Castelli, IET Radar Sonar M. Benidir, Discriminating real objects in radar imaging by exploiting the squared modulus of the continuous wavelet transform, and 1 1 27-37 February Navigation, 2007. Discriminating real objects in radar imaging by exploiting the squared modulus of the continuous wavelet transform. *IET Radar, Sonar and Navigation*, 1, No 1:27–37, February, 2007.

[109] M. Unser, A. Aldroubi, and M. Eden. B-spline signal processing: Part i-theory. part ii-efficient design and applications. *IEEE Trans. Sig. Process*, 41:821–848, 1993.

[110] M. Unser, S. Horbelt, and T. Blu. Fractional derivatives, splines and tomography. *Proc. EUSIPCO*, IV:2017–2020, Tampere, Finland, 2000.

[111] R. Walter. *Principles of mathematical analysis*. Third edition. McGraw-Hill, Inc., New York, 1976.

[112] M. Wang, A.K. Chan, and C.K. Chui. Linear frequency-modulated signal detection using radon-ambiguity transform. *IEEE Trans. Sig. Proc.*, 46(3):571–586, 1998.

[113] P. D. Welch. A fixed-point fast fourier transform error analysis. *IEEE Trans. Audio Electroacoustics*, 17:151157, 1969.

[114] J.C. Wood and D.T. Barry. Linear signal synthesis using the radon-wigner transform. *IEEE Trans. Sig. Proc.*, 42(8):2105–2111, 1994.

[115] Y. Wu and D. C. Munson. Multistatic passive radar imaging using the smoothed pseudo wigner-ville distribution. In *ICIP (3)*, pages 604–607, 2001.

[116] Z. Wu and N. E. Huang. A study of the characteristics of white noise using the empirical mode decomposition method. *Proc. Roy. Soc. London*, 460:15971611, 2004.

[117] Z. Wu and N. E. Huang. Ensemble empirical mode decomposition: A noise-assisted data analysis method. *Adv. Adapt. Data Anal*, 1:1–41, 2009.

[118] X. Xiang-Gen and C. Genyuan Wang. Quantitative snr analysis for isar imaging using joint time-frequency analysis-short time fourier transform. *IEEE Transactions on Aerospace and Electronic Systems*, 32, 2:649 – 659, Apr, 2002.

Résumé

La Décomposition Modale Empirique (EMD) est un outil de traitement de signal piloté par les données et dédié aux signaux non-stationnaires issus ou non de systèmes linéaires. L'idée de base de l'EMD est l'interpolation des extrema par des splines pour extraire de composantes oscillantes appelées modes empiriques intrinsèques (IMFs) et un résidu. Dans cette thèse, un nouvel algorithme de l'EMD est introduit où au lieu d'une interpolation rigide, un lissage est utilisé pour la construction des enveloppes supérieures et inférieures du signal à décomposer. Ce nouvel algorithme est plus robuste au bruit que l'EMD conventionnelle et réduit le nombre d'IMFs "artificielles" (sur-décomposition). En combinant le nouvel algorithme et la méthode de séparation d'énergie (ESA) basée sur l'Opérateur d'Energie de Teager-Kaiser (OETK), un nouveau schéma de démodulation des signaux AM-FM multi-composante appelé EMD-ESA est introduit. Différentes versions de l'EMD-ESA sont analysées en terme de performance. Pour l'analyse Temps-Fréquence (TF), une nouvelle formulation de la carte TF de l'EMD-ESA appelée Transformation de Teager-Huang (THT) est présentée. Cette nouvelle Représentation TF (RTF) ne présentant pas de termes d'interférences est comparée aux RTF classiques telles que le spectrogramme, le scalogramme, la distribution de Wigner-Ville Distribution (WVD), la Pseudo-WVD et la réallocation de la Pseudo-WVD. En combinant la nouvelle formulation de la THT et la transformée de Hough, une nouvelle méthode de détection des signaux multi-composante à modulation linéaire de fréquence dans le plan TF est présentée. Cette méthode de détection est appelée transformation de Teager-Huang-Hough (THHT). Les résultats de la THHT sont comparés à ceux de la transformée WVD-Hough. Finalement, l'analyse TF par THT et par des RTF classiques (WVD,...) de signaux réels de rétrodiffusion par des coques cylindriques de dimensions et de caractéristiques physiques différentes est présentée. Les résultats obtenus montrent l'apport de la THT comme un outil TF.

Abstract: The Empirical Mode Decomposition (EMD) is new data driven signal processing tool dedicated to the analysis of non-stationary signals derived or not from linear systems. In EMD, the core idea is the fitting splines to extrema in the process of extracting the oscillatory components, called Intrinsic Mode Functions (IMFs), and a residual in the decomposition of the input signal. In this thesis a new EMD is introduced where smoothing interpolation instead of exact interpolation is used to construct the upper and lower envelopes of the signal to be decomposed. The new EMD is more robustness against noise compared to conventional one and reduces the number of unwanted or insignificant IMFs (over-decomposition). Combining the new EMD and the Energy Separation Algorithm (ESA) based on the Teager-Kaiser Energy Operator (TKEO), a new approach for demodulating multi-component AM-FM noisy signals called EMD-ESA is presented. Different versions of the EMD-ESA are detailed and their performances analyzed. For Time-Frequency (TF) analysis, a mathematical formulation of the TF map of the EMD-ESA called Teager-Huang Transform (THT) is presented. This TF Representation (TFR) cross-terms free is compared to classical TFRs such as spectrogram, scalogram, Wigner-Ville Distribution (WVD), Pseudo-WVD and reassigned Pseudo-WVD. Combining the new formulation of the THT and the Hough transform (HT), a new tracking scheme (detection and estimation) of multi-component linear frequency modulation signals is introduced and compared to WVD-Hough transform. The introduced detection method is called Teager Huang Hough Transform (THHT) for short. Finally, a TF analysis by the THT and classical TFRs (WVD, Pseudo-WVD,...) of real signals backscattered by a cylindrical shell of different dimensions and physical parameters is performed. The obtained results show the interest of the THT as a TF tool.

Keywords : Signal processing, Time-Frequency Representation and Analysis, Empirical Mode Decomposition, AM-FM Model, Teager-Kaiser Operator, Teager-Huang Transform, Physical Modes of spherical shell and Acoustic Scattering Signals.